OCEANS AND ATMOSPHERE
www.csiro.au

Characterisation of Regional Fluxes of Methane in the Surat Basin, Queensland

Final report

Task 3: Broad scale application of methane detection, and
Task 4: Methane emissions enhanced modelling

EP185211

Report for the Gas Industry Social and Environmental Research Alliance (GISERA)

October 2018

Ashok Luhar, David Etheridge*, Zoë Loh, Julie Noonan, Darren Spencer, Stuart Day

*Corresponding author (David.Etheridge@csiro.au)

ISBN (print): 978-1-4863-1161-3
ISBN (online): 978-1-4863-1162-0

Citation

Luhar, A., Etheridge, D., Loh, Z., Noonan, N., Spencer, D., Day, S. 2018. Characterisation of Regional Fluxes of Methane in the Surat Basin, Queensland. Final report on Task 3: Broad scale application of methane detection, and Task 4: Methane emissions enhanced modelling. Report to the Gas Industry Social and Environmental Research Alliance (GISERA). Report No. EP185211, October 2018. CSIRO Australia.

Copyright

Important disclaimer

Contents

Acknowledgments

We would like to thank the following people for their roles in this work:

Gordon and Sue McConnachie provided access to their land for the Burncluith monitoring station and supported the operation of the facility. Matt Kernke (Origin) helped arrange access and installations at the Ironbark site. Steve Zegelin and Mark Kitchen (CSIRO) managed the flux tower and meteorological measurements at the monitoring stations. Staff of GASLAB at CSIRO Oceans and Atmosphere, Aspendale, provided the atmospheric composition measurement techniques and calibration standards required for this work. Natalie Shaw from Katestone Environmental is acknowledged for leading the bottom-up emission inventory preparation.

Damian Barrett (CSIRO) provided long term advice on this project.

Martin Cope and Mark Hibberd of CSIRO, and Prof. Peter Rayner of the University of Melbourne provided useful comments on the report.

This project is supported by the Gas Industry Social and Environmental Research Alliance (GISERA). GISERA undertakes publicly-reported independent research that addresses the socioeconomic and environmental impacts of Australia's natural gas industries. For further information visit https://gisera.csiro.au.

Executive summary

This is the final report of the GISERA project "Characterisation of Regional Fluxes of Methane in the Surat Basin, Queensland" addressing the following project milestones:

Task 3: Broad scale application of methane detection, and

Task 4: Methane emissions enhanced modelling.

Fluxes (i.e. emissions in the present context) of methane to the atmosphere from the Surat Basin, a large region of coal seam gas (CSG) production and processing in Queensland, are the focus of GISERA research in Greenhouse Gas and Air Quality (https://gisera.csiro.au). Agricultural and coal mining activities are other significant sources of methane in the region. The main aim of the work done under the final Phase 3 of the project reported here was to demonstrate the utility of an inverse (or "top-down") modelling approach for regional scale (~ 100–1000 km) for inferring methane emissions across the Surat Basin, and to examine the inferred methane emissions vis-à-vis available "bottom-up" emissions for the region. The inverse approach uses continuous measurements of atmospheric methane concentrations, atmospheric transport and dispersion modelling, and prior information about emissions, all within a Bayesian probabilistic framework.

A model domain of approximately 350 km x 350 km centred near the town of Miles was considered and is taken to represent the Surat Basin in this report. The CSG emission activities of interest in the Surat Basin and the Ironbark and Burncluith monitoring stations lie within this domain.

Analysis and modelling of continuous, hourly mean methane concentration data from the Ironbark and Burncluith monitoring stations was undertaken for the measurement period July 2015 to December 2016. The two stations, approximately 80 km apart, were established on either side of existing and future-projected CSG activity, and measured concentrations of methane and carbon dioxide (and carbon monoxide at Burncluith), as well as meteorological data. Methane concentration roses for each monitoring site showed higher concentrations when the winds were from the CSG area.

Methane data were filtered to remove transient spikes in concentration caused by occasional cattle passing nearby the monitor inlets and to remove nighttime low-wind stable atmospheric conditions which atmospheric models have difficulty representing. Hours with high observed carbon monoxide concentrations at Burncluith were also excluded as these periods represent local and transient biomass burning events that are not accounted for in the emission inventory and modelling.

A gridded "bottom-up" methane emission inventory for the region for the year 2015 was compiled. It contained the source intensities and their spatial distribution for all major methane sources, and yielded a domain-wide methane emission of 173 x 10^6 kg yr^{-1} of which cattle grazing (54%) is the largest contributor followed by feedlots (24%) and CSG processing (8.4%).

This bottom-up inventory emissions were further processed and used in CSIRO's state-of-the-art regional scale meteorological and air pollution model, TAPM, to simulate methane concentrations

to compare with measurements from the two monitoring stations. This comparison required a methodology to estimate the time-varying regional background concentration of methane.

The above forward TAPM modelling using the bottom-up methane emission inventory provided a credible simulation of the observed methane concentration distributions at both Ironbark and Burncluith, except that the model underestimated approximately the top 15% of the concentration values. The likely reasons for this underestimation include underestimation of emissions from sources close to the monitoring sites; possible presence of time-varying, intermittent or additional sources that are not accounted for in the bottom-up emission inventory; and errors in the modelled meteorology and plume transport.

The forward modelling also showed that the top three contributors (in order) to the overall averaged modelled methane at both Ironbark and Burncluith are Grazing cattle; the combined emission due to Feedlot, Poultry and Piggeries; and CSG Processing. In contrast, the top three contributors to the highest 5% of the modelled concentrations at Ironbark are CSG Processing, Feedlot + Poultry + Piggeries, and Grazing cattle, whereas these at Burncluith are Grazing cattle, Feedlot + Poultry + Piggeries, and CSG Processing.

The regional Bayesian inverse model formulated to infer methane emissions across the region used the hourly mean methane measurements from the two stations, coupled with TAPM running in backward-in-time meteorological and dispersion mode to calculate the required source-receptor relationship. Emissions were inferred for grid points with a resolution of 31 km x 31 km across the domain. As a test, the inverse model was first applied to a 'synthetic' case in which modelled concentrations were treated as ambient concentration measurements. It yielded a stable and sensible solution, giving confidence in the computational technique.

The inverse model was applied with several choices of prior emission information. The results showed that even when no prior information (except for loose bounds on the emission rate) is specified, the information contained in the measured concentration time series from the two monitoring stations is able to constrain the total emissions realistically, but compared to the bottom-up inventory emissions the estimated emissions are more concentrated in a few areas in the middle of the domain and less in the areas further away.

The use of the bottom-up emission inventory as a prior (with an uncertainty of 3%) in the inverse model yielded optimal source emission estimates, as judged from their ability to describe the methane measurements when used in forward modelling compared to the bottom-up inventory emissions. The domain-wide inverse estimate of methane emission is 166 x 10^6 kg yr^{-1} which is slightly lower than the total bottom-up inventory emission. However, in a subdomain of approximately 155 km x 155 km covering areas between and immediately around the two stations, dominated by agricultural and CSG emissions and where there are potentially other sources not accounted for in the inventory, the estimated emissions were 30% higher than the bottom-up inventory emissions.

The development and application of inverse modelling for regional scale conducted in this report demonstrate that, when appropriately formulated with a realistic prior, it can provide a source distribution estimate that is stable and updates the "bottom-up" source distribution for its consistency with atmospheric concentration measurements. An aim of the study was to focus on the emissions between the stations. However, it was also apparent that having only two monitoring stations across the large domain that contains many methane sources is a limitation.

The modelling showed that the two stations do not sample some distant areas adequately, particularly those located in the north-west and south-east of the domain, due to the large distances between those areas and the monitors coupled with the infrequency of winds from those areas towards the monitors. Thus, potential sources in these areas would not have been estimated as well. The limited number of stations across the large area also necessitated the attribution of sources to points within a grid that is relatively coarse.

There are other uncertainties in the inverse modelling that could lead to inaccuracies in the inferred source emissions. The modelling makes assumptions about the sources that contribute to the measured concentrations, including that they are constant in time and are all contained within the model domain. It relies on the source-receptor relationship (derived using the modelled meteorology which carries its own inherent uncertainty) being accurate across the region. These are typical difficulties of inverse modelling.

The present study (both measurements and the emissions inferred from them) does not distinguish between different source sectors. To do source attribution, measurements of tracers specific to source sectors (such as isotopes of methane) would be required, when instrumentation suitable for field deployment becomes available. The inverse modelling will need to be further developed to account for these types of data streams and extended to sources other than point (e.g. area and line sources).

1 Introduction

This report presents the results of a 3-year study of the emissions (or fluxes) of methane from a large region of the Surat Basin, Queensland, Australia. The Surat Basin is a significant region of coal seam gas (CSG) production and processing, as well as agricultural and coal mining activities. Emissions of methane (CH_4) from CSG activities in this and other Australian CSG precincts have been estimated in several studies undertaken under the GISERA framework. In this study, we use atmospheric "top-down" methods, where continuous measurements of atmospheric methane concentrations are coupled with meteorological and plume transport information through an atmospheric model, to infer the methane emissions across a regional domain (~ 100–1000 km). The method is also known as inverse modelling. This can be contrasted with the more commonly used forward modelling in which concentration fields due to emissions from known sources or from sources estimated by "bottom-up" accounting are predicted using an atmospheric transport and dispersion model driven by observed or predicted meteorology. Figure 1 presents a schematic diagram of the forward and inverse problems, with more details of modelling given later in Sections 4 and 5.

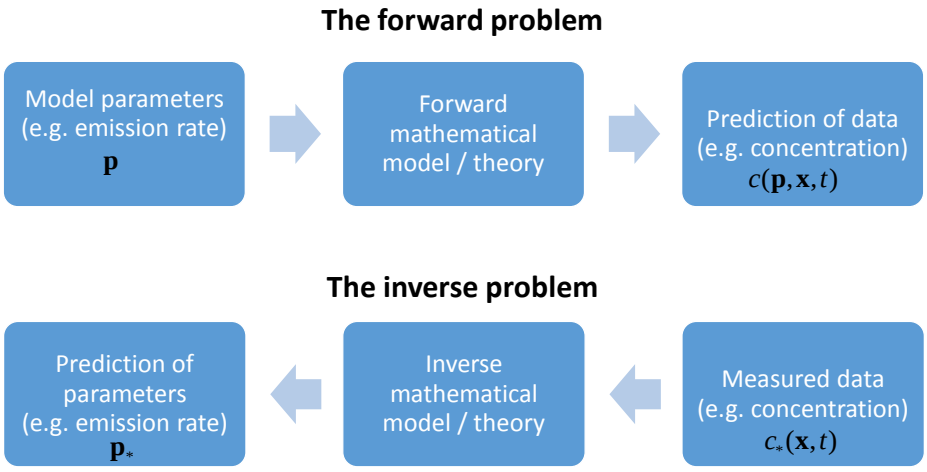

Figure 1. Schematic diagram of the forward and inverse modelling problems.

The inverse modelling results presented in this report complete Phase 3 of the project "Characterisation of the Regional Fluxes of Methane in the Surat Basin. Queensland." Phase 1 provided a literature review of existing methods for detecting and quantifying natural CH_4 seeps, completed in December 2013 (Day et al., 2013). Phase 2 presented results of field trials of suitable methodology identified during Phase 1 at selected locations within the Surat Basin. These included ground surveys, flux chambers, and measurements of methane concentrations using satellite and airborne platforms (Day et al., 2015). Phase 2 also presented forward modelling of the atmospheric methane concentrations that would result from scenarios of emissions from CSG activities across the Surat region, considering some of the smaller scale monitoring results. This

provided the basis for optimally locating monitoring stations for the detection and quantification of the regional methane emissions for the present study. The first monitoring station, Ironbark, was installed during Phase 2, preliminary results were presented and a second monitoring station was recommended. Phase 3 began with the installation of the second field monitoring station (Burncluith) (Figure 2) which was described with initial monitoring data and some hyperspectral remote sensing results in Etheridge et al. (2016). The development of an inverse modelling scheme, and the assessment and screening of the initial monitoring data for modelling and preliminary emissions estimates were presented in Etheridge et al. (2017).

Here we develop that modelling further for the full monitoring period. The modelling methodology is first evaluated in forward and inverse modes, and tested using "synthetic" methane concentration data. A methane emissions inventory for the region, independently prepared by consultants based on Government and industry databases and from the above-mentioned ground surveys, is used in the inversion methodology involving the actual monitoring data and for comparison with the emissions inferred from the inverse modelling.

1.1 Natural gas and the atmosphere

The use of natural gas as an energy source offers potential reductions in greenhouse gas emissions compared to other fossil fuels. Electricity generation with natural gas can produce significantly less carbon dioxide (CO_2) as a combustion product than coal per unit of electrical energy generated. However, because natural gas is comprised mainly of methane, a greenhouse gas 28 times more effective per molecule than CO_2 (over a 100-year period; IPCC, 2014), emissions of methane to the atmosphere during the exploration, production, handling and power generation of natural gas could reduce and even negate these benefits. Global methane concentrations have increased 250% since pre-industrial times (1750 AD) (MacFarling Meure et al., 2006), contributing nearly 20% to the radiative forcing of climate (Meinshausen et al., 2017). Anthropogenic sources over 2000-2012 are mainly agriculture and waste (livestock, rice, landfills; 33% of total methane emissions), fossil fuels (coal mining, gas, oil and industry; 19%) and biomass/biofuel burning (9%) (Saunois et al., 2016). Natural geological emissions are likely to be less than 10% of total methane emissions. Methane is also chemically reactive in the atmosphere and plays a role in the background chemistry, potentially affecting air quality and stratospheric ozone. Loss of natural gas through emissions to the atmosphere also has economic costs due to the value of the lost product and potentially a liability if carbon pricing is established in the future.

Due to its relatively short atmospheric lifetime (about 10 years) compared to CO_2, the global concentration of methane and its climate impact could be quickly reduced by reducing emissions. Anthropogenic methane emissions are amenable to mitigation and doing so could achieve other benefits since emissions represent lost product (in the case of the gas industry), a possible safety hazard (for sufficiently rapid leaks in confined spaces) and potential energy use opportunities (for example by capturing landfill emissions).

Emissions of natural gas from coal seam gas (CSG) are under scrutiny because of the rapid growth of the CSG industry and the large number of potential emission sources across a CSG field. These include wells, pipelines, pumps, pneumatic controls, vents and produced water bodies (Day et al., 2013). Large emissions from gas fields have been found in the USA (Pétron et al., 2012; Brandt et al., 2014; Schneising et al., 2014; Alvarez et al., 2018). High methane concentrations detected

during ground surveys in Australian gas fields have been traced to localised emissions from CSG operations and their individual emissions quantified (Day et al., 2015). However, quantification of net emissions of methane during the production and processing of CSG has remained elusive. It is not practically feasible to measure every potential source component and location to quantify net emissions over a significant proportion of a gas field's operation. Further, disturbance of the subsurface (by well drilling, water depressurisation, gas production, or hydraulic fracturing) may mobilise natural gas and enable it to find pathways to the surface (Lafleur et al., 2016). Emissions of methane from the land to the atmosphere can also occur naturally in gas and coal rich regions and are often referred to as seeps. The location and timing of seeps are poorly known and may occur as multiple point or diffuse locations across a large area (Saddler and Gotham, 2013). Methane seeps in the global context and those specific to the Surat Basin are presented by Day et al. (2013).

1.2 Top-down atmospheric monitoring

Here, top-down atmospheric monitoring essentially means measuring atmospheric methane concentrations that consist of cumulative contributions from various emission sources. While atmospheric methane concentrations can be measured by an increasingly broad array of instruments that can be deployed on various fixed and mobile platforms, the concentration measurements require models or analytical frameworks for methane emissions, or fluxes, to be inferred. The nature of emissions to the atmosphere from the land surface across a region, whether by natural methane seeps or induced by subsurface disturbance, or from a region containing CSG operations, presents a particular monitoring challenge (Rayner and Utembe, 2014). The potential of a monitoring scheme to quantify methane emissions across the Surat Basin using a "top-down" analysis was presented in Etheridge et al. (2017), where methane concentration measurements from two monitoring stations (i.e. Ironbark and Burncluith) were combined with atmospheric dispersion modelling to infer emissions. Here we present the full results for that analysis using the complete monitoring period and better prior information of sources, and discuss their strengths and limitations for quantifying methane emissions across a region containing industrial CSG activities as well as several other methane sources.

2 Measurements and filtering

The Ironbark and Burncluith monitoring stations and the measurements they produced are described in detail in Etheridge et al. (2017). Briefly, Ironbark and Burncluith (Figure 2) began operation on 8 November 2014 and 15 July 2015 respectively. Gaps in data, caused mostly by power failures, were typically short (less than a few days at a time). However, more protracted power outages to the Ironbark site caused extended interruptions from December 2016. The available data when both stations operated thus span more than a year (July 2015-December 2016) and are used in the modelling to infer methane sources across the region. Meteorological measurements were also made at both stations. An eddy covariance flux tower at Ironbark measured micrometeorological data and the fluxes of water vapour, heat and CO_2 (flux data were not necessary for the current study).

Figure 2. Map of the region of the Surat Basin monitoring in this study, showing the Ironbark and Burncluith monitoring stations and towns. The two stations are approximately 80 km apart.

Concentrations of CO_2 and CH_4 were measured at Ironbark and CO_2, CH_4 and CO at Burncluith from 10-m high inlets. The high frequency data were quality controlled (flagged out of the record when key instrument parameter stray outside of acceptable operating conditions) and calibrated using CSIRO produced standards. Careful calibration allows the data to be reported on the appropriate World Meteorological Organisation mole fraction scale; NOAA04 for CH_4, WMOX2007 CO_2 scale

and the NOAA CO scale. Identical measurement methodology and calibrations allow the concentrations from each site (and from other sites in CSIRO's network) to be exactly inter-compared and used in models. The installations are further described in the Milestone 3.1 report (Etheridge et al., 2016).

We use hourly means of the measured concentrations for analysis and modelling. The measured hourly mean concentration time series at Ironbark and Burncluith for the full sampling periods are presented Figure 3 and Figure 4.

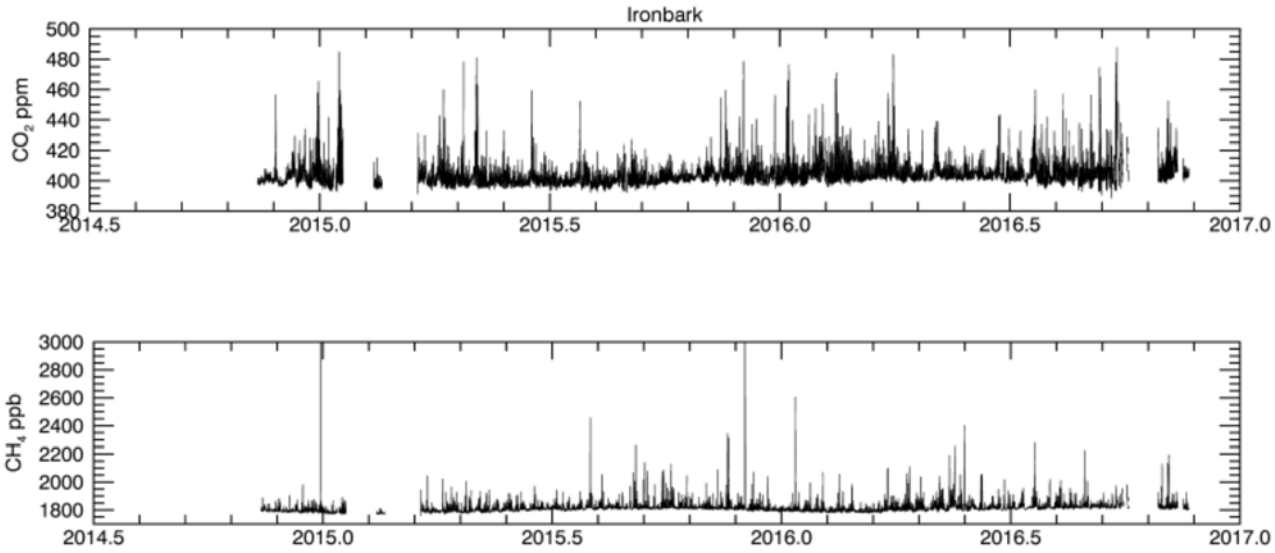

Figure 3. Measured concentration time series (hour means) of CO_2 (parts per million, ppm) and CH_4 (parts per billion, ppb) at Ironbark.

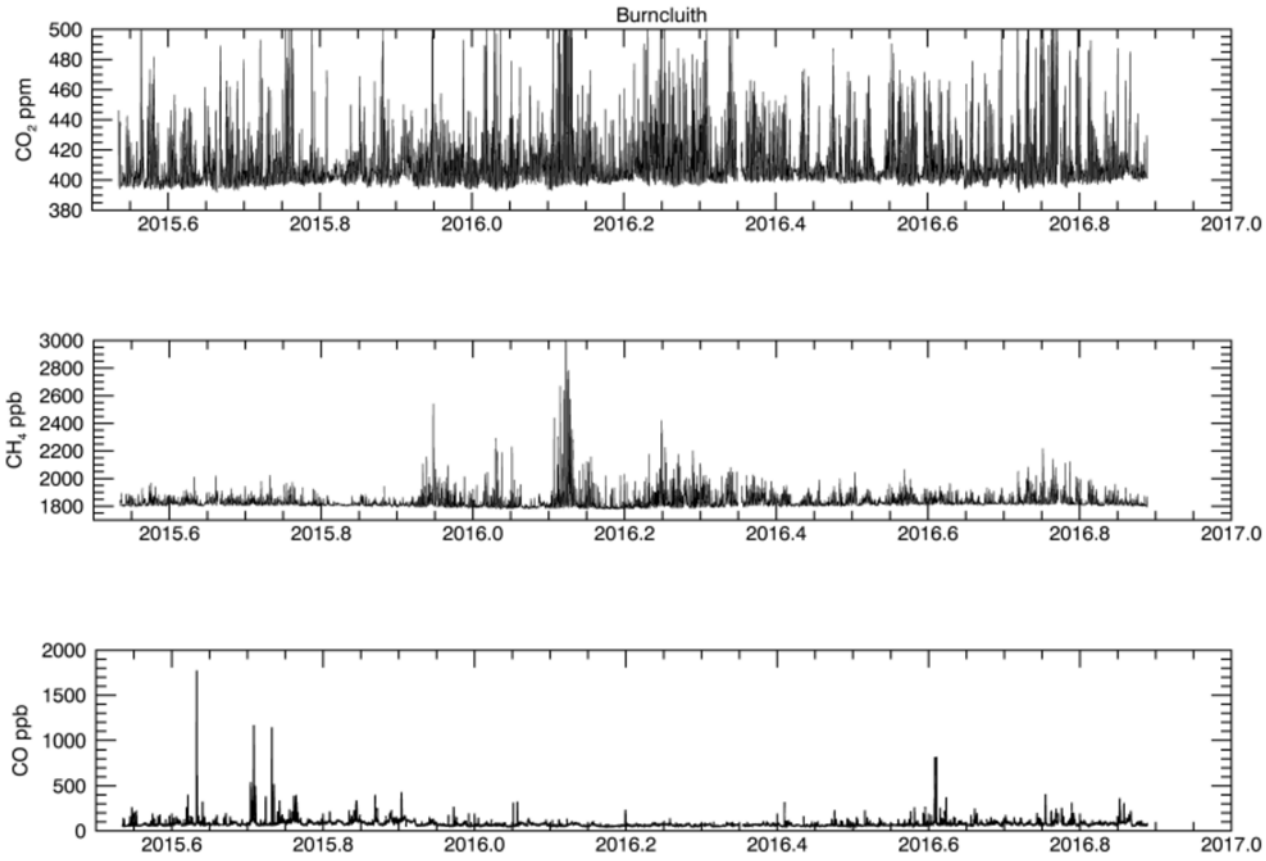

Figure 4. Measured concentration time series (hour means) of CO_2 (ppm), CH_4 (ppb) and CO (ppb) at Burncluith.

2.1 Data filtering

Burncluith is located on a private farm holding and the land owners run a small number (30-40 head) of cattle in the paddocks adjacent to the monitoring station. Due to the proximity of the cattle, the relative size of their emissions can be potentially significant compared to signals from larger, but more distant sources. In order to ensure that contributions from proximate cattle would not undermine the value of the Burncluith record to constrain emissions from the broader Surat Basin – our region of focus – we developed a method to filter the methane record for local cattle emissions which removes rapid spikes due to meandering cows (or stationary cows with meandering winds) without altering the underlying signals and trends in methane concentration (see Etheridge et al., 2017).

There were often significant numbers of cattle immediately upwind of the monitoring locations. In addition, information regarding the use of wood-fired home heater and smoke emissions from nearby controlled burns was supplied by the landholders. Effectiveness of the filter at removing close range point source signals such as these, while preserving signals from more distant and significant sources, such as those from anthropogenic activities in the Surat Basin more broadly, was demonstrated.

The cattle filter removed most large amplitude, high frequency spikes in the measured methane concentrations likely from nearby cows while retaining persistent signals resulting from emissions from sources of possible interest. However, it is not expected to remove signals from the larger population of grazing cattle or feedlots across the region.

The same cattle filter was applied to the Ironbark data, for consistency, although cattle are fewer and further away at Ironbark and have much less impact on the methane measurements.

A considerable amount of elevated concentrations of all measured gases at the two sites occur during the nighttime under light (or low) wind conditions. This is because under these conditions the atmosphere is typically characterised by strong stable stratification and a shallow boundary layer height so that even small local sources can lead to very large enhancements in the local methane concentration due to very little atmospheric mixing. Difficulties in representing dispersion in atmospheric models (which we use) under nocturnal low wind conditions can lead to errors (Luhar and Hurley, 2012; Section 5.6). Such nocturnal conditions can be approximately defined as those with a wind speed at 10-m above ground of less than 2–3 m s^{-1}, which corresponds to a Richardson number (a stability parameter that is the ratio of buoyant suppression of turbulence to shear generation of turbulence in the lower atmosphere) value of greater than 0.2 − 0.3 (Luhar et al., 2009). Thus, one option to circumvent the issue of modelling not being able to properly simulate strong inversion conditions at night is to consider daytime hours (1000–1700 h) irrespective of wind speed, and the remaining hours for which the wind speed is greater than 3 m s^{-1}. The daytime window typically corresponds to periods of strong mixing dominated by convective motions resulting from the solar heating of the ground. For data selection for the two sites, the respective measured wind speeds were used. The daytime window is slightly narrower than the 0900-1900 h time window used earlier (Etheridge et al., 2017).

Finally, we used the measured carbon monoxide (CO) concentration at Burncluith (CO was not measured at Ironbark) as a tracer of emissions from combustion sources. A plot of CO vs CH_4 concentrations in Figure 5 shows a distinct grouping of high CO values (orange circles) most likely from combustion sources. Both methane and CO are emitted from biomass burning, and elevated concentrations were observed during forest fires observed northwest of Burncluith (Etheridge et al., 2017). Biomass burning emissions are not included in the bottom-up methane emissions inventory that we use in our modelling work as they are sporadic and highly uncertain, however they can be identified by CO concentration measurements. Carbon monoxide is not present in other large methane sources of interest, including those compiled in the emissions inventory. Methane emissions from power stations, domestic wood heating and vehicles on the other hand would contain CO, but the modelled CH_4 signals for these sources are predicted to be virtually undetectable at Burncluith (see the modelled concentration roses in Appendix A. The majority (89%) of CSG source emissions in the bottom-up inventory are not from combustion. Importantly, emissions from the less well known migratory or seepage sources, which also do not originate from combustion, would not be screened out by a CO filter. Thus, comparisons of observed CH_4 with model simulations are more accurately made by excluding hourly periods with large CO enhancements above the background CO concentration. We chose an hourly mean CO enhancement of 10 ppb as a cut off, based on CO measurement precision, the closeness of fit of the calculated background record to the lower range of observed values and the variance of the CO measurements. The hourly mean data points after removing the data points with CO values greater than 10 ppb above background concentrations are shown as blue dots in Figure 5. The

background CO concentration was calculated using the same methodology as the background CH_4 (Section 4.1.2). The CO selection filter also helps remove enhanced CH_4 measurements at Burncluith due to emissions from the wood fire in the dwelling adjacent to the monitoring station. Enhancements of CO above background are mostly observed during north-westerly and easterly winds, consistent with the locations of the occasional forest burn offs and dwelling open fire sources respectively.

Unless specified otherwise, we use the filtered hourly mean methane data for analysis and regional scale modelling.

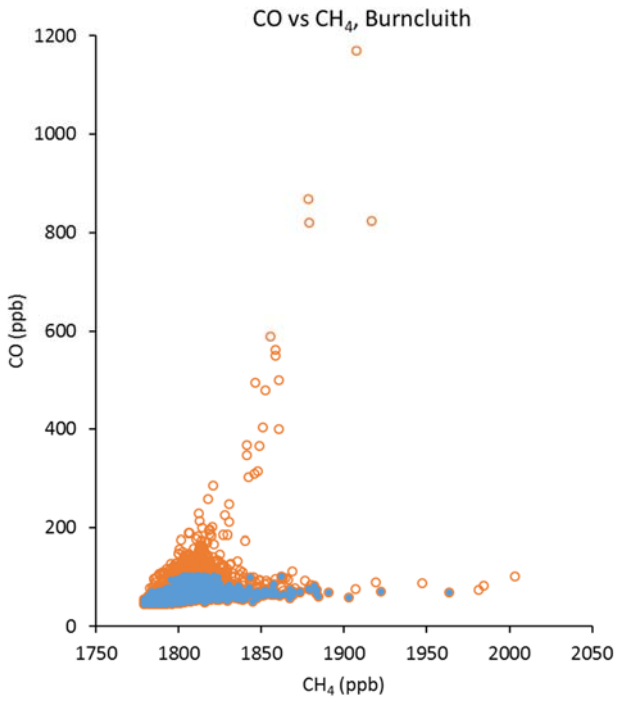

Figure 5. Hourly mean concentrations of CO versus CH_4 measured at Burncluith selected for 1000-1700 for all wind speeds and for 1800-0900 for wind speed greater than 3 m s^{-1} (orange circles). The data group with high magnitudes of CO concentration likely represents dominant contributions from combustion sources. The data marked with blue dots are the measurements when hourly mean CO concentrations are within 10 ppb of the background CO concentration at the time of measurement, and are selected to represent contributions from non-combustion sources.

3 Bottom-up methane emissions

A bottom-up database (or inventory) of the Surat Basin methane emissions from various source categories was developed by consultants Katestone Environmental with feedback from CSIRO. The report “Surat Basin Methane Inventory 2015 - Summary Report” (Katestone, 2018) provides a detailed description of the methane emissions calculation methodology and estimated emission uncertainties, and is given in Appendix B. The domain of the emission inventory was 345 km east-west by 344 km north-south with the centre near the town of Miles. The domain was divided into evenly-spaced grid cells each of 1 km by 1 km. The emissions are for the year 2015.

The emission inventory includes the following sectors and activities:

- Large industry (power stations, coal mines, coal seam gas processing and production)
- Agriculture (feedlots, grazing cattle, piggeries and poultry farms)
- Domestic wood heating
- Motor vehicles
- Other sources (landfills, sewage treatment plants, river seeps and geological seeps).

The emission inventory does not include methane emissions from land clearing, biomass burning, wetlands, registered ground water wells, or fuel usage and material handling associated with mining activities.

Table 1 presents a summary of total methane emissions from the various sectors and sources for the region. There are 14 source categories in total. In general, standard methodologies are used with information from State and Federal Government Departments, such as the National Pollutant Inventory (NPI), National Resource Management (NRM), and National Greenhouse and Energy Reporting (NGER). Although the emission inventory is for 2015, we use it for the full study period (i.e. July 2015 to December 2016) for our modelling, assuming that changes in annual emissions from 2015 to 2016 are small. All the dominant emissions are time invariant. Time variations on diurnal and seasonal timescales included for some sources, namely traffic, wood heating and power plant, are included, but these are amongst the smallest contributors (0.014%, 0.16% and 0.37%, respectively, of the total emissions) and are, therefore, averaged to annual means for computational efficiency in the modelling. CSG sources are broadly categorised in the emission inventory as production (including well head control equipment, separators, maintenance, leaks, well head pumps, flaring, diesel used in vehicles, and backup generators) and processing (including compressor venting, control equipment, gas conditioning, plant compressors, flaring, diesel used in vehicles, backup generators, and collection and storage of produced water). Information on some sources has been provided by or can be compared with estimates from CSIRO monitoring activities. For example, some ground seeps and river seeps were located and their emission rates quantified (Day et al., 2015; Sherman et al., 2014). These were not attributed in the emission inventory to any activity, such as the disturbance of subsurface by CSG activities or other activities such as pumping of ground water. Emissions from CSG wells given in the emission inventory are based on the NGER methodologies and are very close to the average emission rate measured by Day et al. (2014, 2016).

Figure 6 presents a pie chart of the relative inventory emissions from the various sectors reported in Table 1. Cattle grazing has the largest contribution (54%) to the total emissions, followed by feedlots (24%) and CSG processing (8.4%).

Table 1 Surat Basin bottom-up methane inventory emissions (kg/year) by industry sector or source [Katestone, 2018]

INDUSTRY SECTOR OR SOURCE		METHANE EMISSIONS (KG/YEAR)
Agriculture	Feedlot	42,270,444
	Grazing cattle	92,991,979
	Poultry	96,699
	Piggeries	2,358,892
Coal seam gas (CSG)	Processing	14,610,306
	Production	1,918,532
Domestic wood heating		280,324
Landfill		1,905,644
Mining	Coal extraction	14,424,564
Motor vehicles		24,071
Power stations		640,070
Seeps	Ground seeps	127,714
	River seeps	375,909
Wastewater treatment		1,137,905
Total		173,163,053

[Katestone, 2018: Report "Surat Basin Methane Inventory 2015 - Summary Report; Appendix B]

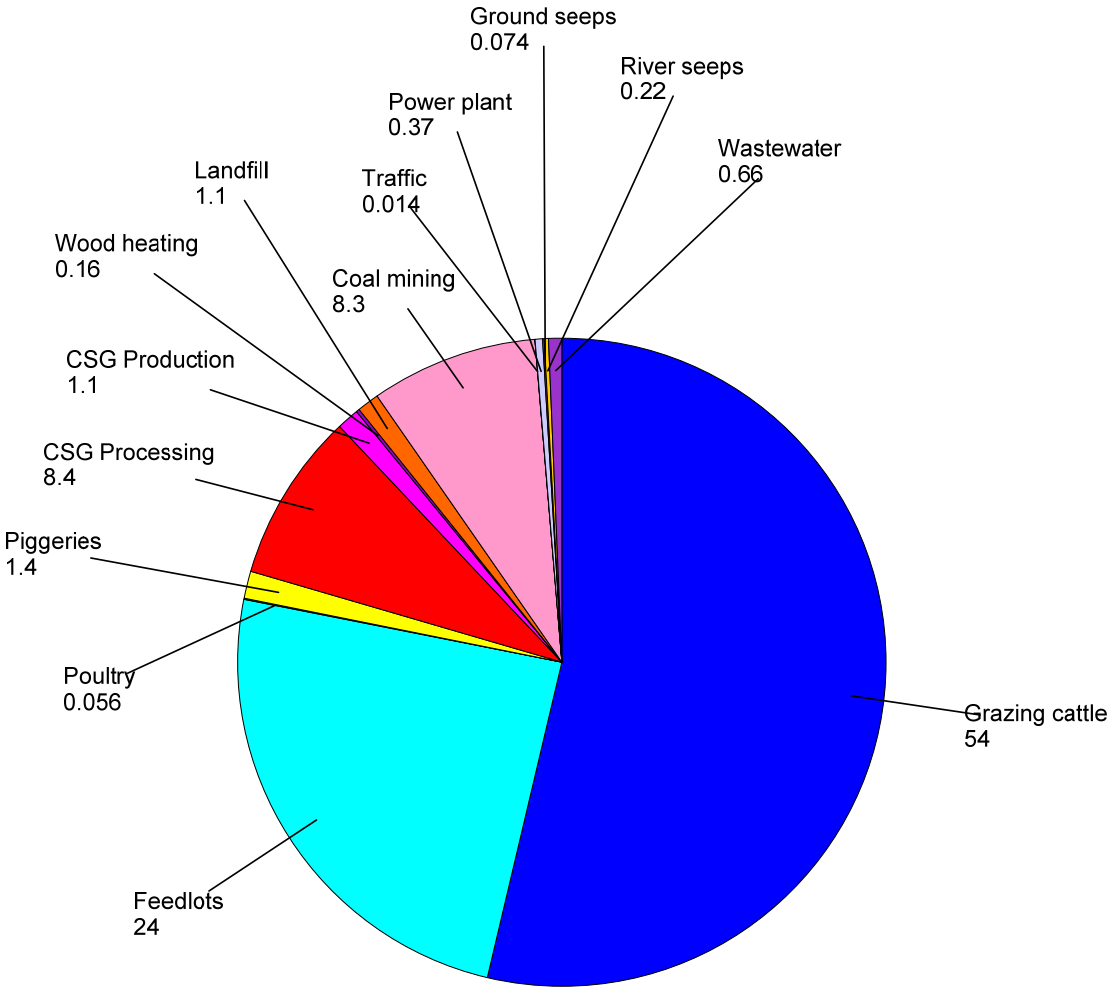

Figure 6. Surat Basin bottom-up methane inventory emissions by industry sector or source (%).

Figure 7 presents total inventory methane emissions across the study domain with grid cells of size 1 km × 1km each. The extensive uniformly coloured areas (green and blue) are cattle grazing emissions.

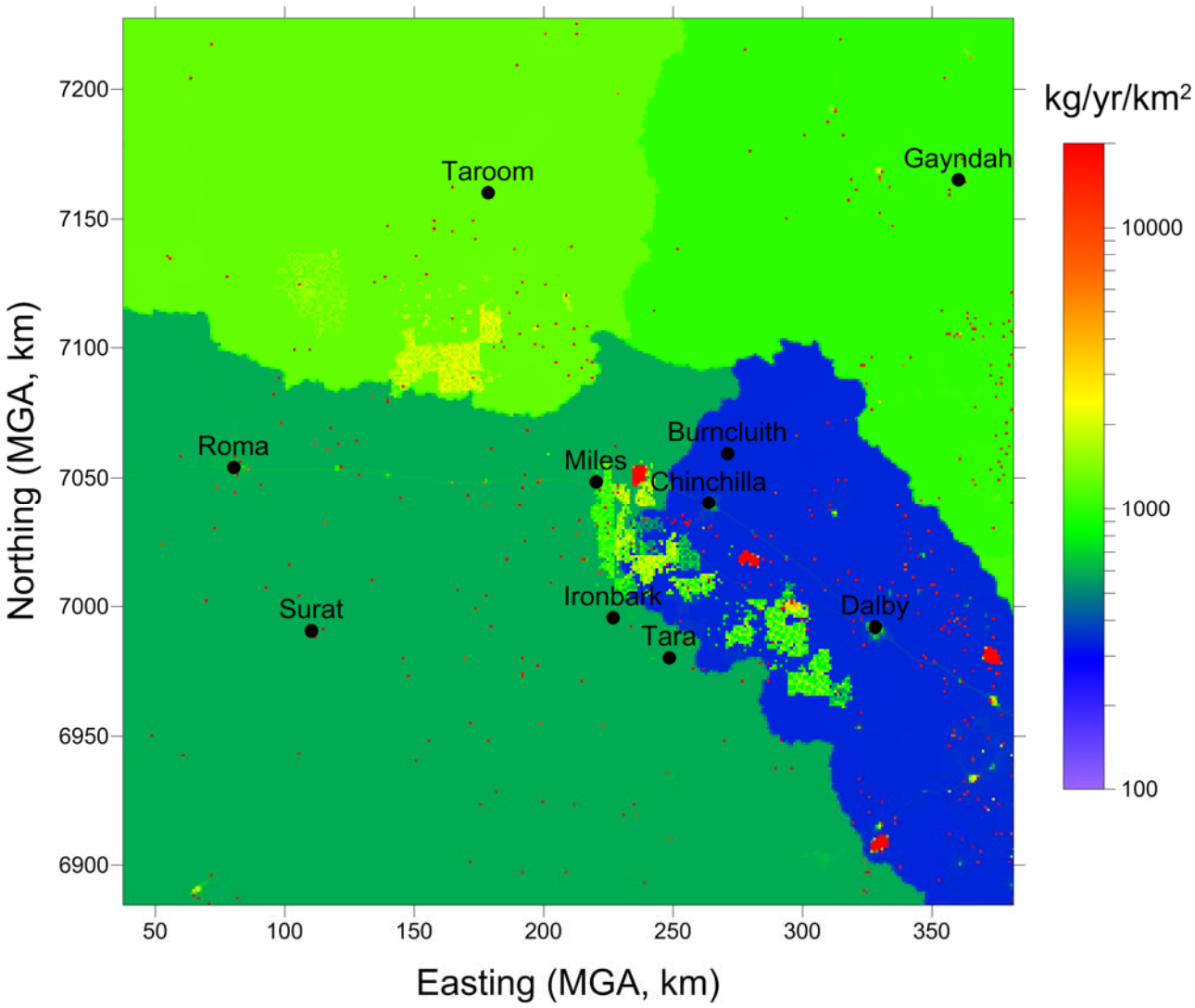

Figure 7. Surat Basin bottom-up methane inventory emissions (kg/year/km^2) based on data from Katestone (2018) for the year 2015. The locations of the Ironbark and Burncluith monitoring stations and some towns in the area are also shown. The coordinates are in the Map Grid of Australia (MGA) system (Zone 56).

4 Atmospheric modelling

The bottom-up methane inventory emissions described in the previous section can be used in a regional transport model to simulate the methane concentration time series at the two stations. These can be compared with the observed time series to test the skill of the model in simulating regional transport and the accuracy of the input emissions. This task is important because the skill of the model also reflects upon its suitability for inverse modelling to infer emissions. In the following section on forward modelling, we use the inventory emissions in a transport model to simulate methane concentrations in the Surat Basin.

4.1 Forward modelling

In forward modelling, concentration fields due to known emissions are predicted using an atmospheric transport and dispersion model driven by observed or predicted meteorology (Figure 1).

4.1.1 Model description and setup

Numerical models used for atmospheric applications are approximate representations of the governing laws of motion and thermodynamics. Atmospheric transport and dispersion modelling calculates the dilution factor for an emission which provides a quantitative relationship between the emission from the source and its detection as concentration at a monitoring station. Forward modelling pertains to simulating the concentration of a species in the atmosphere given the emission of that gas species.

Modelling emission transport at regional scale (~ 100–1000 km) requires an appropriate model coupled with a meteorological modelling capability. We use CSIRO's The Air Pollution Model (TAPM vn4.0.4), which is a three-dimensional, coupled prognostic meteorological and pollutant dispersion model (Hurley et al., 2005) which runs in forward mode. Prognostic models are the most complex of air pollution models, and are used to forecast the time evolution of the atmospheric system through the space-time integration of the fundamental equations of conservation of mass, heat, motion, water and other substances (e.g. air pollutants). They are either stand-alone meteorological models driving air pollution dispersion models, or are fully coupled meteorological and air pollution models (e.g. TAPM). The main advantage of the prognostic approach is that it eliminates the need to have site-specific meteorological observations to drive a pollution transport model.

The global databases required as input to TAPM include terrain height, land use, vegetation leaf-area index, sea-surface temperature, and large-scale weather information (synoptic meteorological analyses). The model can be used in a nestable mode (i.e. a finer domain embedded in a coarser, larger domain) to improve computational efficiency and resolution.

The meteorological component of TAPM predicts the local to regional scale flow at finer temporal and spatial resolution (e.g. sea breezes and terrain induced flows) within a background of larger-

scale meteorology provided by input synoptic weather analyses. The transport and dispersion component uses the predicted meteorology and turbulence from the meteorological component, and consists of a default Eulerian grid-based set of prognostic equations for pollutant concentration.

TAPM has been widely used in Australia for air quality regulatory applications and research problems. Previous applications involving local to regional scale dispersion problems include Luhar and Hurley (2003), Luhar et al. (2008), Zawar-Reza and Sturman (2008), Bandeira et al. (2011), Luhar and Hurley (2012) and Emmerson et al. (2016).

TAPM was run for the Surat Basin for the period 1 July 2015 to 31 December 2016, when both Ironbark and Burncluith monitoring stations operated concurrently. Two nested spatial domains were used in the model: an inner domain of size 370 km × 370 with a horizontal grid resolution of 5 km × 5 km (so 75 x 75 grid points), and an outer domain of size 1110 km × 1110 km with a horizontal grid resolution of 15 km × 15 km (Figure 8). The number of vertical levels in the model was 25, with the lowest five being 10, 25, 50, 100 and 150 m above ground level (AGL). The centre of the domains was -26°35' latitude, 150°4.5' longitude, with the corresponding Map Grid of Australia (MGA) coordinates being 208.657 E, 7056.383 N (Zone 56). The model domains partially fall within MGA Zone 55. All the distances reported here are relative to Zone 56.

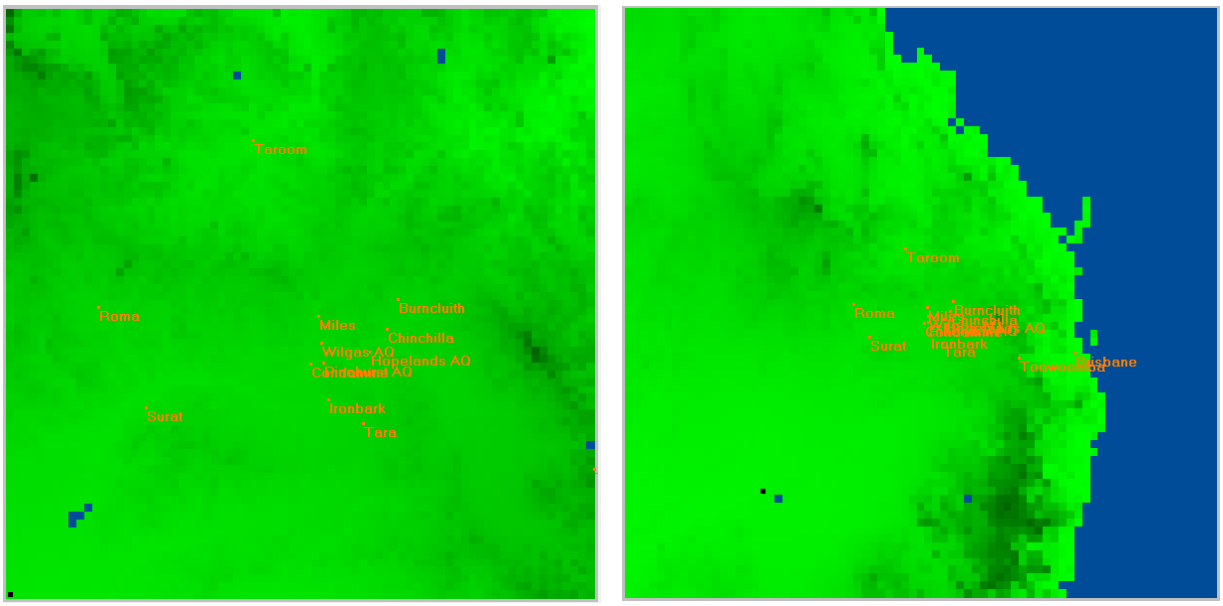

Figure 8. TAPM model domains. Left: inner-grid domain of size 370 km × 370 km with a horizontal grid resolution of 5 km × 5 km, right: outer-grid domain of size 1110 km × 1110 km with a horizontal grid resolution of 15 km × 15 km. Ironbark, Burncluith and other locations are shown. The colour shading represents topography (the darker the colour the higher the terrain elevation), and the blue colour is water.

The input synoptic fields of meteorological parameters, namely the horizontal wind components, temperature and moisture, required in TAPM were derived from the U.S. NCEP (National Centers for Environmental Prediction) reanalyses with a resolution of 2.5° longitude × 2.5° latitude on multiple levels every 6 hours. TAPM is initialised at each grid point within the outermost domain with values of these parameters interpolated from the synoptic analyses.

The methane inventory emissions given at 345 x 344 grid points each with a resolution of 1 km x 1 km lie within the inner model domain. This number of grid points is too large and unwieldy computationally to implement as individual sources in the model so a computer script was developed to regrid these emissions to a more manageable 69 x 69 grid points with each grid cell size being (345/69) km x (344/69) km (≈ 5 km x 5 km), ensuring that the regridding procedure conserved the total emission from the various sectors. The regridded emission cells also matched the inner grid resolution of the TAPM setup. The regridded emission inventory showing contributions from all sources is shown in Figure 9 (note that the colour scale differs from that in Figure 7).

In TAPM, each regridded cell was treated as a surface area source (except the power station emissions which were treated as point sources with stack height and plume rise inputs specified). The emissions were constant with time. TAPM can handle a maximum of 4 tracers in a single run. To keep the computations more tractable, instead of releasing all 14 source category emissions as separate "tracers", emissions were aggregated into nine sectors, which corresponded to various source categories or their combinations, with each sector emission treated as a tracer:

- Tracer 1 (Grazing cattle)
- Tracer 2 (Feedlot + Poultry + Piggeries)
- Tracer 3 (CSG Processing)
- Tracer 4 (CSG Production)
- Tracer 5 (Mining)
- Tracer 6 (River seeps)
- Tracer 7 (Wastewater treatment + Domestic wood heating + Motor vehicles)
- Tracer 8 (Landfill + Ground seeps)
- Tracer 9 (Power stations)

Thus 9 tracers were released from each source grid cell. Three separate TAPM runs were required to handle 9 tracers. Figure 10 presents a pie chart of the relative emissions (%) of the nine tracers used in the TAPM modelling.

Hour averages of the modelled meteorology and methane concentrations extracted for Ironbark and Burncluith were used for analysis. The modelled methane concentrations do not include background methane levels that represent sources and processes outside of the model domain. In the following section, we devise a method to estimate a time-varying background methane concentration which is then added to the modelled methane.

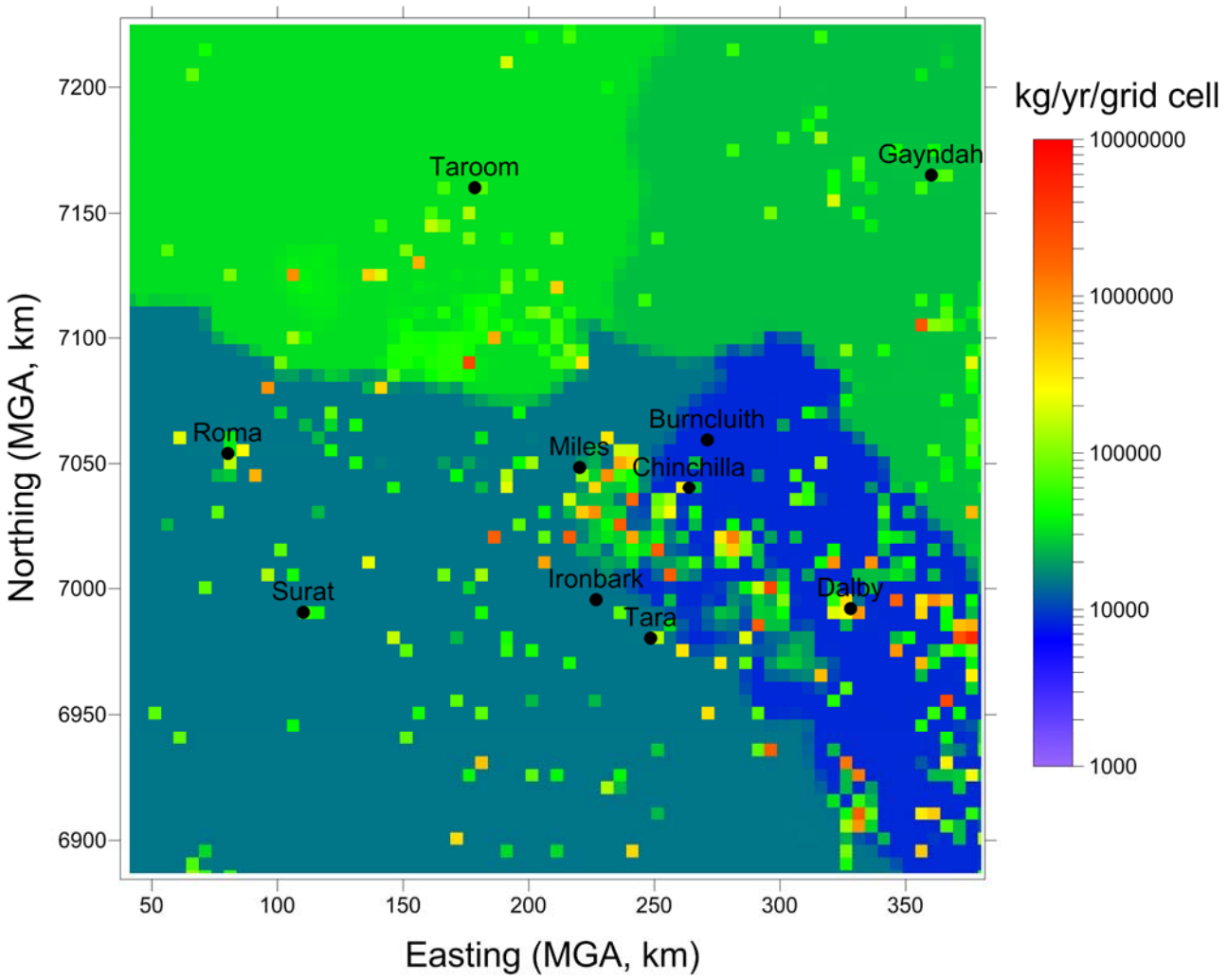

Figure 9. Regridded Surat Basin methane inventory emissions with 69 x 69 grid points (kg/year/grid cell). The grid cell size is 5 km x 5 km. The coordinates are in the Map Grid of Australia (MGA) system (Zone 56).

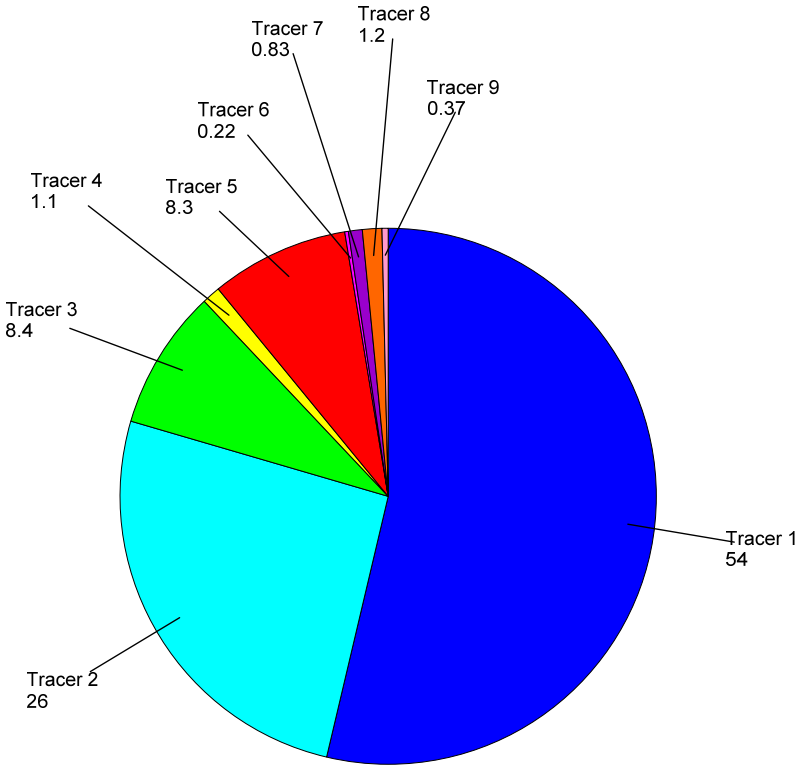

Figure 10. Surat Basin methane inventory emissions by tracer sources used in the modelling (%)

4.1.2 Estimating the background methane concentration

The observed methane concentrations include both background concentration and contributions from sources within the modelling domain. On the other hand, the modelled methane concentrations are only contributions from the prescribed inventory sources, and a background methane concentration needs to be added to the modelled methane for comparison with the methane measurements at Ironbark and Burncluith. Conversely, the background concentration needs to be subtracted from the observed concentrations to obtain methane signals that represent the contributing sources within the domain of interest. A method was devised to estimate the background methane levels for the area under consideration, as described next.

Background methane concentrations for clean, marine air (air having passed over oceans for distances up to thousands of kilometres and thus well mixed and not influenced by identifiable sources) can be found from baseline atmospheric monitoring stations typically situated on coasts. Baseline stations in the Australian region include Cape Grim (Tasmania) and Cape Ferguson (Queensland), both operated by CSIRO. Methane concentrations during baseline conditions at these locations show a marked seasonal cycle and year to year growth but very steady concentrations over shorter timescales.

Background CH_4 concentrations in continental locations like the Surat Basin are slightly higher than concentrations at these baseline stations due to emissions from regional sources upwind of the Basin. To infer the emissions of sources within the domain of interest from concentration data at Ironbark and Burncluith it is important to determine background concentrations within the

domain. We used CH_4 concentrations measured at both the Ironbark and Burncluith sites that best reflect the regional background by selecting conditions that minimise the influence of emissions from within the domain.

A time series of hourly background CH_4 concentration for each of the two sites was constructed as follows. Data from the measured concentration time series were retained if they occurred between 1200 – 1500 h local time (typically the time of highest boundary layer height and maximum trace gas homogeneity during the diurnal cycle) and the hourly standard deviation was less than or equal to 1 ppb, indicating very well mixed conditions. This filtered dataset was then used to derive a smooth curve. Based on the method described by Thoning et al. (1989), the filtered dataset was fitted with a function consisting of cubic polynomial and three harmonics. This function fit is then subtracted from the filtered data and the residuals further filtered with a band-pass filter of 80 days. The original function fit is then added back to the filtered residuals to give a smooth curve fit through the data. These operations are performed iteratively (with hours lying outside twice the standard deviation around the fit excluded) until the fit converges. An interpolation routine then produced the fitted background CH_4 concentrations at each of the hourly timestamps of the original measured data. Figure 11 presents the calculated individual site background CH_4 concentrations, as well as the baseline records at Cape Grim (CGO). The uncertainty in the background fits at both sites is around 3.5 ppb. A regional background CH_4 concentration is given as the arithmetic mean of the two background time series.

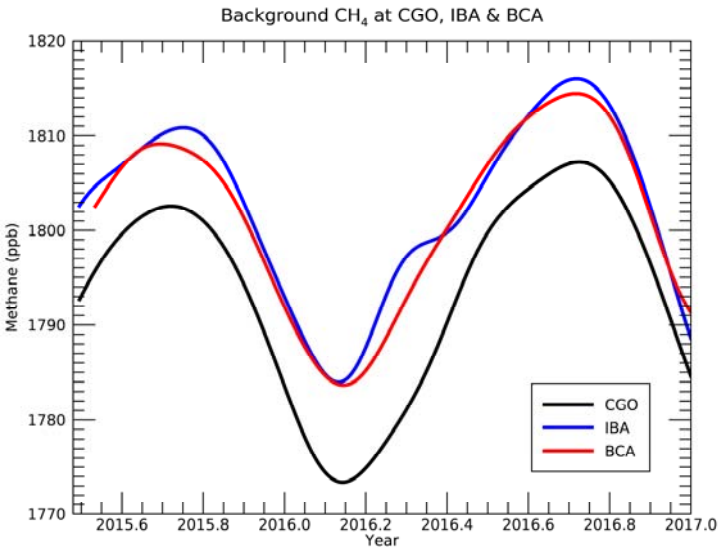

Figure 11. Plot showing the individual site hour mean background CH_4 concentrations and the baseline record at Cape Grim (CGO). The regional background (the average of Ironbark (IBA) and Burncluith (BCA)) was considered an optimal background estimate from which to infer signals from sources within the domain.

The resulting background concentration time series was subtracted from the observed concentration time series to provide an estimate of the concentration signal from emissions in the domain of the Surat Basin, for comparison with the forward model simulations by TAPM using

prescribed sources from the emissions inventory. They are also used in the inverse modelling as described in Section 5.6.

4.1.3 Comparison of near-surface meteorology

Prediction of concentrations at monitoring stations using source emission rates (and conversely inferring source emission rates using concentration data, as done later in Section 5) depends on accurate modelling of the regional wind field which governs atmospheric transport and dispersion. The TAPM modelled winds can be tested at the two stations where we have meteorological measurements.

Figure 12 to Figure 14 present wind roses for Burncluith and Ironbark constructed using the TAPM generated hourly winds and the observed hourly winds for the period August 2015 to December 2016. The TAPM winds are from the inner-nest model output at a height of 10 m while the observed winds are from sonic anemometer measurements made at a height of 7.6 m at Burncluith and 5.8 m at Ironbark. Only those modelled hours for which there are wind data are considered. Figure 12 shows wind data for all hours, Figure 13 shows wind data for daytime hours only (1000 – 1700 h) when atmospheric mixing is generally strong, and Figure 14 shows wind data for nighttime hours (1800 – 0900 h).

The observed winds at Burncluith and Ironbark shown in Figure 12 are qualitatively similar, with winds from the north-east quadrant being the most frequent over the time period shown and both sites showing relatively smaller frequencies of wind from the south-west quadrant. Wind speed at Burncluith is observed to be weaker than that at Ironbark, particularly when the winds are from the north-east quadrant. The TAPM-simulated winds are qualitatively similar to those observed, with the most frequent modelled wind direction also from the north-east quadrant and winds from the south-west quadrant modelled at a relatively smaller frequency in agreement with the observations. The TAPM winds at Burncluith and Ironbark are similar, more so than those observed. At Burncluith the model underestimates the frequency of low wind speed events (< 2 m s^{-1}) and overestimates the frequency of higher wind speed events (> 4 m s^{-1}) from the north-east sector. The wind speed distribution at Ironbark is much better modelled than that at Burncluith.

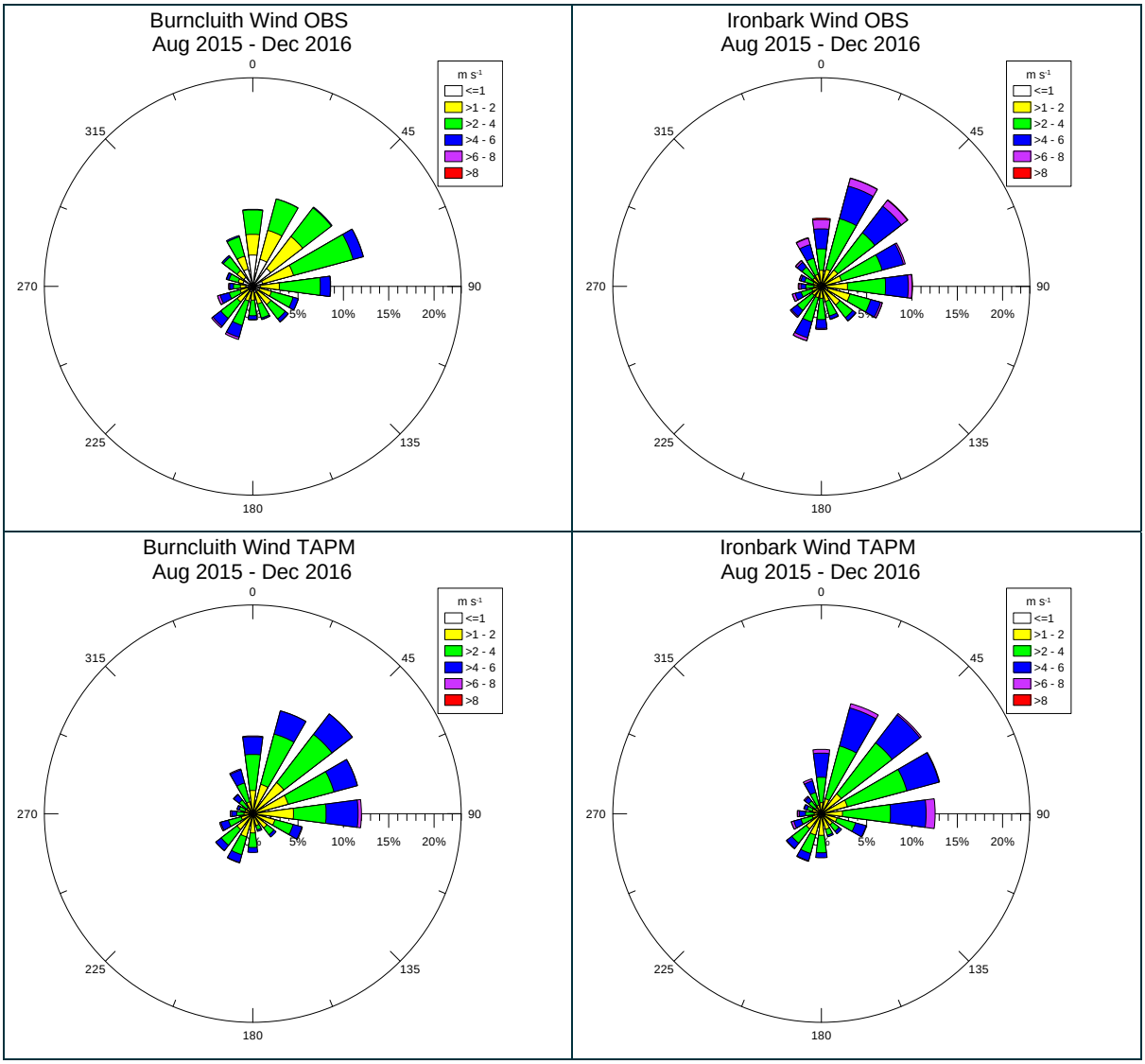

Figure 12. Observed (top) and modelled (bottom) wind roses for the Burncluith and Ironbark monitoring sites (August 2015 to December 2016) (all hours considered).

The daytime wind roses in Figure 13 and the nighttime wind roses in Figure 14 show the observed low wind speeds (< 2 m s^{-1}) at Burncluith occur mostly at nighttime (Figure 14). Low wind speeds at night are associated with a strongly stable nighttime boundary layer with shallow inversion which, as mentioned earlier, most meteorological models have difficulty in reproducing. At nighttime the observed winds are predominantly from the north-east quadrant, with a pattern similar to the all-hours winds (Figure 12). There is generally good agreement between the TAPM and the observed wind direction at nighttime.

The TAPM daytime winds (Figure 13) at Burncluith and Ironbark are similar, with more frequent easterly components and less frequent northerly components than the all hours TAPM winds. The daytime observed winds at Burncluith show a similar pattern while Ironbark observations show a greater frequency of north-northwesterly winds during the day which is not captured by TAPM. Observed at both sites is a greater frequency of south-westerly winds compared to when all hours

are considered. TAPM shows an increase in the frequency of winds from the south-west during the day but not as frequent as observed particularly at Ironbark. Wind speeds at Burncluith are overestimated by TAPM during the day, mostly for winds from the north and the north-east quadrant.

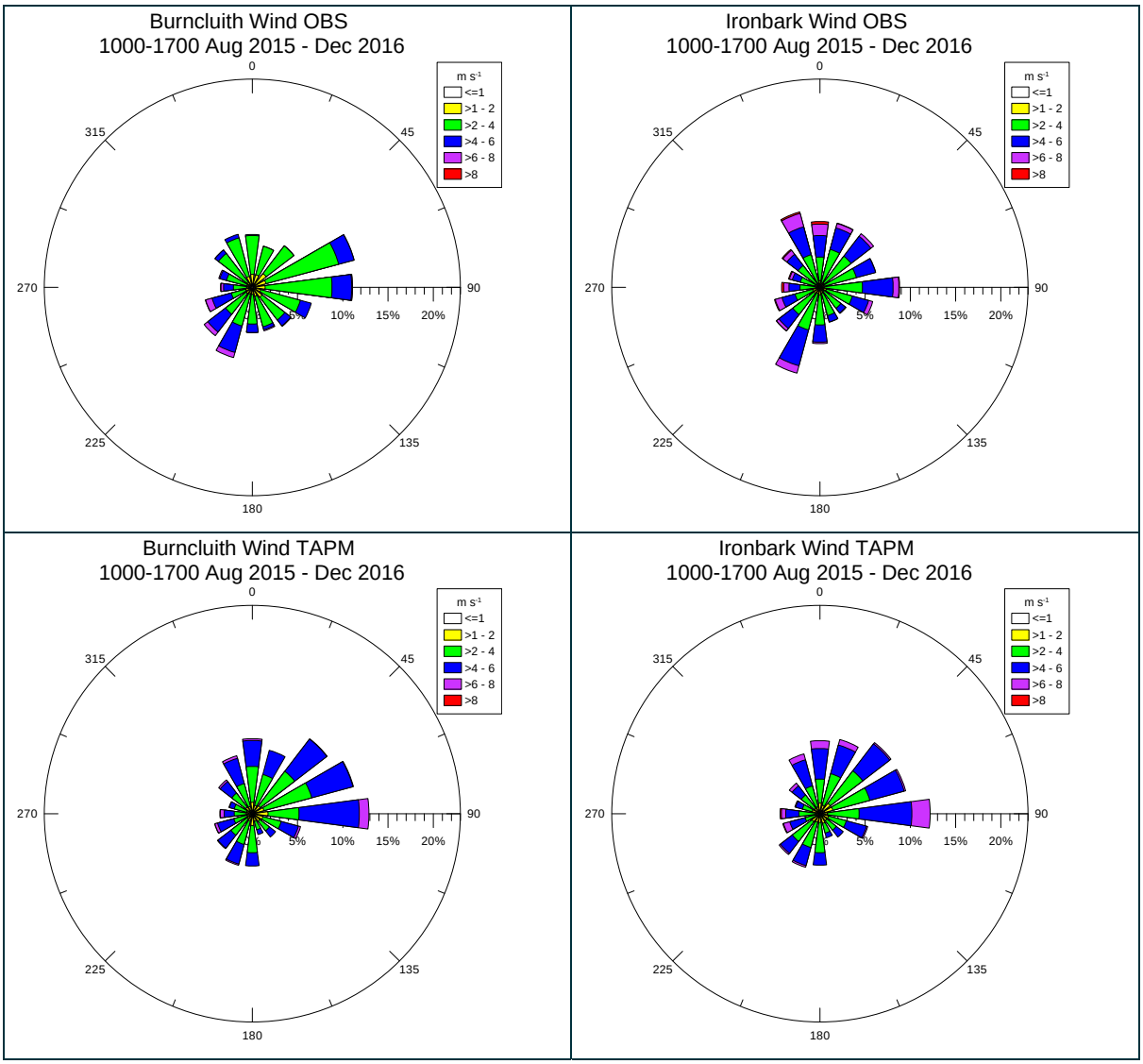

Figure 13. Observed (top) and modelled (bottom) wind roses for the Burncluith and Ironbark monitoring sites for daytime hours only (1000 – 1700 h) (August 2015 to December 2016).

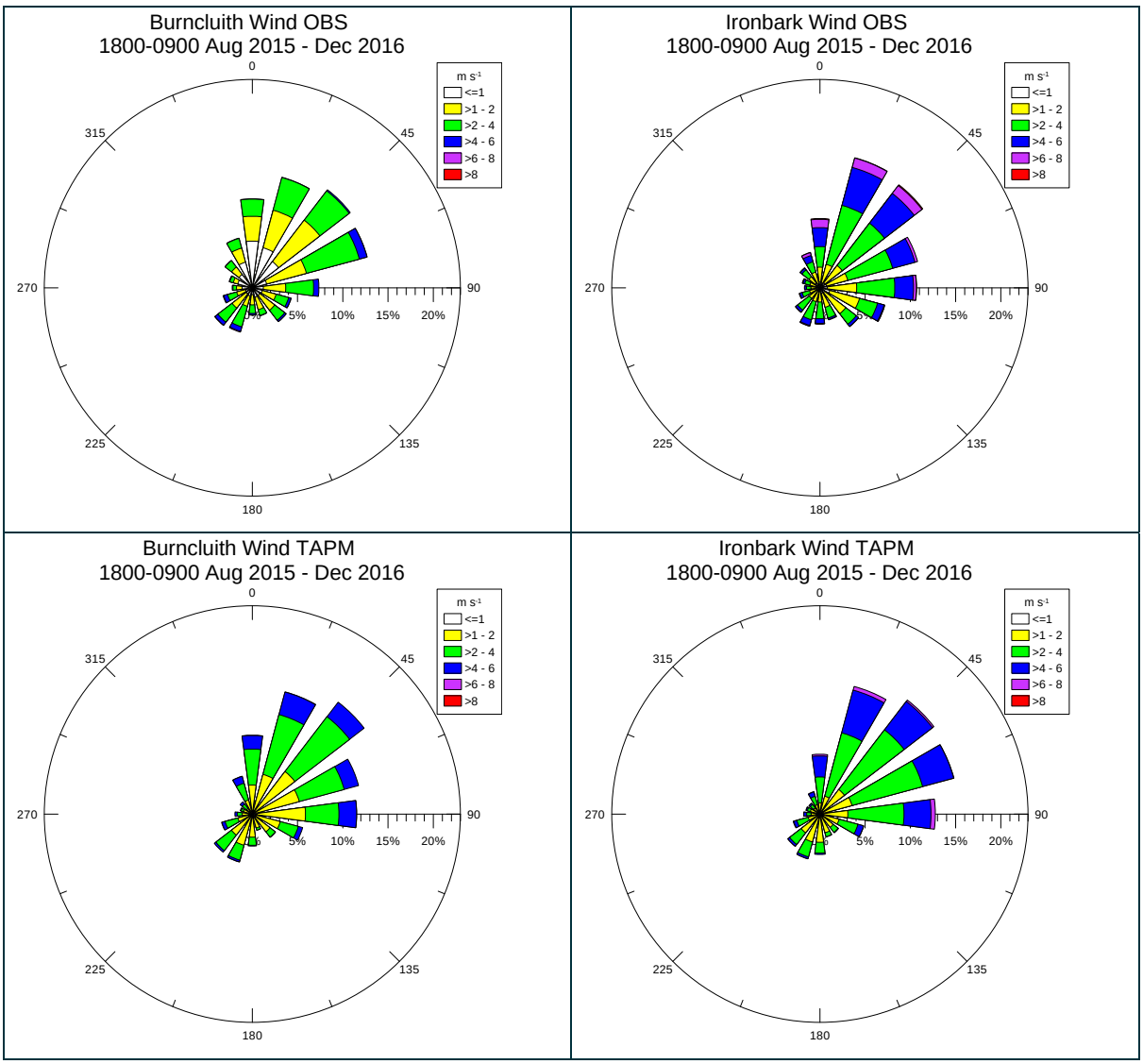

Figure 14. Observed (top) and modelled (bottom) wind roses for the Burncluith and Ironbark monitoring sites for nighttime hours only (1800 – 0900 h) (August 2015 to December 2016).

Wind roses provide a good qualitative means for comparing modelled winds with measurements. The meteorological performance of the model can be examined further in terms of probability (or frequency) distribution functions (pdfs) for wind speed and wind direction. Comparison pdf plots are presented in Figure 15 for all hours, where the pdf values are essentially normalised frequencies (e.g. 0.15 means 15% of the number of data values). A data point is plotted for the mid value of the range, e.g. 2.5 m s^{-1} for the bin 2–3 m s^{-1}. The wind speed pdfs clearly show the low wind speed discrepancy at Burncluith, whereby the observed frequency of low wind speeds is not captured by TAPM well, which mostly occurs at night. However, the Ironbark wind speed is well modelled at all times. The wind direction pdfs show a good overall reproduction by the model of the distribution of wind direction at both sites. There is some overestimation of the frequency of winds from the north-east and underestimation of that from the south-east and north-west at both sites. Overall the model performs better at Ironbark.

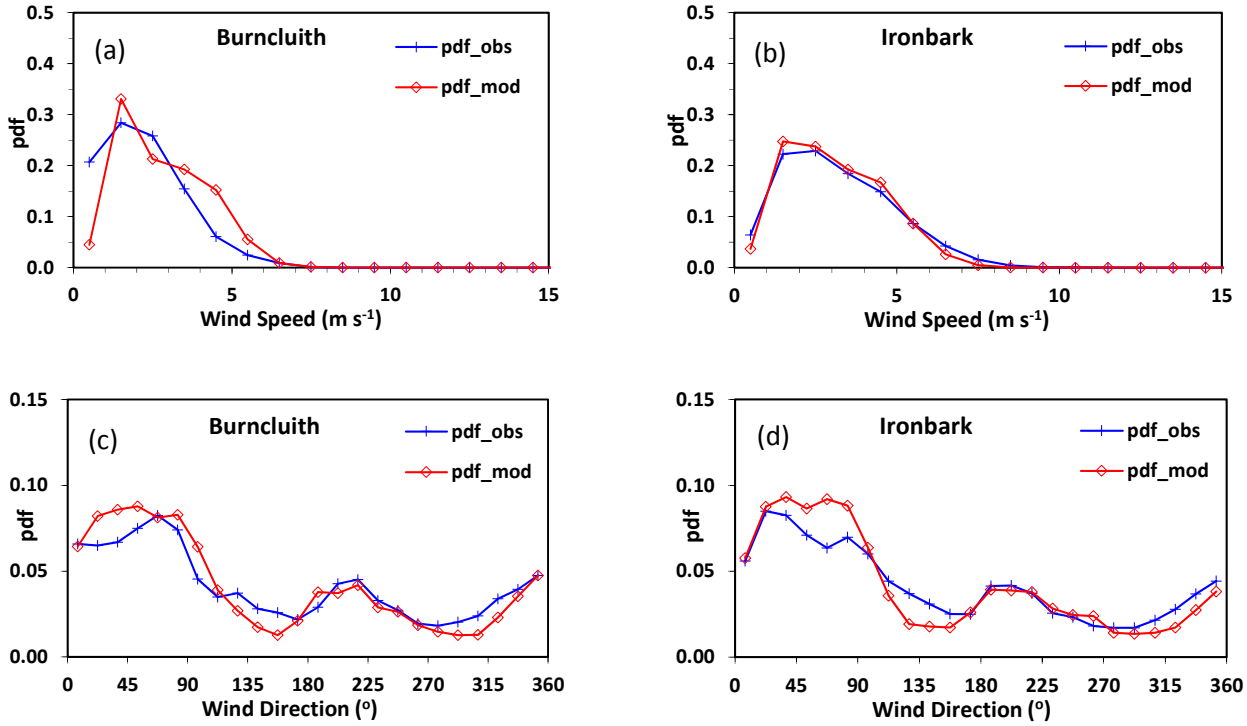

Figure 15. Probability density functions (pdf) of the observed and modelled wind speed and direction at Burncluith and Ironbark. All hours considered.

We also calculated commonly used meteorological model performance statistics for wind speed and its components (*u* and *v*). We refrain from giving all the performance statistics here except to report that the overall correlation coefficient between the observed and modelled wind speed at Ironbark is 0.68 and it is 0.66 at Burncluith. Another parameter, the Index of Agreement (IOA, = 0 no agreement, = 1 perfect agreement), which, unlike the correlation coefficient, is sensitive to differences between the observed and model means as well as to certain changes in proportionality (Willmott, 1981) is 0.82 for Ironbark and 0.76 for Burncluith.

Example time series plots of the modelled and observed winds were given in the interim report (Etheridge et al., 2017), so are not reported here again.

There are a number of reasons for some disagreement between the modelled meteorology and the data. All numerical models such as TAPM are only approximations of the full dynamic and thermodynamic equations that describe the motions of the atmosphere and thus have inherent limitations and uncertainty associated with them.

The performance of an atmospheric model also depends strongly on the accuracy of the boundary conditions. The synoptic weather information from NCEP analyses, which is used as a boundary condition in TAPM, may also be a source of uncertainty and, consequently, of disagreement between the model results and the data for the Surat Basin. The NCEP information is obtained from the output a global meteorological model with assimilation of meteorological observations from a network of stations.

Predictions are also dependent upon the temporal and spatial resolution (both horizontal and vertical) of the model and of the input data (e.g. terrain and land use), presence of complex air flows not described by the model, the quality of meteorological measurements and how well the monitoring stations are sited.

As judged from the IOA values, the overall TAPM performance for winds for the Surat Basin is satisfactory and comparable to those in other studies (e.g. Hurley et al., 2005, 2008; CSIRO, 2004)[1]. Based on this we can conclude that TAPM is suitable for modelling plume transport in the Surat Basin.

4.1.4 Observed and modelled methane concentrations

The modelled hourly concentrations due to the 9 tracer source categories were summed up and compared to the observed CH_4 concentrations in the following figures. Figure 16 presents concentration roses for Burncluith and Ironbark constructed using the observed CH_4 concentrations and wind direction, and the TAPM generated concentrations and wind direction. Only those modelled hours for which there are wind and CH_4 observations are considered and the period shown is from August 2015 to December 2016. For ease of comparison the regional background concentration has been subtracted from the observed CH_4. The CH_4 roses in Figure 16 show that at Ironbark CH_4 is observed at greater concentrations when the wind is from the north-east sector while at Burncluith high CH_4 concentrations are observed under all wind directions, with north-east being the most frequent direction. TAPM concentrations at Ironbark are larger when the wind is from the north-east sector, in agreement with the observations, however the modelled concentrations are not as large as those observed. At Burncluith, the TAPM concentrations are larger when the wind is from the south-west sector and somewhat smaller when the wind is from the north-east sector unlike the observations which have larger values from all directions. The modelled concentrations at Burncluith are also not as large as those observed.

[1] Also see papers in TAPM citation database https://scholar.google.com.au/scholar?oi=bibs&hl=en&cites=13876071272134760358.

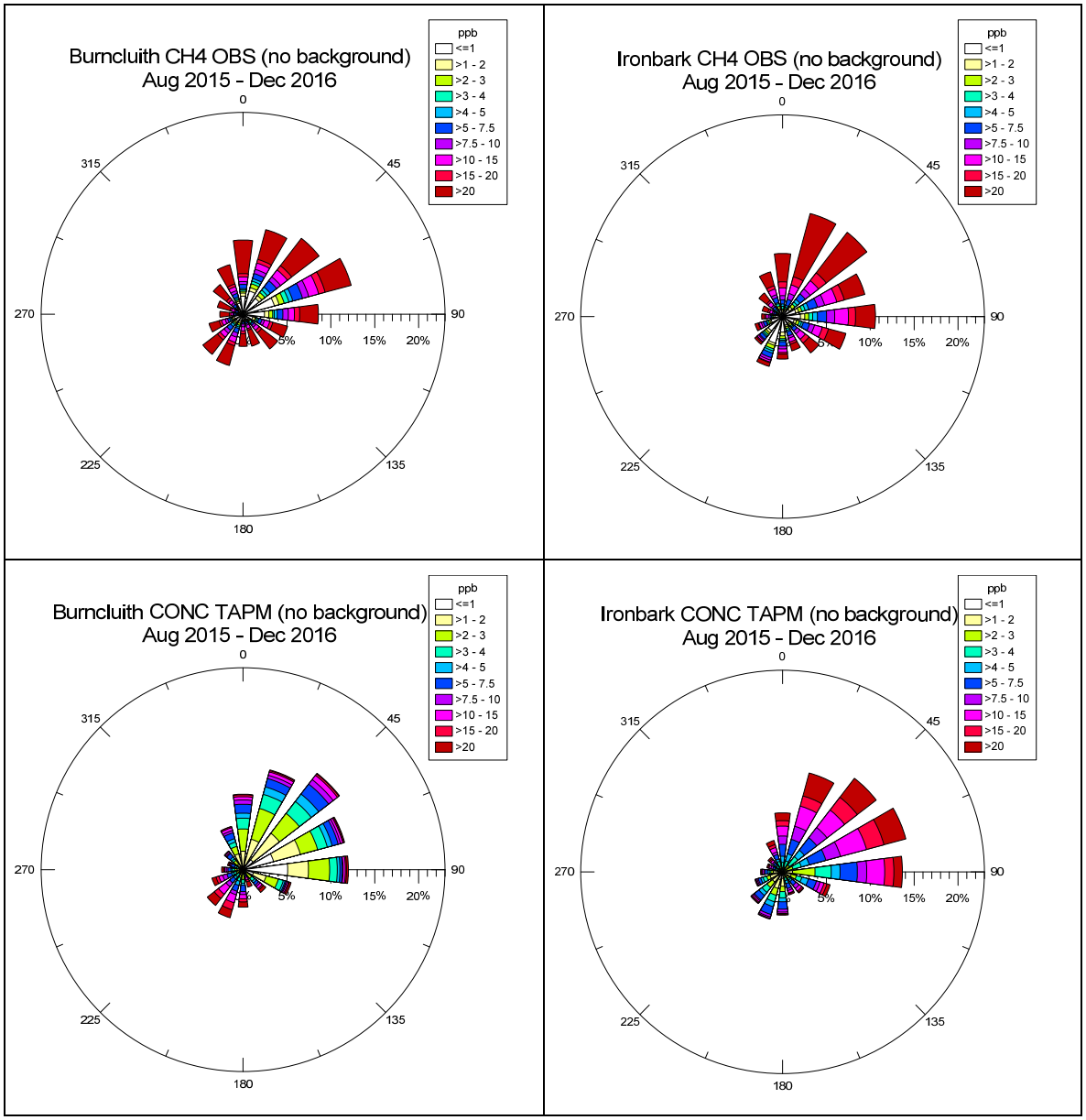

Figure 16. Observed (top) and modelled (bottom) methane concentration roses for the Burncluith and Ironbark monitoring sites (August 2015 to December 2016). Observed concentrations have had the regional background concentration subtracted. All hours considered.

The corresponding concentration roses for daytime and nighttime are shown in Figure 17 and Figure 18, respectively. The nighttime observed concentration roses are similar to those for all times (Figure 16), showing relatively small increases in the frequency of winds from the north-east sector and hence more frequent CH_4 from that sector. The observed CH_4 at Burncluith during the daytime shows much lower CH_4 from the north-east sector than for all times (Figure 16). TAPM captures this but underestimates the concentrations. At Ironbark, the frequency of winds from the north-east sector is reduced and that from the south-west sector is increased compared to all times, with corresponding changes in the observed CH_4 from those directions. The model broadly captures these changes but underestimates the concentrations.

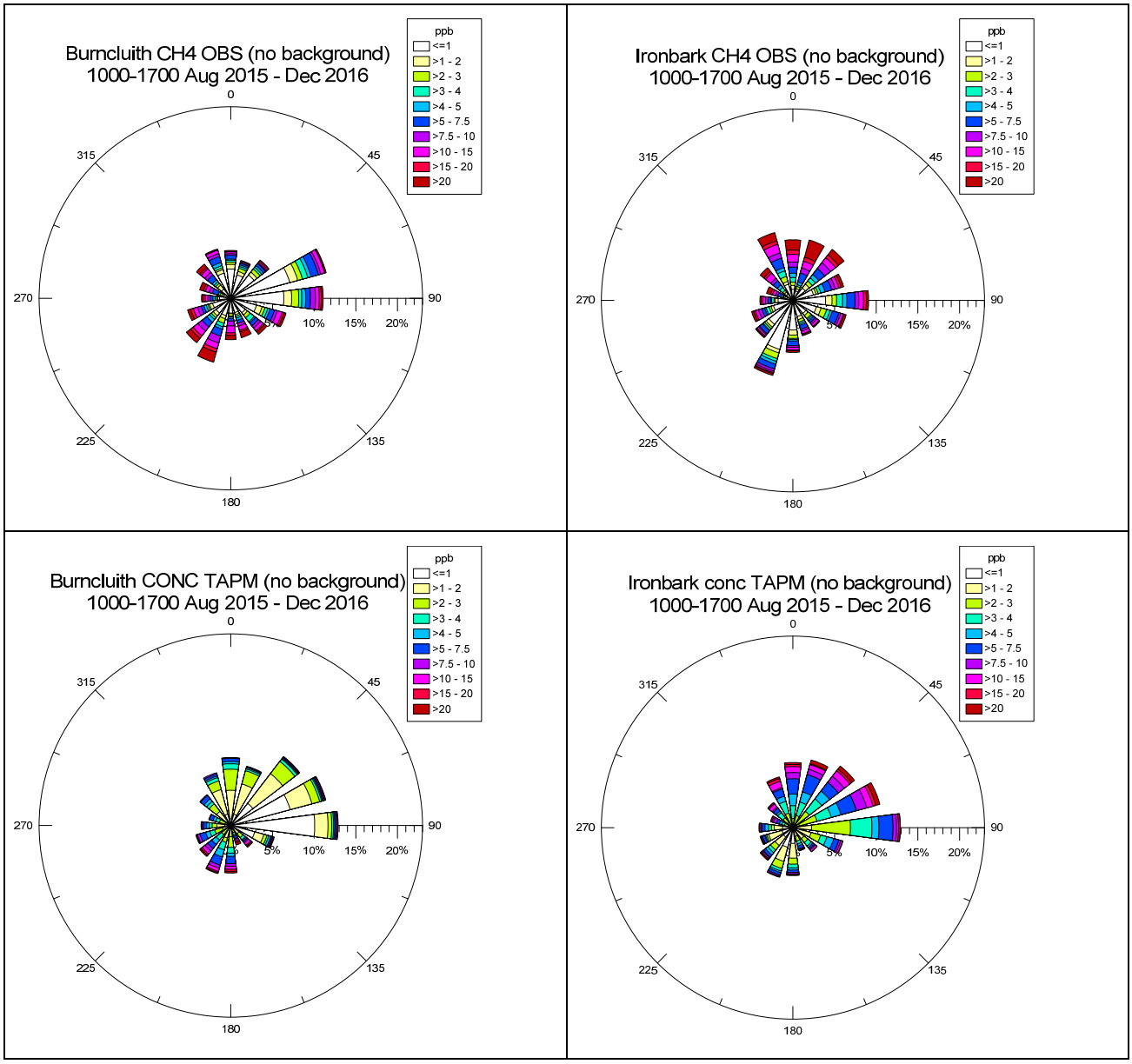

Figure 17. Observed (top) and modelled (bottom) methane concentration roses for the Burncluith and Ironbark monitoring sites for daytime hours only (1000 – 1700 h) (August 2015 to December 2016). Observed concentrations have had the regional background concentration subtracted.

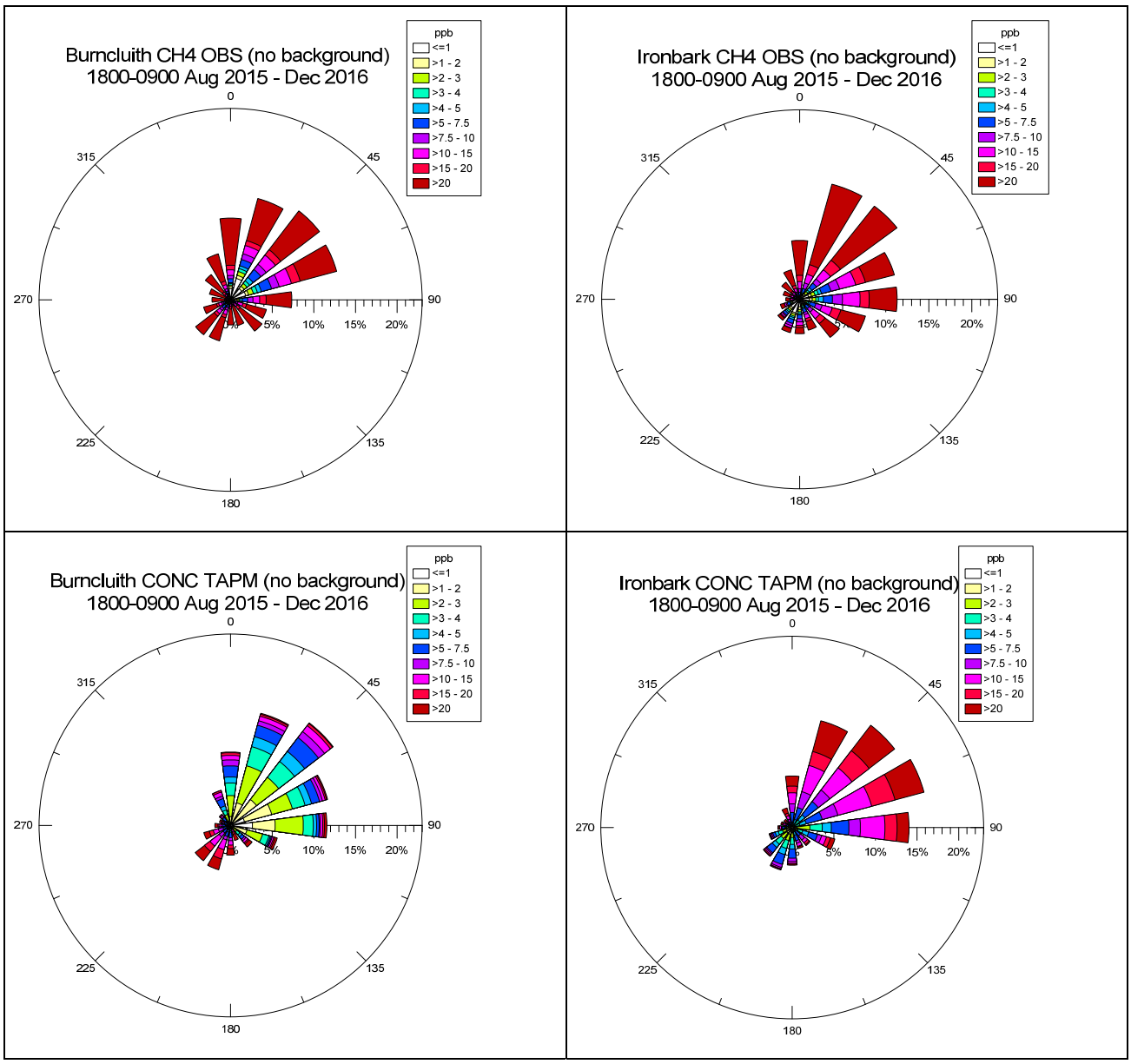

Figure 18. Observed (top) and modelled (bottom) methane concentration roses for the Burncluith and Ironbark monitoring sites for nighttime hours only (1800 – 0900 h) (August 2015 to December 2016). Observed concentrations have had the regional background concentration subtracted.

Generally, most flow and transport models (including TAPM) have significant limitations when it comes to simulating low-wind meteorology and associated transport under nocturnal conditions. Therefore, as discussed earlier, at each site only those hours were considered that lie within the daytime period 1000–1700 h (end hours) regardless of the wind speed, and also those from the rest of the diurnal period (i.e. 1800 – 0900 h) with an observed wind speed greater than 3 m s^{-1} (additional discussion given in Section 5.6). Further, at Burncluith the hour mean data for which the measured CO enhancements (above the background) were greater than 10 ppb were excluded since these occasional periods may have been influenced by biomass burning to the north-east and woodheater emissions from the house next to the monitoring station (these sources are also not included in the bottom-up emission inventory). This CO filter further removed about 22% of the filtered Burncluith data. After the above filtering the number of useable hours was 6432 for

Ironbark and 4149 for Burncluith (so the total sample size for model comparison purposes (and inverse modelling in Section 5) was 10581). These numbers can be compared with the original, nonfiltered, valid number of hours of 10938 for Ironbark and 12660 for Burncluith.

Figure 19 presents scatter plots of the hourly-averaged modelled vs. measured methane concentrations at Ironbark and Burncluith. There is considerable scatter in these plots, which is not uncommon for such evaluation of dispersion models driven by modelled meteorology and utilising hourly concentrations paired in both space and time (e.g. Luhar et al., 2008). But it is clear that at Ironbark the model generally underestimates the measured concentrations. Some of the largest observed concentrations are underestimated by the model. Similarly, on occasions the model predicts high concentrations but they are not present in the measurements. For Burncluith, the comparison looks somewhat better. For Ironbark, the correlation coefficient (r) is 0.57 and it is 0.74 for Burncluith.

Possible reasons for the model-data differences include uncertainty in the bottom-up emissions, their potential time variation and some being intermittent, not all sources being included in the emission inventory, the source gridding under-representing the actual proximity of some sources to the monitors, and the regional and local atmospheric processes (e.g. meteorology) not fully/accurately represented by the model at every scale. Further, regional prognostic models such as TAPM are ensemble-mean and volume-averaged models, in contrast to the observations which are collected at single point locations.

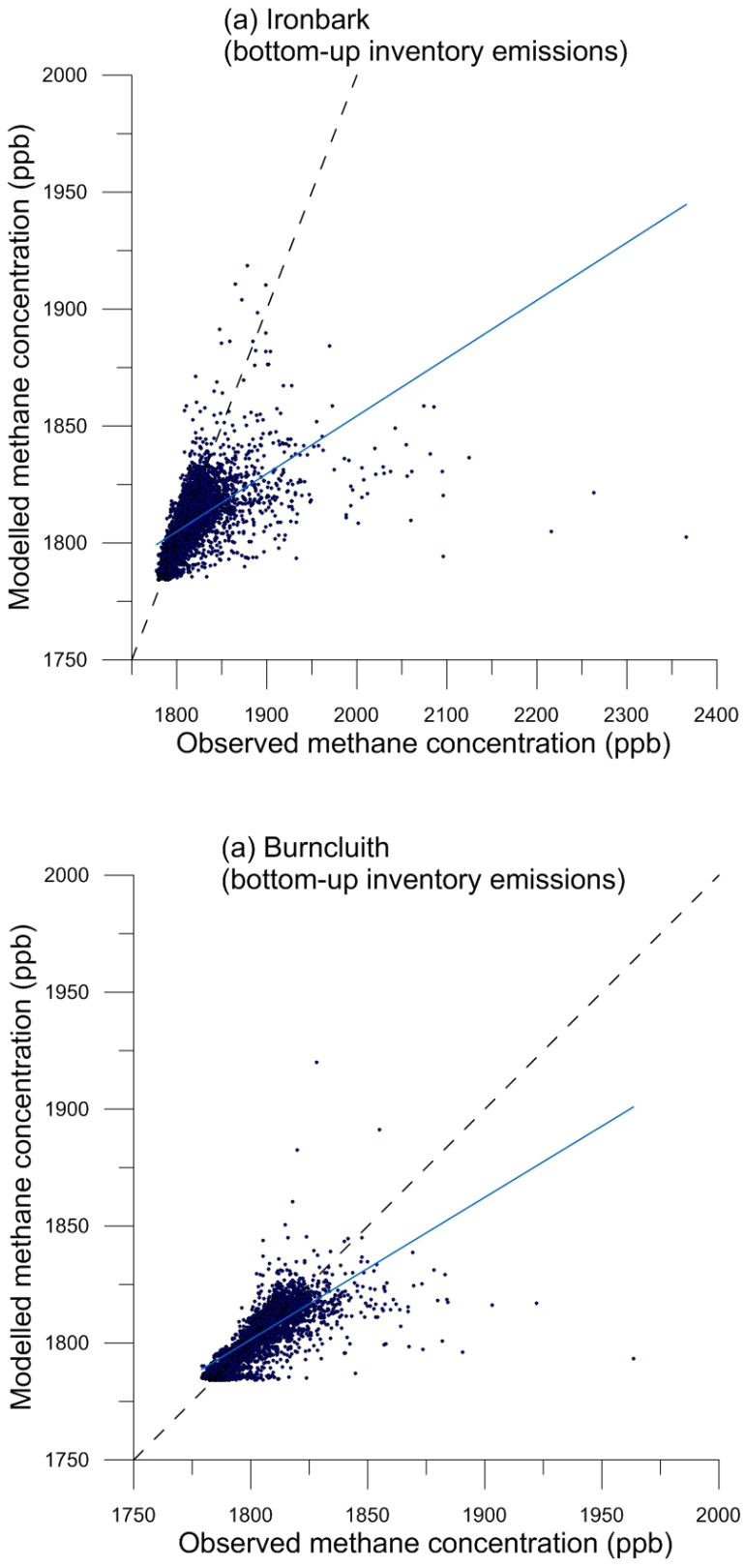

Figure 19. Scatter plot of the hourly-averaged modelled vs. measured methane concentrations at the (a) Ironbark and (b) Burncluith sites in the Surat Basin. The dashed line is the line of 1:1 correlation and the solid line is the linear regression fit.

Comparing hourly mean observed and modelled concentrations paired in both space and time, as done in Figure 19, is a stringent test of a dispersion model, particularly a regional dispersion model that is driven by modelled meteorology. Atmospheric dispersion is stochastic in nature and is influenced by the instantaneous, random motions of the air (i.e. turbulence) which are difficult to predict accurately by a model at hourly intervals. As an example, small differences between the wind direction fields determined by the model and the actual fields can cause the location and magnitude of the predicted concentration at a point to be quite different from the observed values at the same point at the same time. Under these circumstances it is more meaningful to compare the observed and predicted concentration distributions formed using values that are unpaired in time and/or space. In our case, with two monitoring stations sampling different source contributions, concentrations unpaired in time at each monitoring station is appropriate (those unpaired in space will be more relevant when a single source is sampled for a short period by a large number of monitors located almost the same distance around it), which thus disregards errors with timing that show up with the paired data.

One method to compare the unpaired observed and modelled concentrations is the so-called quantile-quantile plot (also called a q-q plot), which is used commonly in air quality model evaluation studies (e.g. Paumier et al., 1992; Venkatram et al., 2001; Luhar and Hurley, 2003). This graphical technique is an effective method for determining whether two datasets with equal sample size (i.e. observed and predicted concentrations) come from populations with a common distribution. Normally, a q-q plot is a scatter plot of the quantiles of the first data set against the quantiles of the second data set. A quantile here means the fraction (or percent) of points below the given value. That is, the 0.9 (or 90%) quantile is the point at which 90% of the data fall below and 10% fall above that value. However, it is common to directly plot the one data set against the other. That is, the actual quantile level is not plotted. For a given point on the q-q plot, we know that the quantile level is the same for both points, but not what that quantile level actually is (see http://www.itl.nist.gov/div898/handbook/eda/section3/qqplot.htm). Hence, in an air pollution model evaluation application, the q-q plot is essentially a plot of the sorted observed concentrations against the sorted predicted concentrations. If the two sets come from a population with the same distribution, then all of the points fall on the 1:1 (or x = y) line. The greater the departure from this reference line, the greater the evidence for the conclusion that the two data sets have come from populations with different distributions. Thus a good model will have a slope in this plot similar to that of the 1:1 line. With the use of a q-q plot, several distributional aspects can be simultaneously tested. For example, shifts in location, shifts in scale, changes in symmetry, and the presence of outliers can all be detected from this plot.

Figure 20a presents a q-q plot for Ironbark in which sorted modelled concentrations are plotted against sorted observed values. It shows that the model simulates the observed concentration distribution well for observed concentrations less than 1820 ppb with the variation almost following the line of perfect (1:1) agreement. But beyond this value, the model underestimates the observed concentration distribution. The total number of data points below 1820 ppb is approximately 75% of the sample at Ironbark, so it can be said that overall the model is underestimating the top concentrations in 25% of the cases.

The q-q plot in Figure 20b for Burncluith is qualitatively similar to that for Ironbark, but with a lower amount of model underestimation of higher-end observed concentrations. Again, as at

Ironbark, the model described the observed concentration distribution well for observed concentrations less than 1820 ppb, which amounts to 90% of the total hours at this station.

The above comparison suggests that the model is mostly getting the distribution of the observed methane concentration right (which in a scatter plot sense means that the points in the plot are almost equally distributed around the line of the perfect fit), but a small number of concentrations which correspond to higher-end values are underestimated by the model. The likely reasons for this underestimation are thought to include underestimation of emissions from sources close to the monitoring sites which are generally responsible for the higher-end concentration levels than farther sources and/or presence of time-varying, intermittent or additional sources that are not accounted for in the bottom-up emission inventory. Additionally, any bias in the predicted wind flow compared to the actual flow patterns, especially between nearby, high emissions sources and the monitoring sites, could be a reason.

In section 5.6, we apply inverse modelling to estimate emissions based on the methane concentration measurements from the two monitoring stations. We then validate the estimated emissions by using them in a forward model configuration and comparing the resulting concentrations to the concentration data.

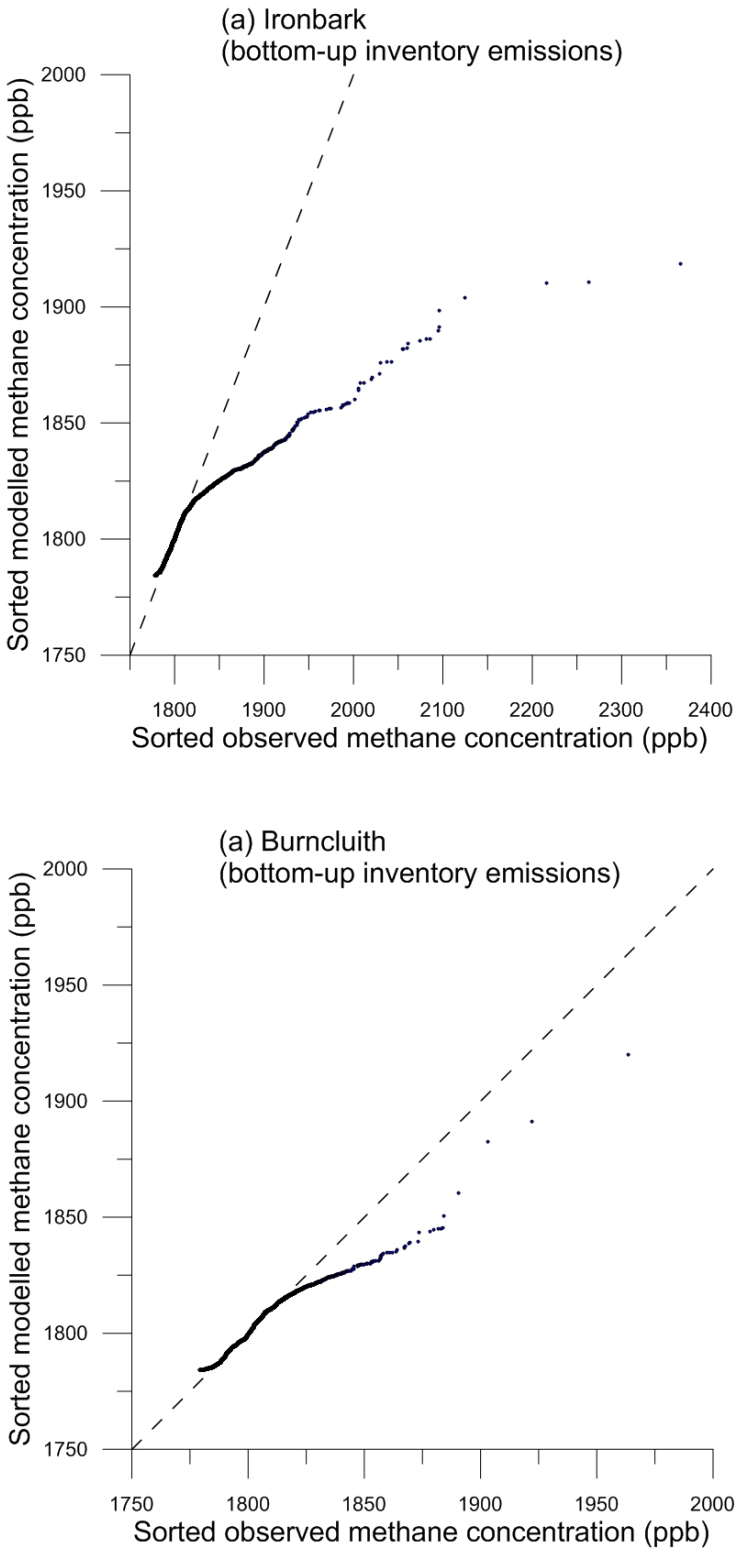

Figure 20. Quantile-quantile (q-q) plot of the sorted hourly-averaged modelled vs. sorted measured methane concentrations at the (a) Ironbark and (b) Burncluith sites in the Surat Basin. The dashed line is the line of perfect (1:1) agreement. Filtered data used.

4.1.5 Modelled contributions by various source categories

TAPM was run with nine tracers corresponding to the various combinations of source categories, therefore concentration output at Burncluith and Ironbark can be separated into different categories dependent on the source of the emissions. Figure 21 presents the overall relative (%) contribution by the various source categories to the total modelled methane concentration averaged over the whole simulation period (without the background concentration) at the Ironbark and Burncluith sites. According to the modelling, the top four contributors to the Ironbark methane are Grazing cattle (45%), Feedlot + Poultry + Piggeries (25%), CSG Processing (19%), and Mining (5.5%). These for Burncluith are Grazing cattle (69%), Feedlot + Poultry + Piggeries (17%), CSG Processing (6.4%), and Mining (4.1%).

Figure 22 is the same as Figure 21 except that it presents contributions by the various source categories to the highest 5% of the modelled methane concentrations. In contrast to Figure 21a, it is apparent from Figure 22a that the largest contributor to these highest concentrations at Ironbark is CSG Processing (35%), followed by Feedlots + Poultry + Piggeries (27%) and Grazing cattle (25%). At Burncluith (Figure 22b), the top three contributors to the highest concentrations are Grazing cattle (28%), Feedlots + Poultry + Piggeries (25%) and CSG Processing (22%). CSG Processing contributes more to the top 5% modelled concentrations than to the simulation average concentration because there are localised sources of this source component between the two monitoring stations that cause spikes in concentration when the winds are favourable. The Grazing cattle, and Feedlots + Poultry + Piggeries sources dominate the average modelled concentration as signals from these sources reach the monitoring stations under most wind conditions as they are almost uniformly distributed throughout the domain.

Additional results on the modelled contributions by the various source categories in terms of concentration roses together with diurnal difference are given in Appendix A.

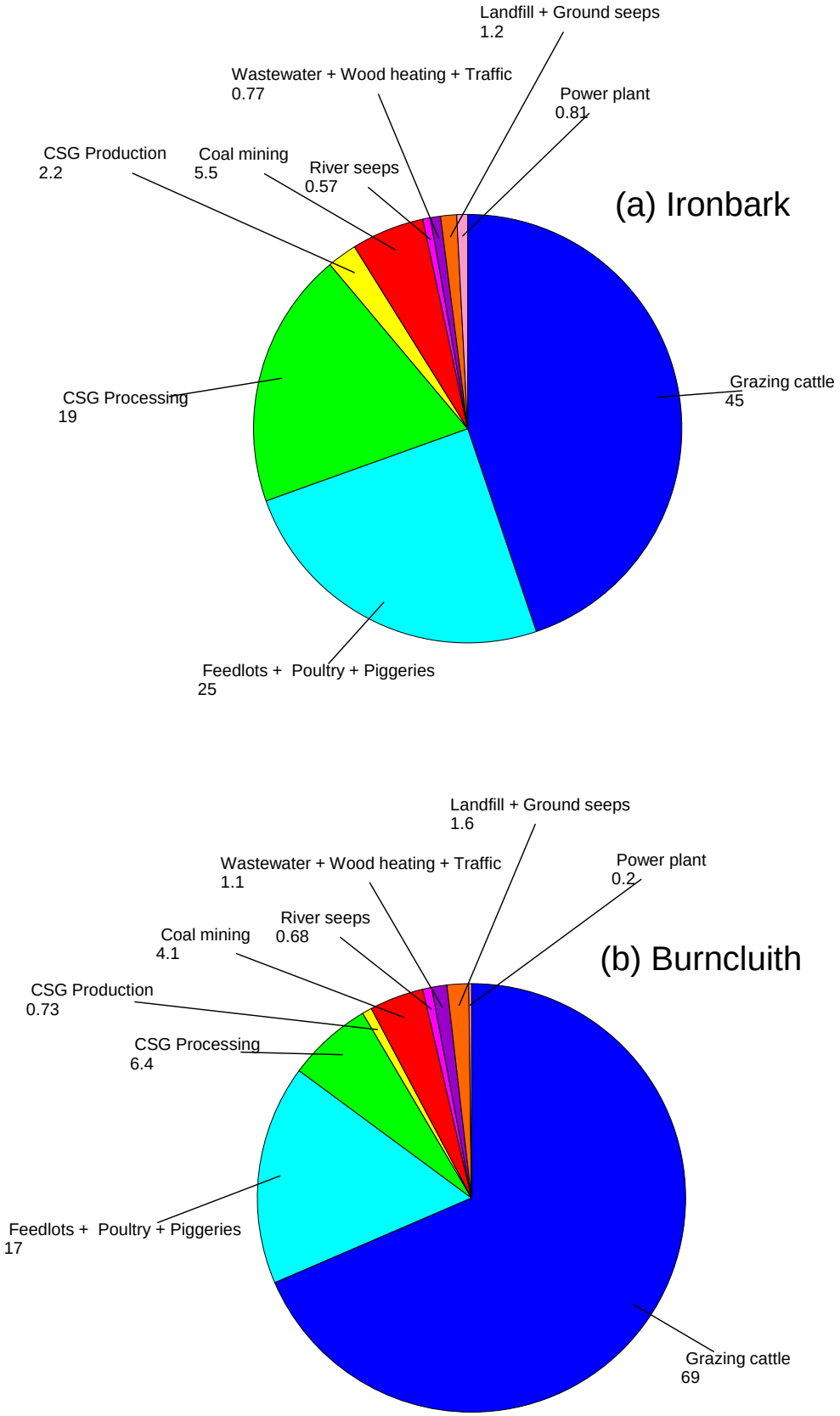

Figure 21. Relative (%) contribution by the various source categories to the total averaged modelled concentration at the (a) Ironbark and (b) Burncluith sites in the Surat Basin.

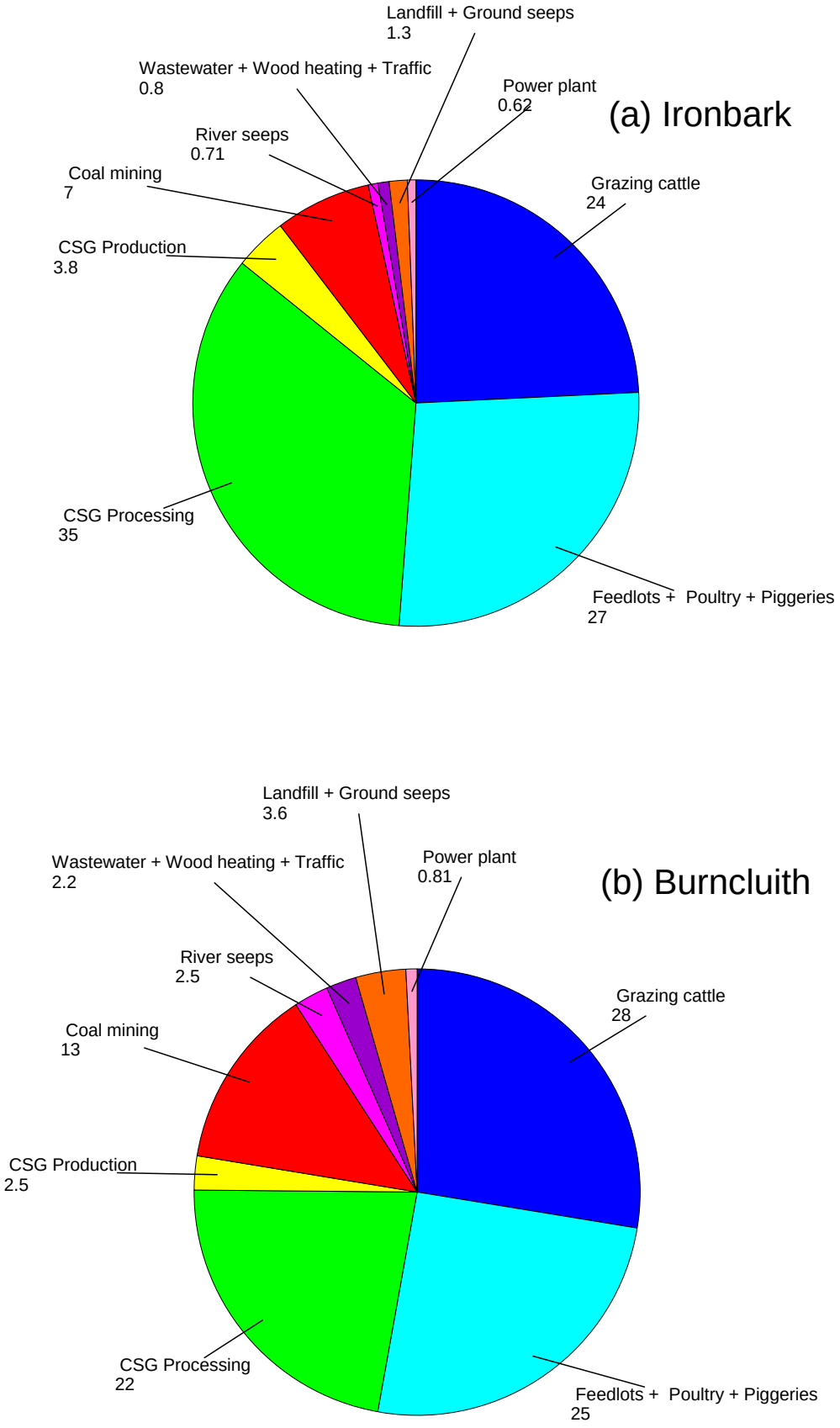

Figure 22. Relative (%) contribution by the various source categories to the top 5% of the modelled hourly concentrations at the (a) Ironbark and (b) Burncluith sites in the Surat Basin.

5 Atmospheric modelling for source estimation

In this section, we formulate and apply an inverse modelling approach to determine methane emissions from the Surat Basin.

5.1 Modelling approaches

Here we formulate and apply the regional transport modelling for source estimation using an inverse approach. Some of the introductory inverse modelling material presented below was given in the interim report (Etheridge et al., 2017), but is given here again for completeness and for making cross-referencing easier with regards to the use of various modelling terms.

Atmospheric dispersion modelling calculates the dilution factor as emissions are transported and dispersed in the atmosphere, and provides a quantitative linkage between the emission from the source and its detection as concentration at a monitoring station. For a unit source emission rate, this relationship is often termed as the source-receptor relationship or the coupling coefficient, and depends on receptor locations and meteorology (which governs transport and dispersion).

Using modelling, information about emission sources such as their release rates can, in principle, be inferred from measurements of their atmospheric concentrations coupled with the source-receptor relationship and available prior information about source characteristics. In practice, however, source estimation is a difficult problem because it usually involves many degrees of freedom which are generally not well constrained due to the limited availability of concentration observations. For example, the number of sources or source parameters to be estimated can be larger than the number of monitoring stations, a case which without having a sufficiently large amount of concentration data can lead to an unstable, non-unique or singular inverse solutions.

There are two broad modelling approaches to determining the source-receptor relationship required in inverse modelling (Rao, 2007): forward dispersion modelling (which was discussed earlier in Section 4 for modelling methane concentrations) and backward dispersion modelling. In the first approach, concentration fields due to sources are predicted for a unit emission rate given the source locations and meteorology of the area. For a single tracer source, a simple back calculation for the emission rate can be performed using the measured concentrations and the modelled dilution factor. However, if there is a large number of sources then there could be a large number of possible solutions unless there is sufficient amount of information available to constrain the solution(s). At the regional scale, plume transport and dispersion from a source are non-translatable, meaning that at a given time the plume distribution calculated for a source cannot be taken to represent that for another source just by shifting the plume distribution to the second source. This is because at this scale the terrain is inhomogeneous and the flow and turbulence that govern transport and dispersion varies spatially. Thus, the source-receptor relationship for each source and for each hour needs to be pre-determined separately by using forward modelling and then used in an optimisation algorithm that minimises the difference between the measured concentrations and the modelled concentrations for a particular solution of source emission rate(s). The problem becomes even more difficult and computationally

inefficient if, along with the source emission rates, the source locations are also not known, in which case every point in the spatial domain needs to be considered as a potential source and the corresponding source-receptor relationship determined, with the optimisation done over all these sources.

The second approach involves tracking plumes backwards in time from each monitor location. The value of the modelled backward concentration at a particular point is equivalent to the relative contribution made by a potential source at that point to the measured concentration at the monitor. Thus, a single backward source-receptor relationship field can be used to obtain the relative contributions made by each location point within the domain (whereas in the forward modelling each location point needs to be treated as a separate source and its plume transport determined). This is then combined with concentration measurements in an optimisation or inference method to yield source parameter information. If the number of potential sources to be considered is greater than the number of monitors, then the backward modelling is more efficient. Typically, in a source optimization scheme, e.g. that based on the Bayesian approach (described below), the number of source hypotheses that needs to be considered is larger than the number of available concentration measurement stations, and therefore the backward approach provides a substantially more efficient procedure. Another advantage of the backward approach is that it can be pre-run without regard to the details of the eventual source geometry. Forward modelling, on the other hand, is more deterministic and easier to formulate and comprehend. Thus, the difference between the two approaches is essentially computational, if they are working correctly both calculate the same matrix.

Because we treat methane as a passive tracer at regional scale, both forward and backward problems are linear in emission rate, in that concentration distribution calculated for a particular emission rate can be linearly scaled for a different emission rate without re-running the model.

Based on a previous modelling study (Day et al., 2017), Figure 23 illustrates the concept of backward and forward plumes involving a monitoring station A. The backward concentration distribution in Figure 23a means that the value of concentration at any point within the domain is the concentration at the monitoring station A caused by a source at that point for a fixed emission. In other words, the backward concentration value at a particular point is a measure of the probability a source located at that point contributes to the concentration at A. Thus, a single backward plume dispersion provides the relative contribution due to any potential source in the domain. So, if there are 7 sources (S1–S7), the largest (probability of) contribution to A is from S3 followed by S2 and S5, with the other sources not contributing. This is qualitatively confirmed by the forward concentration fields due to the seven sources in Figure 23b, in which there is a direct plume impact at A of S3, with diluted plumes from S2 and S5 also passing through A and the plumes from the other sources missing the receptor. So, the advantage of the backward approach is clear here in that just one dispersion simulation provides information on contribution to A from any potential source within the domain whereas the in forward approach dispersion from all potential sources needs to be simulated individually.

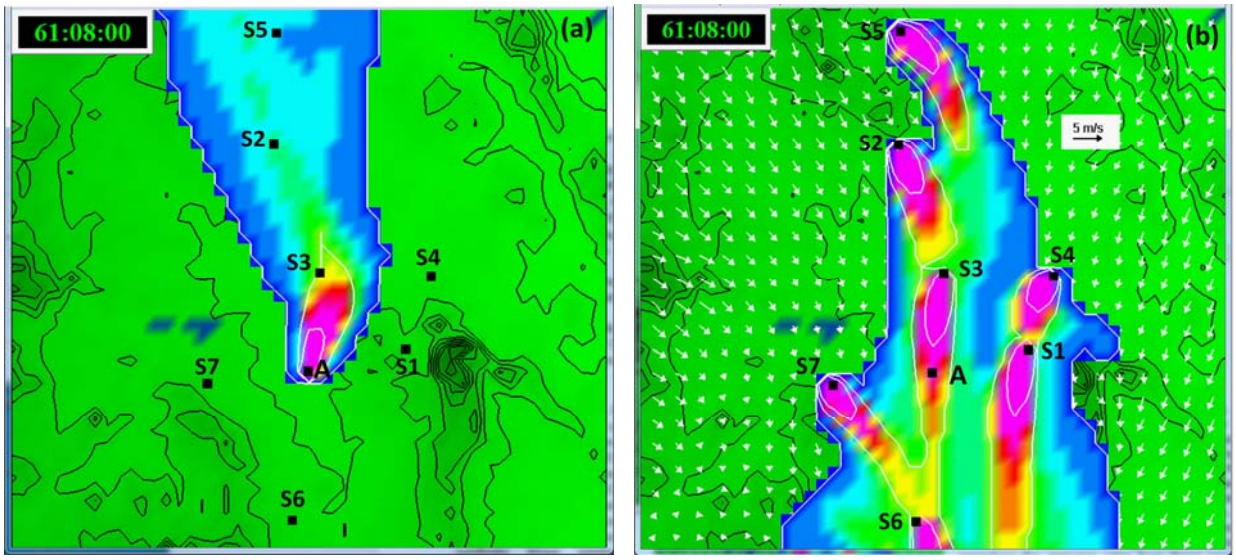

Figure 23. (a) Modelled backward hourly-averaged surface concentration field, and (b) forward modelled surface concentration field due to the seven sources S1–S7 at the same time. The domain size is 250 km x 250 km. The black contours represent the topography. The plume contours (white) and colours in (a) and (b) represent the same concentration values (from Day et al., 2017).

Although the above dispersion modelling approaches are available for source quantification, the success of their application depends on a number of factors, such as the number and type of source parameters to be estimated, the quantity and quality of concentration measurements available and their uncertainty, the skill of the dispersion model used for calculating the source-receptor relationship and the associated uncertainty, the background concentration, and the quantity and quality of prior information available on source characteristics.

For the current problem, we consider backward dispersion modelling to be the best approach.

5.2 Backward plume dispersion modelling

When monitoring stations and the sources contributing to concentration signals at these stations are spatially far apart, the problem takes the dimension of regional scale (i.e. ~ 100–1000 km). For local scale (~ 5 km) applications, the meteorology given at a single location can be assumed to be spatially uniform so that it represents the whole local domain (e.g., Luhar et al., 2014). Also, the dispersion process can be assumed to be steady state since the time it takes for a plume to reach a monitor from a source is much shorter than the concentration averaging time and also much shorter than the time scale of variability in the meteorology governing dispersion. In contrast, modelling emissions at regional scale is complex because surface conditions are usually inhomogeneous and the meteorology governing transport (and hence the source-receptor relationship) is spatially variable. Thus, the dispersion process is also spatially variable, and can be unsteady as plume travel times can be considerable compared to the concentration averaging times. The source-receptor relationship for each source location possibility is spatially unique (and thus non-translatable), and the source signals may not be strong enough to be detected at a distant monitor. Additionally, monitoring on regional scales represents integrated emissions from all source types contributing to measured methane concentration signals within the study area.

Modelling sources at the regional scale requires an appropriate plume transport model coupled with a meteorological modelling capability and an optimisation method. A backward transport modelling method that uses TAPM in backward time mode was used to provide the source-receptor relation required in the Bayesian inference inversion used for optimisation (described below)which estimates emission rates of multiple sources given their locations and atmospheric concentrations. The current setup is summarised as follows.

The TAPM forward model (described earlier) was first run for meteorology only (without dispersion) for the full period of interest (1 July 2015–31 December 2016). The predicted horizontal wind components were reversed (i.e. the signs were changed). Subsequently, TAPM's transport and dispersion module was run backward in time for the full period by using the previously modelled reversed wind components. The (inverted) vertical velocity was calculated from the continuity equation by using the reversed horizontal wind components. TAPM's Eulerian dispersion module uses (positive) diffusivities without any vertical counter-gradient flux correction, so was not changed for the backward calculation for the present passive tracer case. The receptors (i.e. the Ironbark and Burncluith sites) were considered as sources (with unit emissions) for backward calculations and the resulting dispersion field was used as the source-receptor relationship, which is required for source estimation in the Bayesian inference method described below.

5.3 Bayesian inference for source estimation

The backward plume provides a means to map the source potentials of a geographical area, but it does not apportion the actual contribution of that source area to the concentrations measured at the receptors. An objective/optimisation methodology is required to do that. We use the Bayesian probabilistic or inference approach for that purpose. Given the source-receptor relationship from the backward transport model, model and observational uncertainties, and prior constraints on the source parameters, this approach updates our knowledge of source parameters as new concentration measurements become available and are considered. This overall methodology is referred to as inverse modelling. In contrast to approaches that find a single optimal solution, the Bayesian approach explores all domains of plausible or permissible values of source parameters and assigns them probabilities. Thus, it accounts for the fact that although many different source configurations may be plausible and consistent with the observed concentration measurements, some will be more probable than others. Applications of the Bayesian approach have been reported for a range of source estimation problems (e.g., Yee and Flesch, 2010; Humphries et al., 2012; Luhar et al., 2014; Feitz et al., 2018) as well as network design studies (e.g. Ziehn et al., 2014). Depending on the type of concentration measurements and the amount of prior information available, the Bayesian approach can in principle be used to determine both the emission rates and locations of multiple sources, as well as other source characteristics.

Bayes' theorem or rule in the present context can be written as (Jaynes, 2003):

$$p(\mathbf{q}\,|\,\mathbf{c}) = \frac{p(\mathbf{c}\,|\,\mathbf{q}).\,p(\mathbf{q})}{p(\mathbf{c})}, \qquad (1)$$

where $p(\mathbf{q})$ is the *prior*, which is the probability density function (PDF) of the source parameter vector **q** that encapsulates our knowledge of the source parameters before the receipt of the concentration measurements **c**; the *likelihood* function $p(\mathbf{c}|\mathbf{q})$ is the probability of observing the concentration data **c** for a particular **q** and is derived using a source-receptor relationship; $p(\mathbf{q}|\mathbf{c})$ is the *posterior*, which corresponds to the update of our prior knowledge of **q** through the modulation of $p(\mathbf{q})$ by the likelihood function which brings in the new information contained in the acquired concentration data **c**; and $p(\mathbf{c})$ is referred to as the *evidence* and is essentially a normalisation constant (Yee and Flesch, 2010). The likelihood function is derived using a source-receptor relationship obtained from a backward dispersion model, and its accuracy depends on how good the model is in explaining the concentration measurements. It mediates the transformation from the prior distribution to the posterior distribution through incorporating the information obtained in the acquired concentration data **c**. The Bayesian formulation considers measurement and model uncertainties, which are assumed here to be normally distributed. One advantage of the Bayesian approach is that any information known a priori about the source field can be considered through $p(\mathbf{q})$ to reduce the degree of under-determinacy of the problem and help obtain a physically meaningful solution.

The prior PDF $p(\mathbf{q})$ needs to be specified. If the a priori information about the model parameters is Gaussian, then the posterior can be generally written in the matrix form as (Tarantola, 2005)

$$p(\mathbf{q}|\mathbf{c}) = \exp(-J)/Z_1 \tag{2}$$

where

$$J = \frac{1}{2}(\mathbf{c}_\mathrm{m}(\mathbf{q}) - \mathbf{c})^T \mathbf{C}_D^{-1}(\mathbf{c}_\mathrm{m}(\mathbf{q}) - \mathbf{c}) + \frac{1}{2}(\mathbf{q} - \mathbf{q}_\mathrm{prior})^T \mathbf{C}_M^{-1}(\mathbf{q} - \mathbf{q}_\mathrm{prior}), \tag{3}$$

$\mathbf{C}_D$ is the covariance matrix representing the addition of measurement and model uncertainties, $\mathbf{C}_M$ is the covariance matrix representing the uncertainty in the prior, $\mathbf{c}_m$ is the modelled concentration calculated using the source-receptor relationship for a given hypothesis of $\mathbf{q}$, the vector $\mathbf{q}_\mathrm{prior}$ is the prior source information, and Z_1 is a constant. The quantity J can be viewed as a cost function whose minimisation corresponds to the peak in the posterior, and hence to the solution.

When there is no prior information available about the source parameters the prior PDF can be assigned a uniform distribution within given bounds of parameter values. In that case the cost function is simply:

$$J = \frac{1}{2}(\mathbf{c}_\mathrm{m}(\mathbf{q}) - \mathbf{c})^T \mathbf{C}_D^{-1}(\mathbf{c}_\mathrm{m}(\mathbf{q}) - \mathbf{c}). \tag{4}$$

The posterior distribution $p(\mathbf{q}|\mathbf{c})$ provides probabilities of all the hypotheses about the values of the source parameters, and is integrated to obtain various mean source statistics of interest.

The TAPM source-receptor relationship obtained from the backward run is used as the likelihood function in the Bayesian probabilistic approach. To make the Bayesian computations tractable, a Markov Chain Monte Carlo (MCMC) method involving the Metropolis-Hastings algorithm is used to

sample the posterior PDF of the source parameters (see Luhar et al., 2014). The methodology can determine emissions and their uncertainties from multiple sources depending on the amount of information available through concentration measurements. In the present configuration, source locations at evenly spaced grid points are specified as prior knowledge.

5.4 Modelled backward plume: source-receptor relationship

The backward TAPM setup used involved the same two nested spatial domains as in the forward modelling: an inner domain of size 370 km × 370 with a horizontal grid resolution of 5 km × 5 km, and an outer domain of size 1110 km × 1110 with a horizontal grid resolution of 15 km × 15 km (Figure 8).

Tracers were released from the Ironbark and Burncluith monitoring sites to generate the backward plumes with a nominal tracer emission rate q (g s^{-1}). A backward plume provides the hourly source-receptor relationship required in the Bayesian analysis (which can then be scaled for any emission rate within the prior specification for source hypothesis). The backward concentration fields for the inner domain were used in the inverse modelling.

Figure 24a shows the scaled modelled backward field of ground-level concentration (C/q, s m^{-3}) averaged over the simulation period 1 July 2015 – 31 December 2016, representing the source-receptor relationship for Ironbark. As indicated earlier with reference to Figure 23a, essentially what Figure 24a implies is that the concentration value at any point within the domain is the (forward) concentration at Ironbark if there were a source at that point emitting at q = 1 g s^{-1}. The backward concentration value at a particular point can also be interpreted, after a suitable normalisation, as the probability a unit source located at that point contributes to the concentration at Ironbark. It is mainly a result of the prevailing meteorology of the area and the distance between the source and the receptor. This example of a backward plume simulation demonstrates the considerable advantage of the backward modelling approach over the forward approach, in that a large number of source hypotheses (which may include multiple sources with varying emission rates) can be explored using a single backward model run for a given monitoring site.

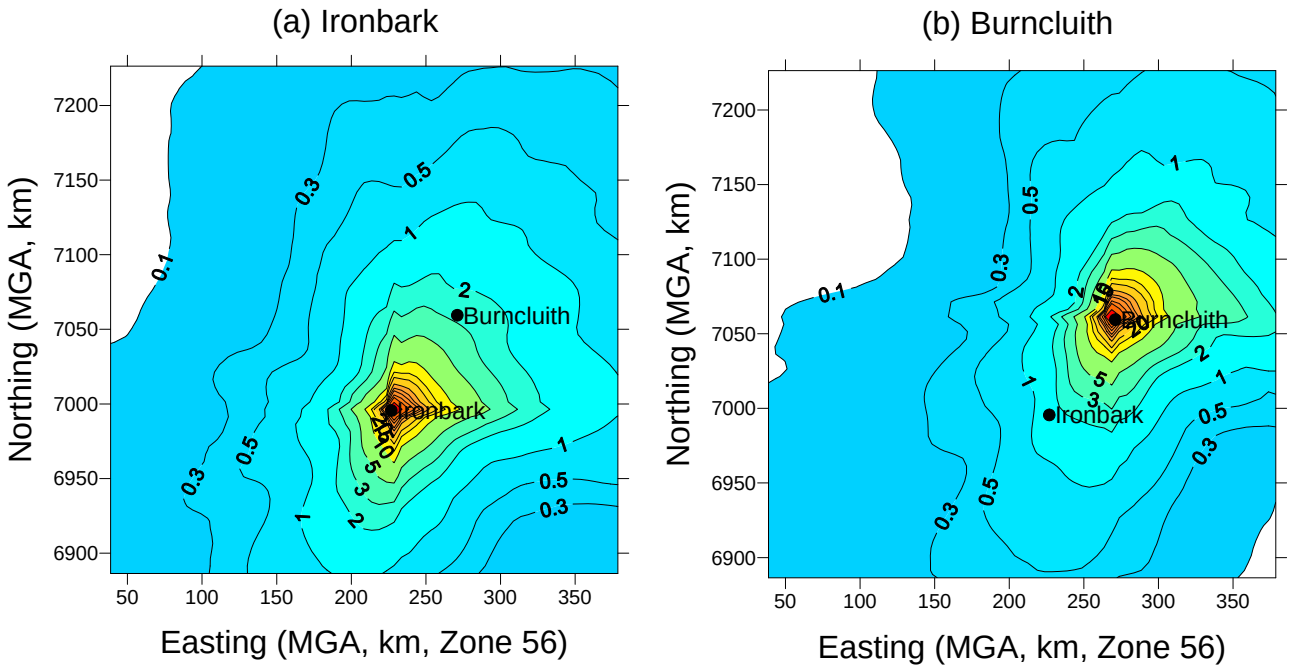

Figure 24. Scaled modelled backward field of ground-level concentration (C/q, s m^{-3}) averaged over the simulation period 1 July 2015 – 31 December 2016, representing the source-receptor relationship for (a) Ironbark and (b) Burncluith. The contour values are to be multiplied by 10^{-9}.

In Figure 24a, the low contour values near the north-west, south-west and south-east corners of the domain suggest that the Ironbark monitoring site will generally have low probability of sampling potential sources located in these areas (i.e. these sources will be under sampled). The main reason for this is that the modelled wind direction frequency distribution for the area is such that plumes from these sources do not often impact Ironbark, coupled with the fact that these sources are distant from the monitoring station so any plumes from these sources reaching the monitoring station will be very diluted and thus not register large signals. However, if emissions from these sources are sufficiently strong they can be registered at Ironbark but with smaller frequency due the infrequent wind directions from these sectors. Conversely, Figure 24a suggests that for the same emission rate, potential sources located near Ironbark and along the NNE to ESE and SSW sectors relative to the monitoring station will be better sampled by Ironbark.

Figure 24b for Burncluith is very similar to that for Ironbark, with a shift of the backward plume distribution towards north-east relative to Ironbark. Thus, if Burncluith is used for inverse modelling, generally speaking sources located in the north-east sector will be better sampled compared to those in the south-west.

As expected, there is a qualitative correspondence between the backward plume distributions in Figure 24a and Figure 24b in which there are large source contribution probabilities from the north-east quadrant followed by the south-east quadrant, and the modelled wind roses at the two sites (see Figure 12) in which the highest frequency of winds is from the north-east sector followed by the south-east one. The area best sampled by the combination of the two monitoring stations also contains much of the CSG activity of the region and was the main intention of the monitoring network design (Day et al., 2015; Etheridge et al., 2017).

An advantage of having two or more stations is that additional information is available to go into inverse modelling to constrain sources better. Combining the concentration data from both stations should, generally, improve the source estimate through better source triangulation. But it is clear from Figure 24 that even if the two stations are combined, potential source areas near the north-west, south-west and south-east corners of the domain remain under sampled and this will influence emission calculations using the inverse methodology. One reason for that is that the two stations are located quite close to each other (approximately 80 km apart) compared to the large size of the study domain and they also lie on a line along the prevailing NE-SW wind sectors, so as far as the spatial coverage of sources within the domain is concerned do not add considerably to the information available through the individual stations. The accuracy of emission estimations depends on how optimised the monitoring station locations are in terms of sampling the source distribution of interest.

Note that the plots in Figure 24 are averaged over 1½ years and there will be some seasonal variations to the backward plume patterns (which are all taken into account in the inverse modelling which used hourly versions of Figure 24). The backward plume distributions given for a unit emission rate are scaled for various emission rate hypotheses for use in the Bayesian inversion.

5.5 Emission determination – 'synthetic' inversion

The goal of our Bayesian inverse modelling is to infer methane emissions across the domain given the observed methane concentrations and prior source knowledge. The robustness of source inference (or estimation) depends on the quantity and quality of the prior information, the amount of spatial and temporal coverage of the concentration measurements that bring in new information and update the prior, and of course on the number of unknown source parameters (e.g. emission rates, location) to be estimated.

Before we do the proper inversion, we formulate a 'synthetic' test case in which we do a forward model run using the bottom-up emission inventory and use the resulting modelled concentration time series at Ironbark and Burncluith in our inverse methodology to investigate to what extent the original bottom-up emissions could be recovered. This case is termed synthetic because the observed methane concentrations from the two monitoring stations are not used, only the modelled concentrations are used.

5.5.1 Model setup

In the forward modelling reported earlier, a source array of 69 x 69 with a resolution of about 5 km x 5km was considered. This is a very large number of sources and almost impossible to estimate (i.e. 69 x 69 = 4761 unknowns) for a nonlinear inverse methodology with a limited prior knowledge about the sources and information available from the two monitoring sites. Additionally, this is also too large a number to handle computationally in the Bayesian method because generally for n number of unknown, independent sources, the number of source possibilities (or hypotheses) to explore is n^m where m is the number of emission rate possibilities to consider within a given emission rate range for each source. Thus, to keep the computations tractable we consider a smaller array of 11 x 11 sources (instead of 69 x 69) uniformly spaced

within the model domain. This is still a large number of unknowns (i.e. 121 emission sources) within the Bayesian analysis but our use of the MCMC technique for posterior PDF sampling makes the associated computations feasible. In the case where the prior, and model and data uncertainties are assumed to be normally distributed and the modelled concentration is a linear function of emission rate, it is possible to use the simpler classical matrix method (Michalak et al., 2005; Tarantola, 2005) to infer emission rates. We use these assumptions here, so the matrix method could have also been adopted instead of the more complex approach involving MCMC that we have used. However, our approach with MCMC provides a more flexible and general inversion framework in that non-Gaussian forms of the prior and uncertainties can also be included if desired, which is not possible with the classical matrix method.

The Katestone bottom-up emissions were regridded for an array of 11 x 11 sources with a grid cell size of approximately 31 km x 31 km. The regridded emissions (kg/year/grid cell) are shown in Figure 25. Our inverse model is currently configured to handle only point sources. Therefore, for consistency first a forward TAPM model run was performed with a uniformly-spaced array of 11 x 11 point sources with all other model settings the same as in Section 4.1.1 (simulation period 1 July 2015 to 31 December 2016, inner-grid modelling domain of size 370 km × 370 km with a horizontal grid resolution of 5 km × 5 km). The emission rates of these point sources were the same as the bottom-up emission inventory gridded to 11 x 11 grid points. The locations of these point sources are shown in Figure 25 as solid circles. Thus, the sources are treated as point sources and are assumed to represent the gridded source areas. The modelled hourly concentration time series of methane at Ironbark and Burncluith were extracted and used in the inverse modelling. The aim was to test to what extent the inverse model could recover the emissions from the 11 x 11 point sources used in the forward modelling based on the modelled concentration time series at the two monitoring stations. In this synthetic case, specification of a background methane concentration was not necessary, and therefore was not used.

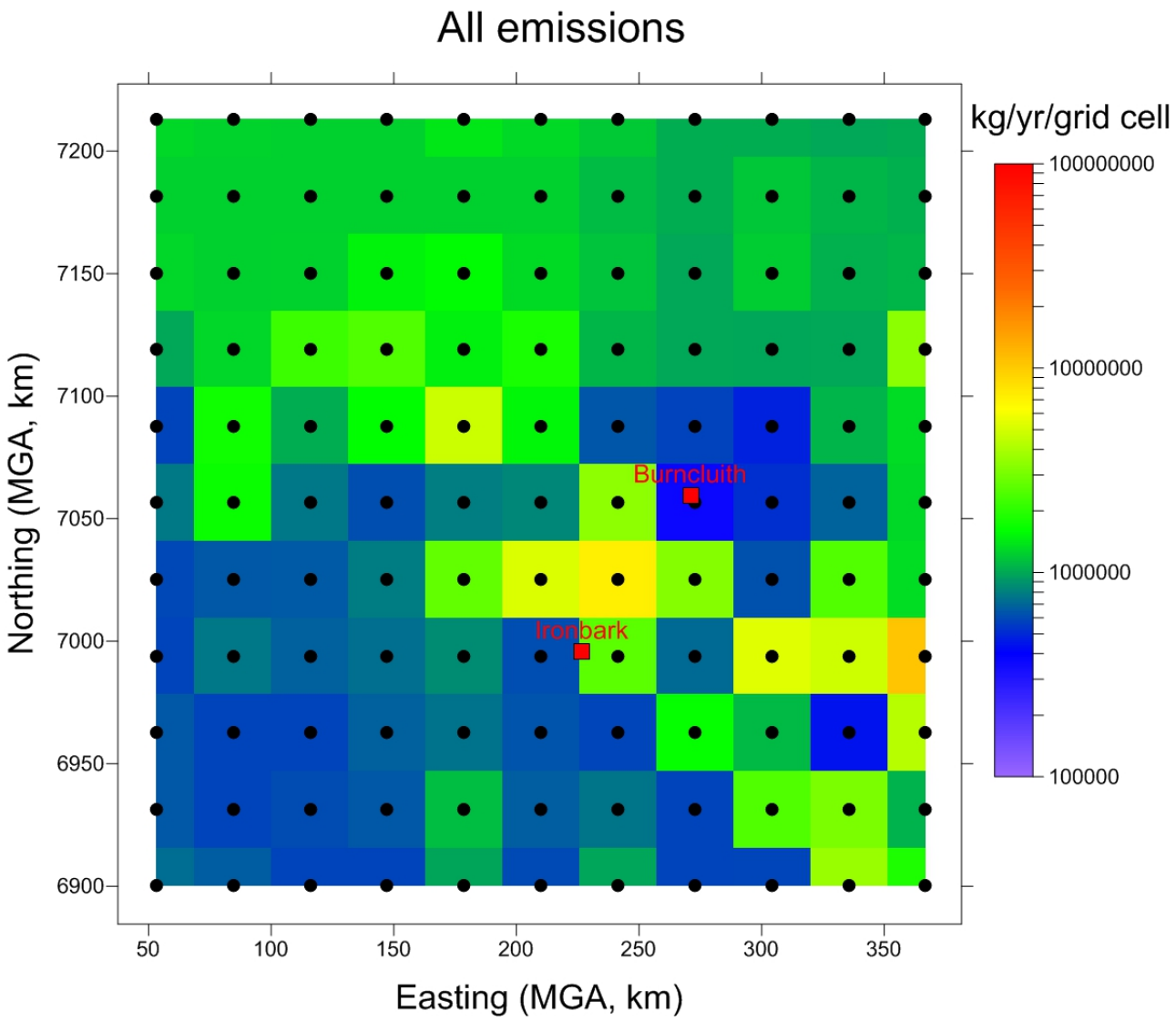

Figure 25. Regridded Surat Basin methane emissions with 11 x 11 grid cells (kg/year/grid cell) derived using the bottom-up emission inventory. The grid cell size is approximately 31 km x 31 km. The 11 x 11 dot points are the point source locations, which correspond to the regridded cells, used in the inverse modelling. Note the logarithmic emission scale. The monitoring site locations are also shown.

5.5.2 Specification of the source prior and other parameters

Specification of a prior through the use of the PDF $p(\mathbf{q})$ in Eq. (1) in the Bayesian inverse modelling is an important step, particularly when the number of unknowns is large. The prior encapsulates our knowledge of the source parameters before the new information received through concentration data is used to modulate the prior information. The prior provides the initial direction or guidance to the inverse modelling algorithm as to what source parameter space to start exploring and with what uncertainty. Generally, the better the quality of and confidence in the prior, the better the source estimate.

The hourly source-receptor relationships obtained by the backward plume TAPM for Ironbark and Burncluith were used as the likelihood function. As is the case with the given inventory emissions, the inverse modelling assumes that all sources emit at constant rate throughout the selected

period, which enables the use of all valid hourly concentration data in one Bayesian calculation to determine the emission rates. The posterior PDF in the Bayesian analysis provides probabilities of all the hypotheses about the values of the source emission rate, and is integrated to obtain the mean and standard deviation of the emission rate.

Even the synthetic case considered here needs a good prior because the amount of information available (i.e. modelled concentrations from Ironbark and Burncluith) and the number of unknown sources (i.e. 121) to estimate are still the same as what would be considered in the real inversion case discussed in the next section. Here we consider the following prior specification.

We first specify a generic Gaussian prior PDF $p(\mathbf{q})$ that is the same for each of the 121 sources. The mean of the prior PDF is taken to be the domain-wide average of the emission rates of the 121 sources in Figure 25, which is calculated to be $\overline{q}$ = 45.37 g s^{-1} (≈ 1.431 x 10^6 kg yr^{-1}) per source and is assigned to each source (Figure 26). A small standard deviation (σ_q) of 0.5% of the mean value is used in the Gaussian prior. In all our calculations, we also impose the constraint that the probability of negative emissions is zero. Generally, in our calculations if the standard deviation of the prior is too large it would bias the posterior towards high probability emission rates whereas if it is too small it would bias the posterior towards the prior distribution.

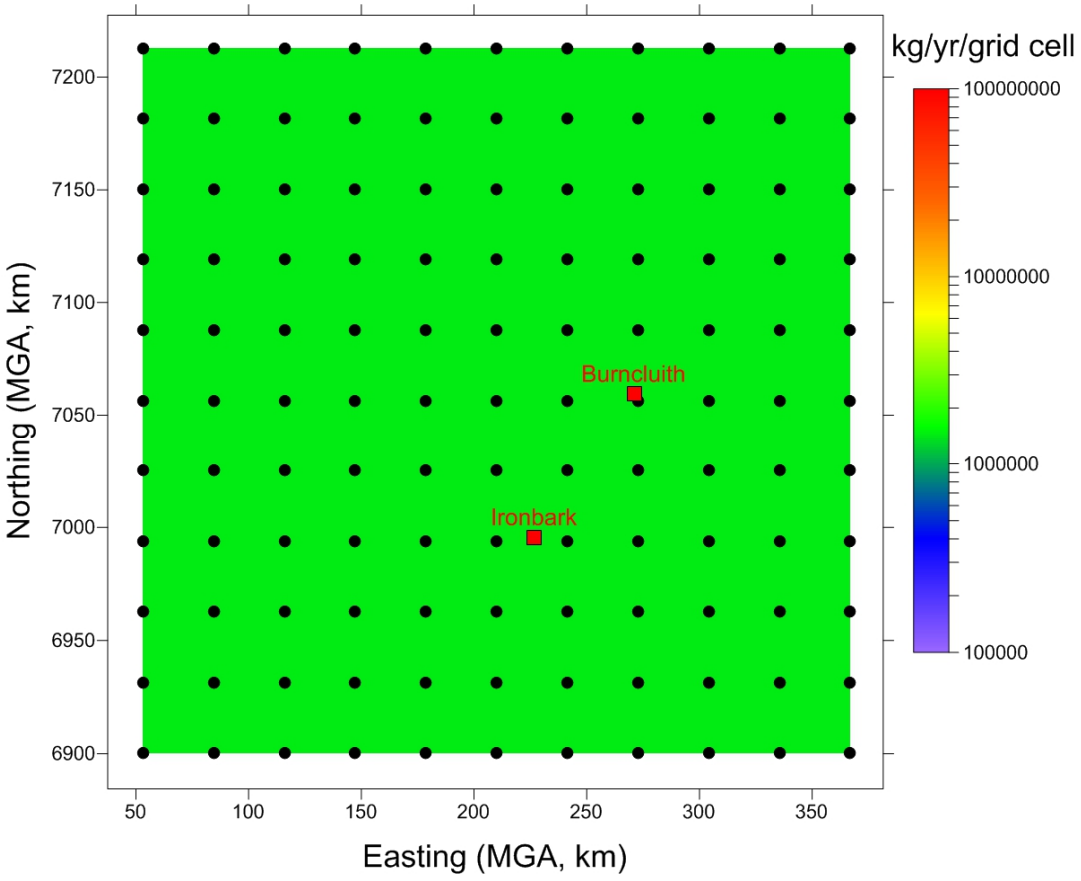

Figure 26. A uniform mean value of 1.431 x 10^6 kg yr^{-1} (or 45.37 g s^{-1}) per source across the domain of 11 x 11 sources used in the Gaussian prior PDF for the synthetic inverse case. The mean value is specified such that the total emission across the domain is 121 x 1.431 x 10^6 = 173.15 x 10^6 kg yr^{-1}, the same as the total bottom-up inventory emission.

The Bayesian inverse methodology adjusts the above uniform prior of 45.37 g s^{-1} per source based on the new information brought in by the modelled hourly concentration time series at Ironbark and Burncluith coupled with the hourly likelihood function given as the scaled modelled backward concentration field for each of the monitoring sites (the average of which is shown in Figure 24).

We also need to know the approximate range of emission rates for each grid source that is needed in the MCMC posterior PDF sampling module. This range is taken as 10–5500 g s^{-1} for each source. The cattle grazing emissions in the inventory are spread over all the grid cells within the domain. The lower limit is the lowest value of the cattle grazing emission rate within a grid cell. The upper (very unlikely) limit is a very large value, approximately the total emission rate from the whole domain localised in a single grid cell.

The uncertainty in the transport model used to construct the likelihood function and the uncertainty in the concentration time series need to be specified. For the former, a nominal uncertainty of 5% in the modelled source-receptor relationship is used. This low value is used because in the present synthetic case the modelled concentrations at the two sites are used to recover the emissions that were used in the forward modelling, so essentially the model uncertainty is zero. (In Section 5.6, a larger model uncertainty of 20% is used for inversions based on the measured methane data.) Here the concentration time series data are the modelled values so again, essentially, there is no uncertainty. Therefore, for the latter, a nominal value of 0.3 ppb was used, which is about a tenth of the uncertainty in the real concentration data used in Section 5.6.

All modelled concentrations greater than 0 were considered (which is basically all the hours (i.e. 13200) because the modelled concentrations are always non-zero since there are sources in all grids of the model domain). A total of 155 MCMC samples of the posterior were drawn. There is a "burn-in" period for MCMC sampling where initial samples are discarded, but this is typically short. In our current application, the first 5 samples were discarded, with the result that the remaining 150 samples were used in the determination of emissions.

5.5.3 Results

Figure 27 presents the emission rates obtained from the synthetic inversion using the modelled concentrations of methane at both Ironbark and Burncluith. It shows how the inverse model has adjusted the uniform prior emission rate of 45.37 g s^{-1} ($\approx$ 1.431 x 10^6 kg yr^{-1}) for each source shown in Figure 26 based on the information contained in the concentration time series at the two sites. The synthetic inversion yields a total emission across the domain of 162.3 x 10^6 kg yr^{-1}, which is only about 6% smaller than the total bottom-up inventory emissions used in the forward modelling to derive the concentration time series.

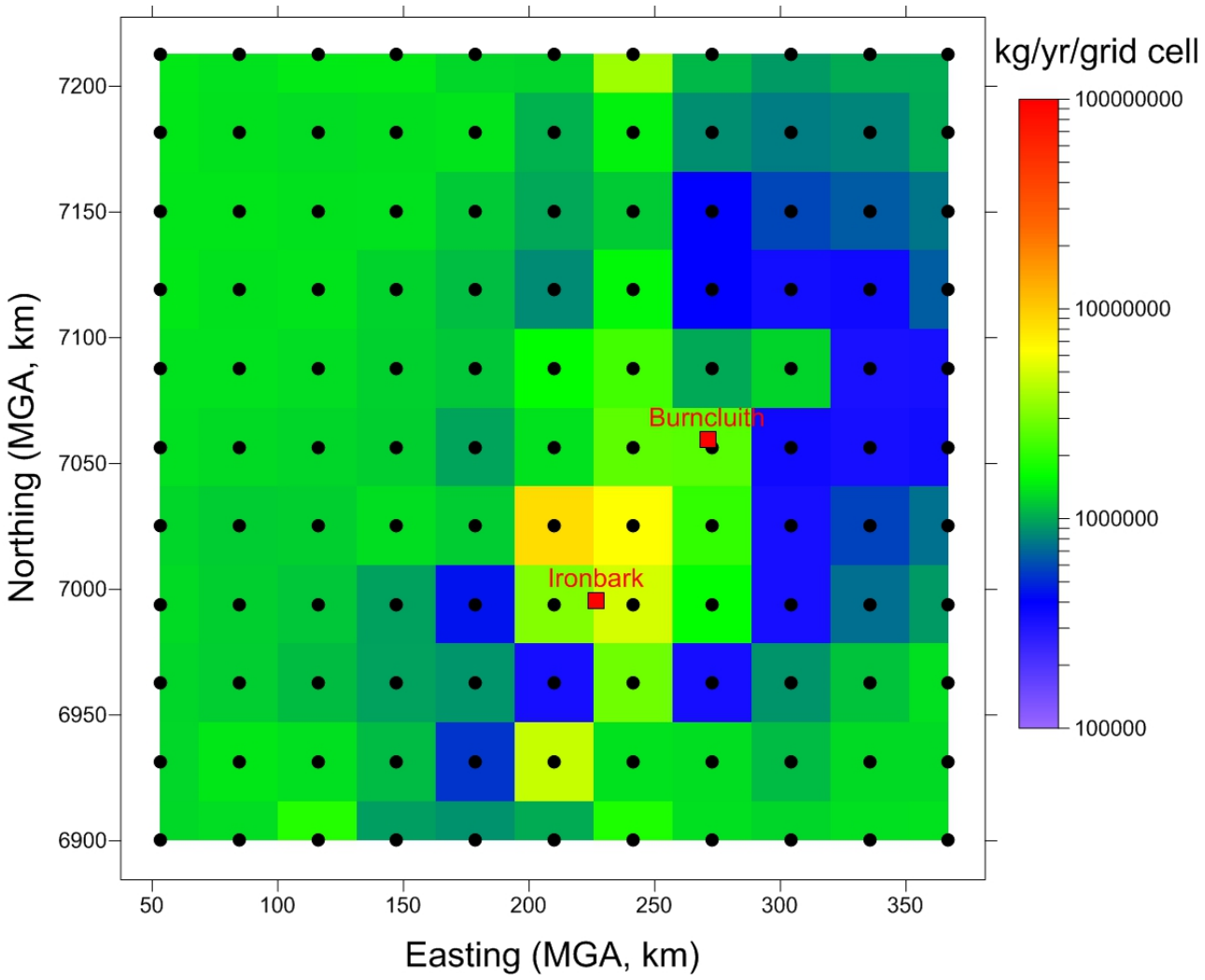

Figure 27. Methane emission rate (kg yr^{-1}) per source grid cell inferred by the inverse model for a uniformly-spaced source array of 11 x 11 sources (a total of 121 source areas) using the modelled hourly-averaged methane concentrations (synthetic case) at Ironbark and Burncluith for July 2015 – December 2016. Note the logarithmic emission scale. The monitoring site locations are also shown.

Comparing Figure 27 with the inventory emission distribution in Figure 25 suggests that the synthetic inversion is correctly obtaining the high emission source area immediately to the north of Ironbark. The inverse model does not yield a strong source area east of Ironbark near the edge of the domain, despite this being in the inventory emissions in Figure 25 that were used to generate the concentration time series for the synthetic inversion. This is probably due to the fact the south-west corner of the domain is not sampled adequately by the two monitoring stations (as discussed in the section 5.4 on backward plume concentration fields). Additional stations and/or specification of a stronger prior for the source areas that contribute little to the concentrations at the two monitoring stations would improve this mismatch. There are other differences in the source patterns too, but again these differences would reduce if we impose better and stronger priors and there is additional information available through more monitoring stations. Overall the model is credible in that it is returning the total emissions and correctly identifying the highest emission areas even with a uniform prior and information from only two stations. For the case of

real inversions below, we have the choice of a more informative prior in the form of the Katestone bottom-up emission inventory, so in hindsight the synthetic case with the less informative uniform prior used is an overly stringent case compared to the real inversion described below.

The intent of performing the synthetic inversion above was to test the feasibility of the inverse methodology, coupled with the stability and effectiveness of MCMC, and to obtain some feel for the degree of prior uncertainty required to achieve a realistic inversion, before the methodology can be used for data-forced inversion (below). The synthetic inversion work showed that the prior uncertainty needs to be small for the present application and that an MCMC sample size of ~ 150 is adequate.

5.6 Emission determination – inversion based on the methane data

In this section, instead of using the forward modelled concentration time series we use the measured methane concentrations at Ironbark and Burncluith in the inverse methodology to infer emissions. The hourly background methane concentrations were subtracted from the time-matched hourly measured concentrations (this occasionally yields small negative concentration deviations).

As mentioned in Section 2.1, for sources near the ground, high ground-level concentrations typically occur during low-wind (< 2–3 m s^{-1}) nocturnal inversion conditions when the ambient stability is strong, turbulent mixing is suppressed, the inversion layer is very shallow, and the flow field is most sensitive to the local terrain features. These are some of the most difficult conditions to simulate by a flow and dispersion model, particularly in a regional scale operational model such as TAPM. There are various reasons for that, including insufficient understanding of the physics of low-wind processes and their parameterisation in the model and limited horizontal and vertical resolutions (e.g. Luhar and Hurley, 2012, and references therein). High concentrations of methane at night are evident in the data, particularly from Burncluith, and to a lesser extent from Ironbark (Figure 18). This is consistent with the larger frequency of nocturnal low winds at Burncluith than Ironbark. The inability of TAPM to estimate the frequency of nocturnal low winds, particularly at Burncluith, was shown earlier in section 4.1.3. For the inverse modelling, the same data selection filter as for the forward modelling was applied, i.e. all daytime hours (1000–1700 h) irrespective of wind speed, all remaining hours for which the observed wind speed is greater than 3 m/s, and further at Burncluith all hours for which the measured CO enhancements above the background are greater than 10 ppb are not considered.

As discussed in Section 2.1, at Burncluith the signature of biomass burning to the north-west and woodheater emissions from the house next to the monitoring station (these sources are also not included in the Katestone bottom-up emission inventory) is evident as enhancements in the CO measurements at that station. The selected CO cut-off value of 10 ppb to remove the influence of these sources is about twice the one standard-deviation uncertainty in the observed CO around the background CO variation without considering the CO enhancement periods (so this uncertainty was calculated as the root mean square of the deviations of the hourly CO concentrations (c_t) from the hourly varying CO background (c_{bt}) over the number of hours when $c_t \leq c_{bt}$.

As mentioned in Section 4.1.2, a background methane concentration uncertainty (σ_b) of 3.5 ppb was calculated based on the background concentration analysis, and this value was specified as the uncertainty in the observed concentrations. A model uncertainty of 20% in the source-receptor relationship was used (Luhar et al., 2014).

5.6.1 Selection of the prior and inverse emission estimates

In this section, three separate cases of the inverse modelling are considered. They vary in the way priors are specified – from simple to complex.

Case 1: We first consider a rather extreme case where we do not specify any prior except for the bounds on the emission rate required by the MCMC technique. The minimum emission rate is taken to be 10 g s^{-1} and the maximum 10,000 g s^{-1} for each of the 121 gridded sources. This is a very broad range where the ceiling value is almost twice the total of the bottom-up emissions from the domain and from a single source cell. The high ceiling on emission rate was chosen to make sure that with the absence of a prior PDF the ceiling does not put an artificial limit on inferred sources whose emission rates could be higher than the ceiling value.

Figure 28 shows the distribution of the mean methane emission rates (kg yr^{-1} per source) inferred by the model. (Note that all types of methane source sectors are represented in the model-inferred emission estimates.) Despite virtually no prior provided, the inversion yields a total emission across the domain of (162.1 ± 5.3) x 10^6 kg yr^{-1} that is very close to the bottom-up emission inventory value of 173.163 x 10^6 kg yr^{-1}. Note that there is no expectation that the inverse model, even if perfectly able to determine the emissions, should give exactly the same emissions distribution or total as the inventory, since the inventory has uncertainties and does not include all potential methane sources, as discussed earlier. The maximum source emission rate in Figure 28 is approximately 1132 g s^{-1}, almost a tenth of the specified ceiling value, which implies stability of inversion computations with the given information.

Generally speaking, the modelled larger emissions between Ironbark and Burncluith and in the middle of the domain are consistent with the bottom-up emissions shown in Figure 25, but the magnitude of the inferred emissions is larger (note the logarithmic emission scale). Conversely, away from the regions of these high inferred emissions the bottom-up emissions are greater than the inferred emissions.

The above results suggest that the information contained in just the concentration time series from the two monitoring stations without a proper prior (only a broad range of possible emission rate is specified) is able to constrain the total emissions realistically, but compared to the inventory emissions the estimated emissions are more concentrated in some grids in the middle of the domain and less in the areas further away.

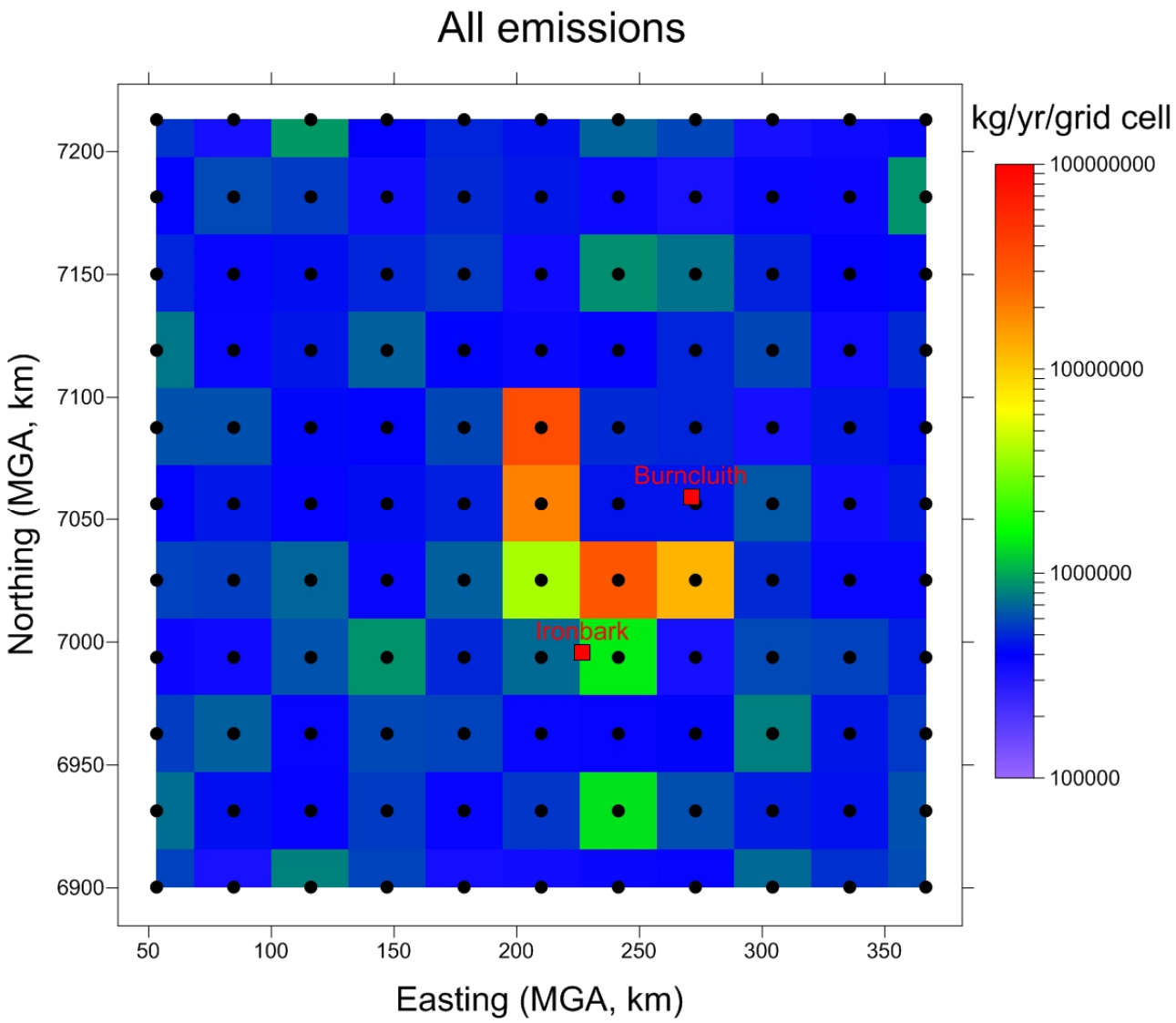

Figure 28. Methane emission rate (kg yr^{-1}) per source inferred by the inverse model without a prior (only a broad range of possible emission rate is specified) for a uniformly-spaced source array of 11 x 11 sources (a total of 121 source areas) using the measured hourly-averaged methane concentrations at Ironbark and Burncluith for July 2015 – December 2016 (Case 1). Note the logarithmic emission scale. The monitoring site locations are also shown.

Case 2: Next we constrain the prior slightly more realistically. In addition to specifying a range of 10–10000 g s^{-1} for each source, a Gaussian prior PDF with a mean uniform emission rate of 45.37 g s^{-1} (≈ 1.431 x 10^6 kg yr^{-1}) per source is used throughout the domain, as in Figure 26 for the synthetic case. A standard deviation (σ_q) of 10% of the mean value is used in the Gaussian prior (which is larger than that used in the synthetic case, as are the uncertainties in the methane background concentration and the modelled source-receptor relationship in this real inversion case).

Figure 29 presents the distribution of the mean emission rates inferred by the model, which is qualitatively similar to that in Figure 28. It is, however, clear that compared to Figure 28 the emission rates for sources located between the two stations and those in the middle of the domain are less pronounced, but the rest of the sources generally have larger emission rates. This inversion yields a total methane emission across the domain of 142.6 (± 1.5) x 10^6 kg yr^{-1}.

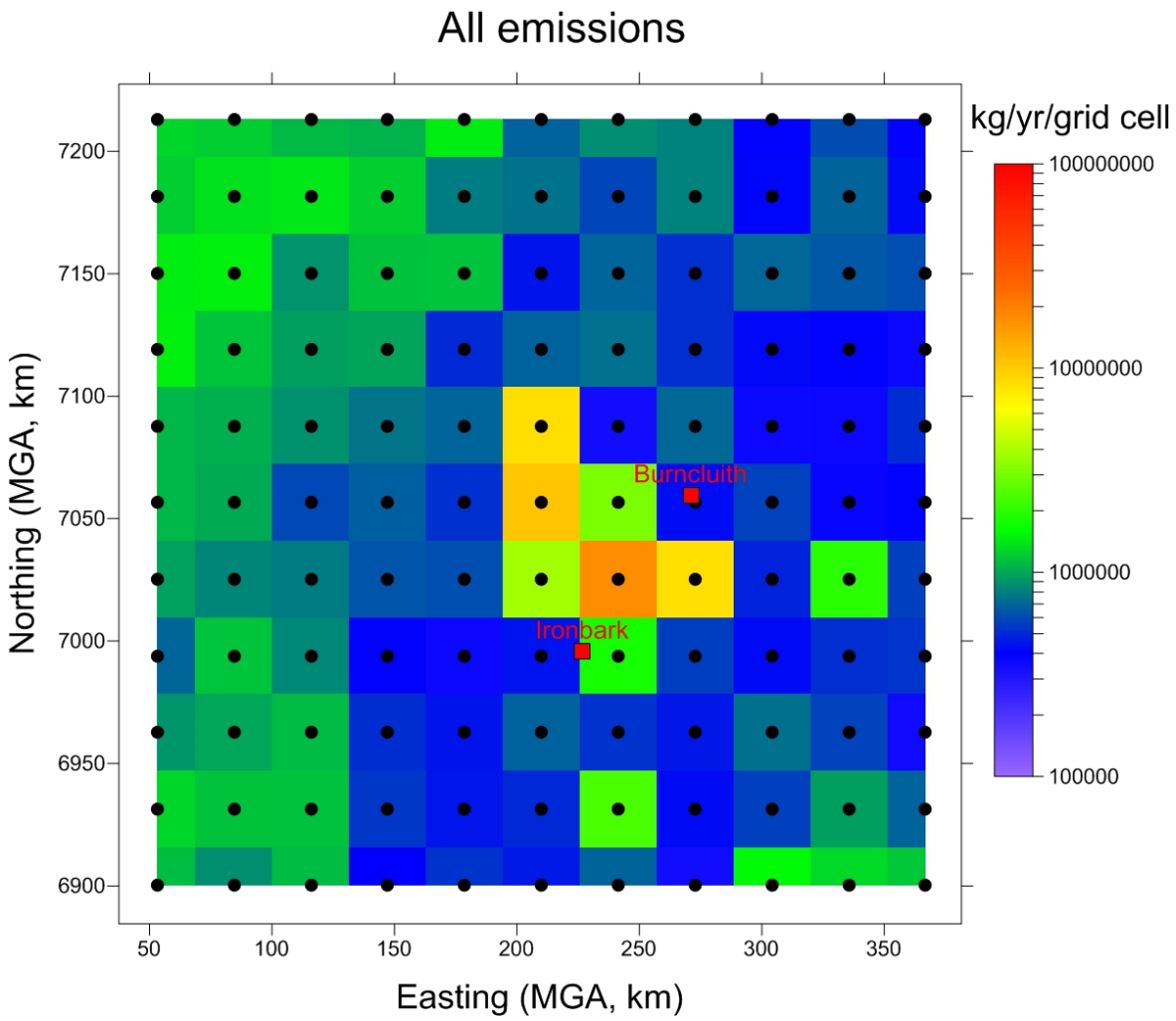

Figure 29. Methane emission rate (kg yr^{-1}) per source inferred by the inverse model for a uniformly-spaced source array of 11 x 11 sources (a total of 121 source areas) using a Gaussian prior PDF with a prescribed uniform mean emission rate of 45.37 g s^{-1} per source cell across the domain and the measured hourly-averaged methane concentrations at Ironbark and Burncluith for July 2015 – December 2016. A standard deviation of 10% of the mean value is used in the Gaussian prior (Case 2). Note the logarithmic emission scale. The monitoring site locations are also shown.

Case 3: In this case, we specify a Gaussian prior PDF for each source with a mean emission rate equal to the bottom-up inventory emission rate for each source (so the prior is the same as Figure 25). Because each source now has a specific prior, the corresponding prior uncertainty (σ_q) is taken to be smaller than that used in Case 2, which was 10% of the mean.

We first use two values of σ_q: 1% and 5%. Figure 30 is the distribution of the mean emission rates inferred by the model with σ_q = 1%. Comparing this figure with the bottom-up emission inventory plot in Figure 25 suggests that the two are very similar, even the strong source area east to Ironbark near the edge of the domain is largely reproduced even though the south-west corner of the domain is not sampled adequately by the two monitoring stations. What this means is that the prior used with a small uncertainty of 1% is a bit too stiff which tends to force the inverse

methodology to yield a solution that is not too different from the prior information, thus effectively dominating the information contained in the concentration data.

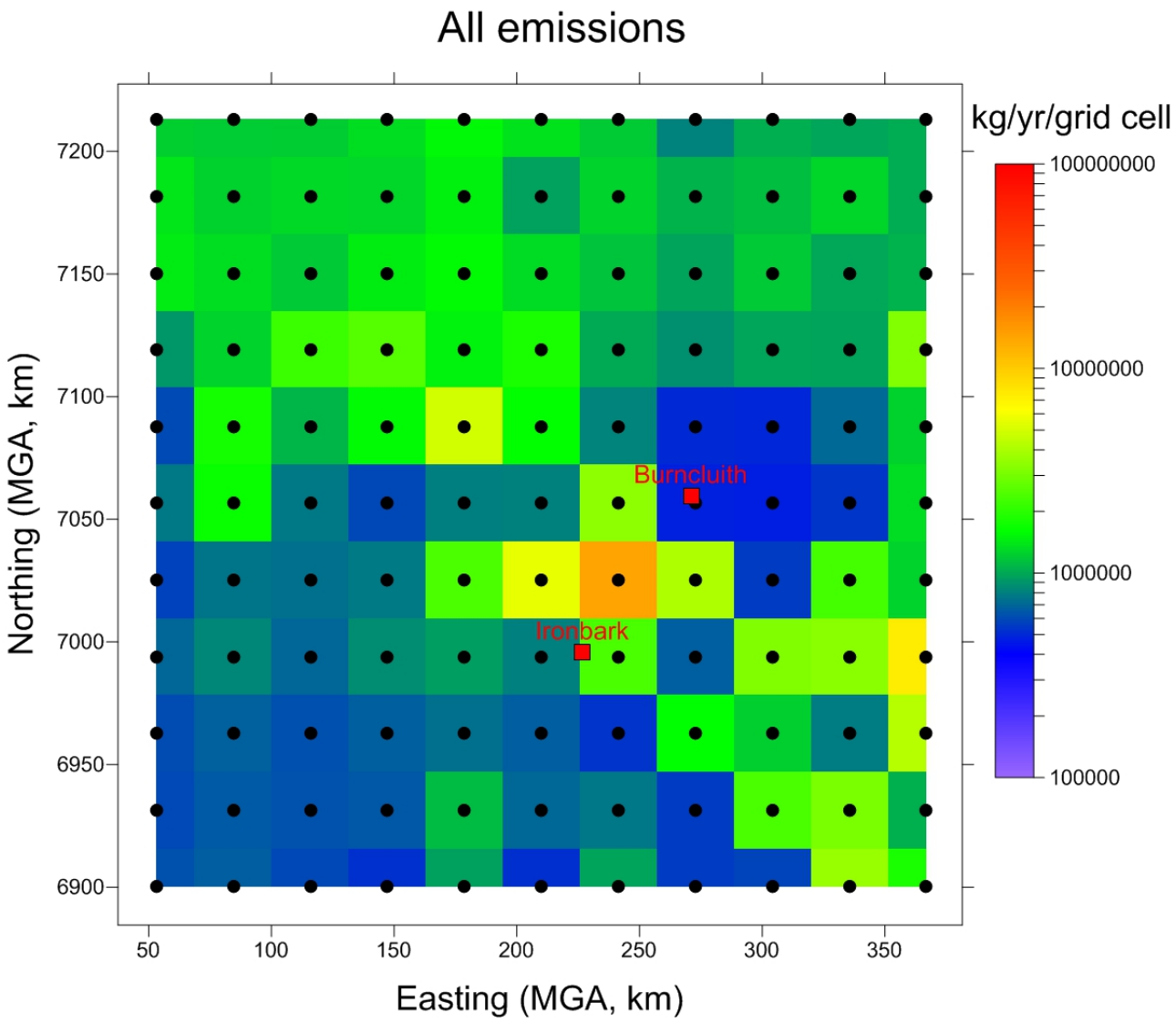

Figure 30. Methane emission rate (kg yr^{-1}) per source inferred by the inverse model for a uniformly-spaced source array of 11 x 11 sources (a total of 121 source areas) using Gaussian prior PDFs with mean values across the domain the same as the bottom-up inventory emissions (Figure 25) and the measured hourly-averaged methane concentrations at Ironbark and Burncluith for July 2015 – December 2016. A standard deviation of 1% of the mean value is used in the Gaussian priors (Case 3). Note the logarithmic emission scale. The monitoring site locations are also shown.

Figure 31 is the same as Figure 30 except with some relaxation in the prior uncertainty with σ_q = 5%. With this relaxation the sources around the middle of the domain and between the two monitoring sites become more pronounced whereas the source area east of Ironbark near the edge of the domain and those in the south-west corner almost disappear as the concentration data exert more influence in the stronger areas of their source-receptor relationship (Figure 24). It is clear that the results are sensitive to the value of σ_q, but it can be seen that a prior uncertainty between 1–5% is a good choice which provides a balance between the desirability of the inversion

coming close to reproducing the prior in source areas for which the probability of monitors sampling the signal is low and at the same time ensuring that the prior does not override the information contained in the concentration data in deriving the posterior probability. Hence we have done another inverse modelling run with σ_q = 3% and the results are shown in Figure 32, which essentially lies between the emission distribution calculated for σ_q = 1% and 5% and this is the final result for Case 3. The inversion in Figure 32 yields a total emission across the domain of 165.8 x 10^6 kg yr^{-1}.

The uncertainty estimates associated with the Katestone bottom-up inventory (Table 31 in Appendix B) vary with emission category and are generally much larger than the single uncertainty value selected above (σ_q = 3%) for the prior. In our calculations, if the standard deviation of the prior is too large it biases the posterior towards high probability emission rates (as is clear from Figure 30 and Figure 31). This perhaps suggests that our inversion is not specified adequately, in that the number of monitoring sites is not adequate and/or better prior uncertainties that are specified separately for each source grid cell are needed.

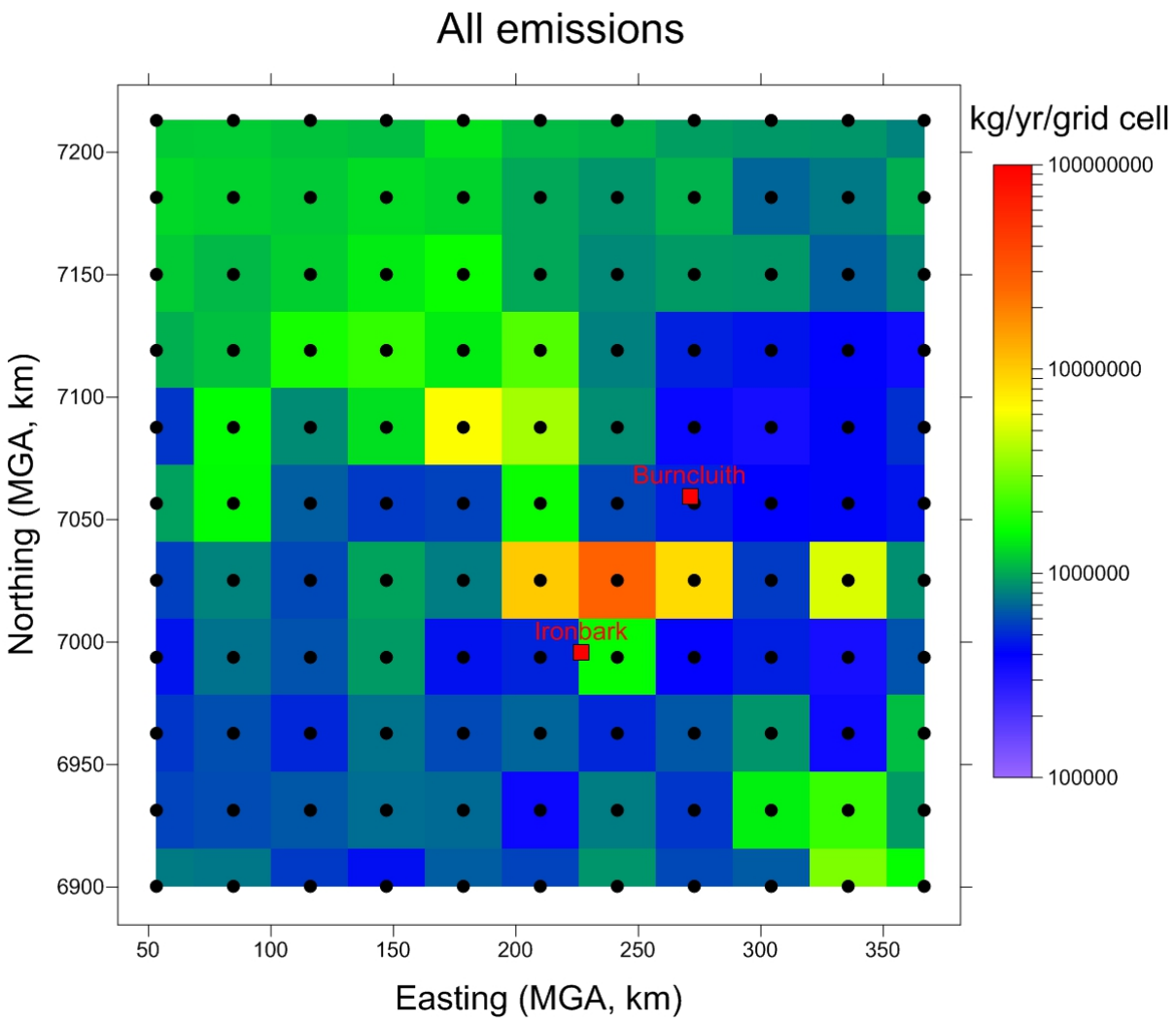

Figure 31. Methane emission rate (kg yr^{-1}) per source inferred by the inverse model for a uniformly-spaced source array of 11 x 11 sources (a total of 121 source areas) using Gaussian prior PDFs with mean values across the domain the same as the bottom-up inventory emissions (Figure 25) and the measured hourly-averaged methane concentrations at Ironbark and Burncluith for July 2015 – December 2016. A standard deviation of 5% of the mean value is used in the Gaussian priors (Case 3). Note the logarithmic emission scale. The monitoring site locations are also shown.

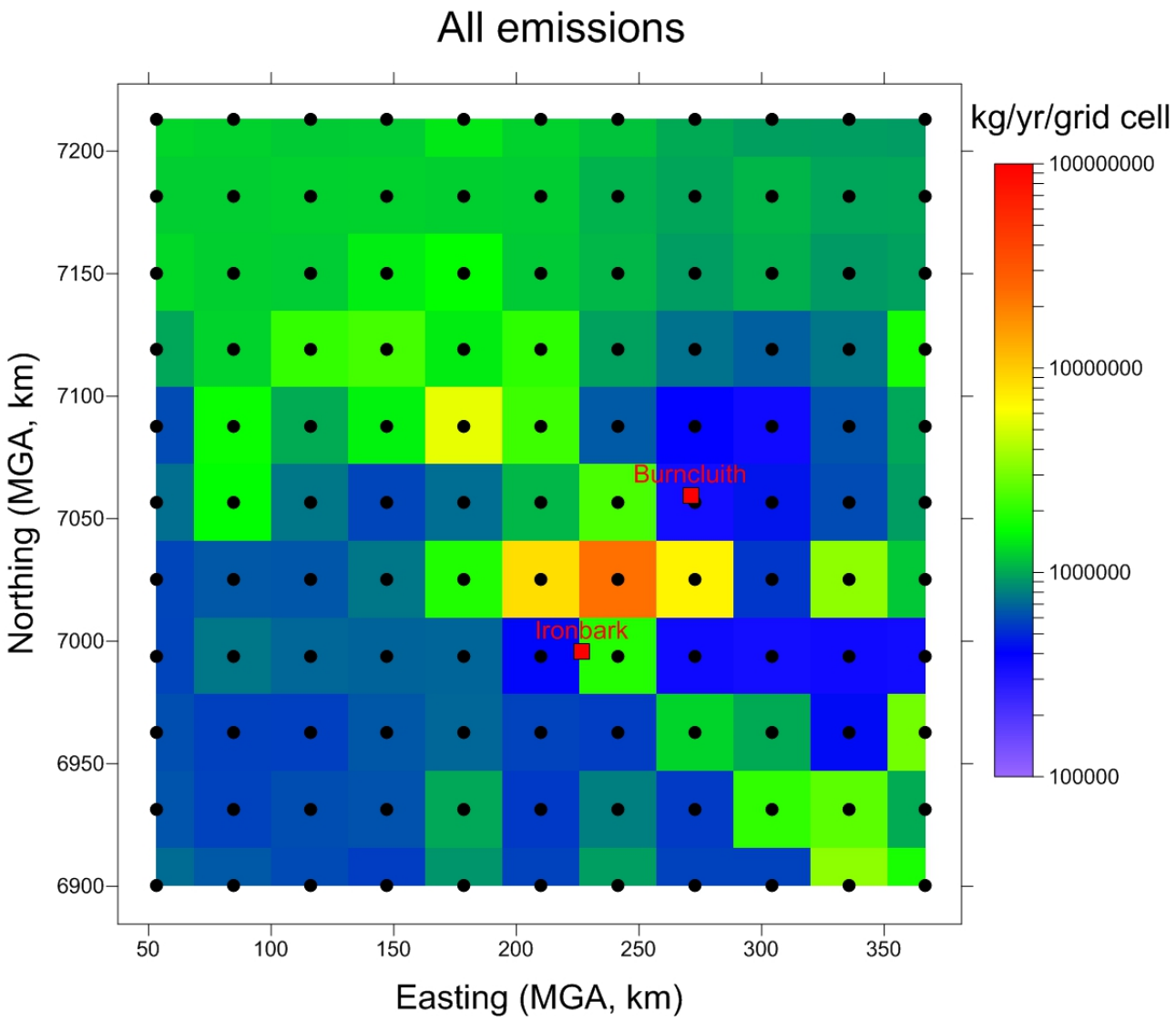

Figure 32. Methane emission rate (kg yr^{-1}) per source inferred by the inverse model for a uniformly-spaced source array of 11 x 11 sources (a total of 121 source areas) using Gaussian prior PDFs with mean values across the domain the same as the bottom-up inventory emissions (Figure 25) and the measured hourly-averaged methane concentrations at Ironbark and Burncluith for July 2015 – December 2016. A standard deviation of 3% of the mean value is used in the Gaussian priors. Note the logarithmic emission scale (Case 3). The monitoring site locations are also shown.

Uncertainty in the inferred emissions: The uncertainty in the inferred emissions can be calculated for each source point by taking the standard deviation of the MCMC samples of the emission rate for that source point (there were 150 samples). Figure 33 presents the standard deviation of the inferred methane emission rate (kg yr^{-1}) per source for the case presented in Figure 32. Compared to the mean values in Figure 32, the standard deviations are smaller by approximately one to two orders of magnitude. In absolute terms, generally, the higher the inferred emission rate the higher the standard deviation. However, it is interesting to see that the grid point with the highest emission rate in Figure 32 which is located between Ironbark and Burncluith has less uncertainty than the two grid points east and west of this grid point (in Figure 33). The overall standard deviation is very small (less than 1% of the total inferred emission) and is dominated by the high emission rate grid points. What this suggest is that the inverse methodology constrains the high source areas well given the methane concentration data from two stations. One reason for these

posterior emission uncertainties being very small is the small uncertainty in the prior, as discussed above.

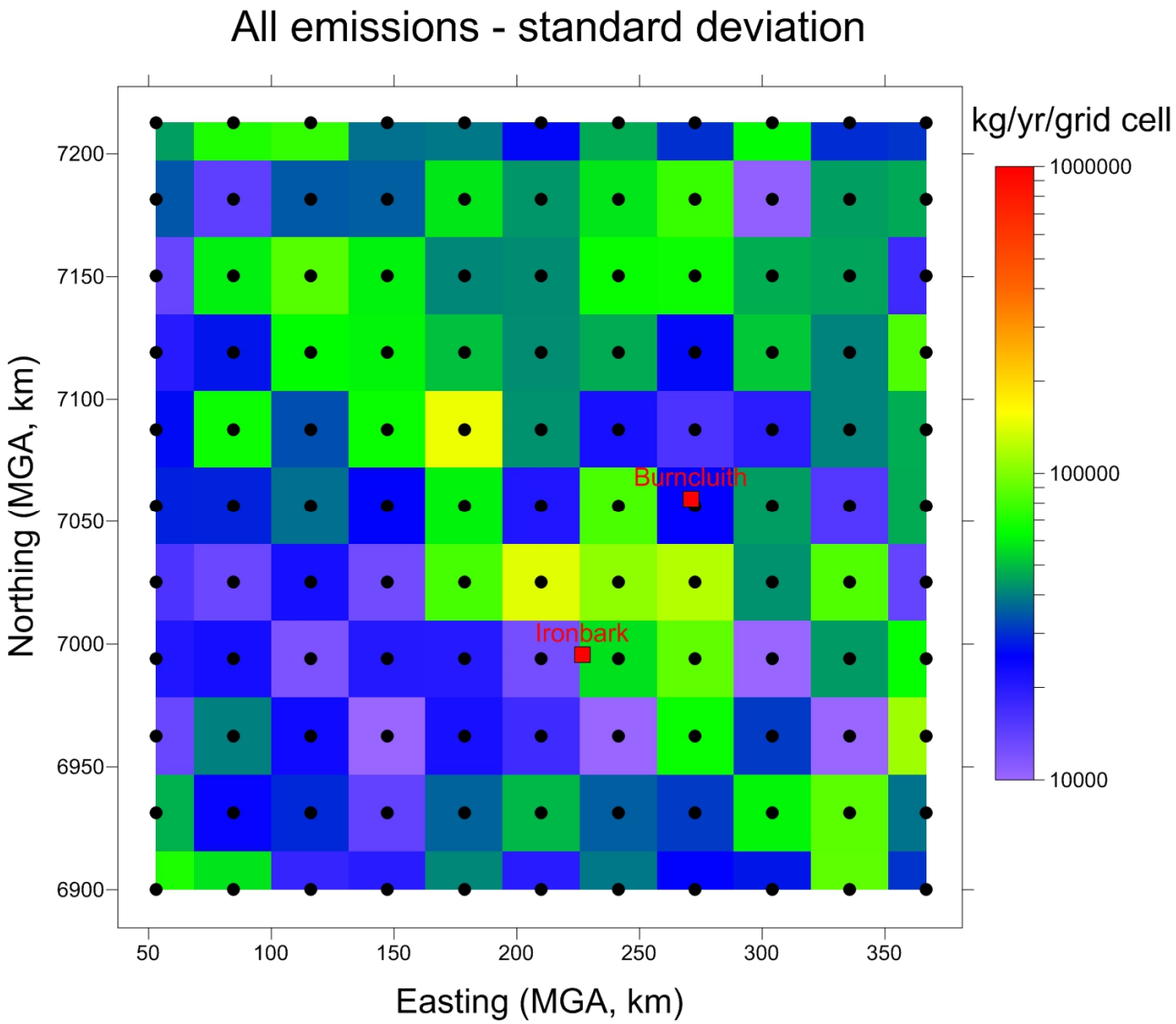

Figure 33. Standard deviation (or uncertainty) of the methane emission rate (kg yr^{-1}) per source inferred by the inverse model in Figure 32.

5.6.2 Sensitivity to the background concentration

A method was devised in Section 4.1.2 to estimate the methane background concentration by selecting conditions that minimise the influence of emissions from within the selected Surat Basin domain on the measured concentrations. The method yielded slightly different background concentration variations for Ironbark and Burncluith (Figure 11), which were averaged and then used for the purposes of model-data comparison and inverse modelling. The averaged background concentration time series was treated as the domain-wide background concentration that represented the contribution of methane sources outside the model domain.

Specifying a regional methane background concentration is a difficult problem. Different locations within the study domain may be influenced by different background emission and transport sectors depending on the meteorology and methane sources located outside the model domain.

An alternative approach to account for the background concentration in regional modelling could be to use a global chemical transport model for methane and use the globally modelled methane concentrations at the boundaries of our regional domain as boundary conditions in the regional modelling. The required methane concentrations at the boundaries can also come from suitably located methane monitors outside and around the study domain if available. We have not attempted either of such approaches here. In our present case, we are limited by having methane data from only two monitors within the study domain, which are used to derive the regional methane background concentration.

Figure 11 suggests that the calculated background concentration variations for Ironbark and Burncluith are slightly different. We conduct an inverse modelling sensitivity test by using separate background methane concentrations for Ironbark and Burncluith, rather than using the background averaged over the two sites.

Figure 34a shows the observed deviations of the hourly methane concentration (c) from the time-matched hourly background (c_b) when separate background values are used for Ironbark and Burncluith versus those when the averaged background values ($c_{b(av)}$) are used. Positive deviations as high as 600 ppb are measured indicating strong influence of sources within the domain. Small, negative deviations (magnitude no greater than 12 ppb) are also present which indicate uncertainty in the background. The root mean square of the negative deviations is 4 ppb for Ironbark and 3 ppb for Burncluith, which are very similar to the background uncertainty value of 3.5 ppb used in the inverse modelling.

In Figure 34a, the two sets of deviations are more or less the same, but when they are plotted on a logarithmic scale in Figure 34b (with only the positive values used), there are significant differences between the two for small values, but most of these differences are within or of the order of the uncertainty in the background (i.e. 3.5 ppb, shown by dashed lines).

Figure 35 shows the same inverse case as in Figure 32 for the inferred methane emission rate except that separate background methane concentrations for Ironbark and Burncluith are used. Compared to Figure 32 based on the averaged background, there is virtually no change in the inferred source distribution in Figure 35, except for some very minor changes in low emission rate areas. The total emission across the domain in Figure 35 is 164.8 x 10^6 kg yr^{-1} compared to 165.8 x 10^6 kg yr^{-1} in Figure 32. The inferred emission uncertainties are also found to be virtually the same in the two cases.

Given the negligible difference between the two inversion cases involving two different prescriptions of the background concentration, we only further consider calculations based on the background methane that is the average of the two sites.

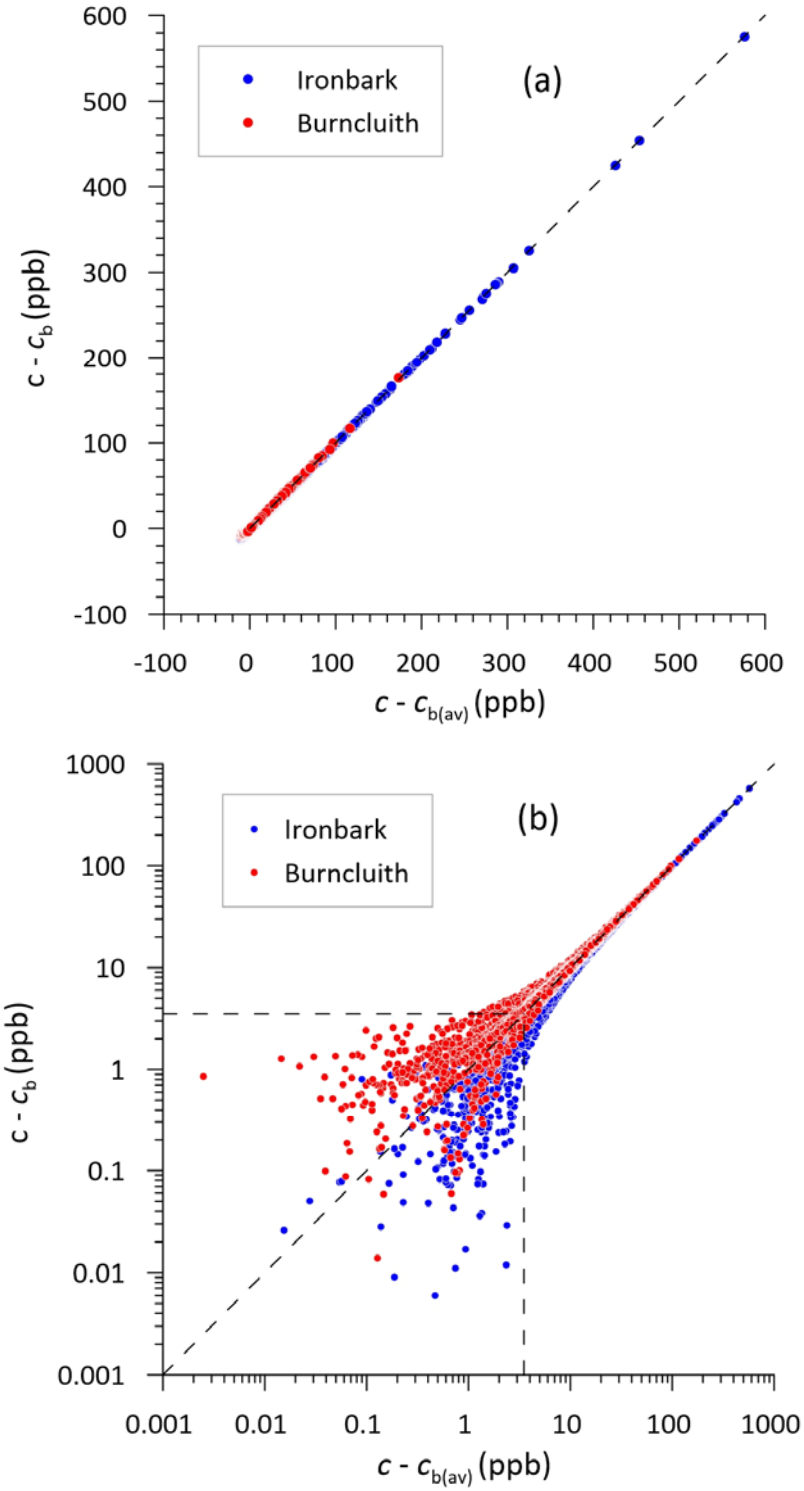

Figure 34. (a) Observed deviations of methane concentration (c) from the background (c_b) when separate background values are used for Ironbark and Burncluith versus those when the averaged background values ($c_{b(av)}$) are used; (b) same as (a) but on a logarithmic scale with only the positive deviations are plotted. Filtered data used.

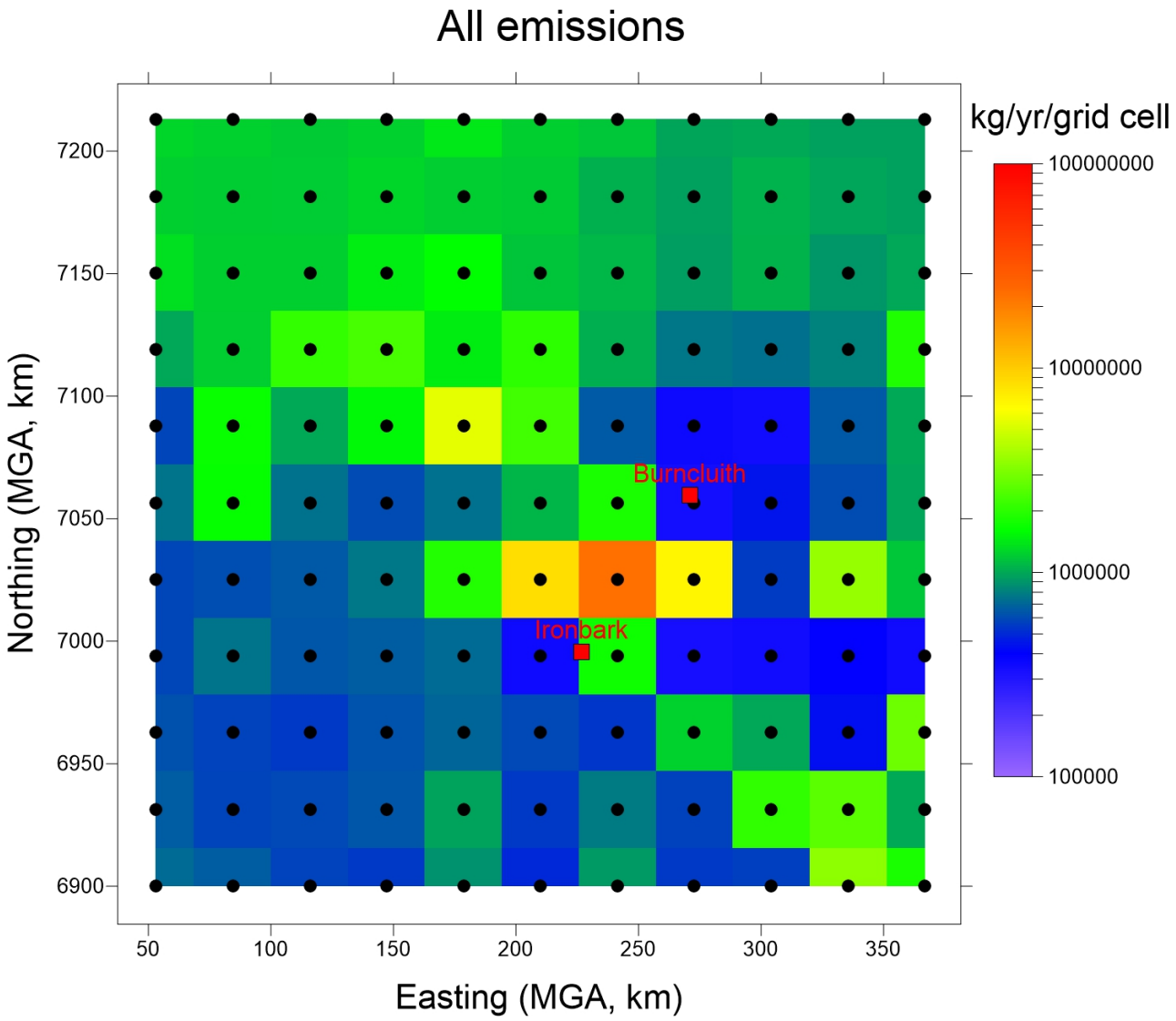

Figure 35. Same as Figure 32 for the methane emission rate (kg yr^{-1}) per source inferred by the inverse model (Case 3) except that separate background methane concentrations for Ironbark and Burncluith are used (rather than using the background averaged over the two sites).

5.6.3 Validation of the inverse emission estimates

The inverse methodology has yielded methane emission rates for the 121 sources uniformly distributed within the domain based on the concentration obtained during July 2015 to December 2016 from the two monitoring stations. However, a question remains as to whether these derived emissions truly represent the measurements, to a better degree than the bottom-up emissions. One way to address that question is to perform a forward model run using the emission rates derived from the inversions and compare the modelled concentrations to the methane concentration measurements. If the comparison demonstrates a better performance of the model with the inversion derived emissions than when the bottom-up emissions are used then we can deduce that the inversions have the ability to represent true emissions with a higher degree of confidence (of course assuming that the meteorology has been modelled sufficiently accurately). Consistency between a forward run using the inferred emissions and concentration measurements is necessary (but not sufficient) and reflects that the forward and inverse models are consistent. In order to enable such a comparison, we conducted three separate forward TAPM runs

corresponding to the emissions rates from the inversion Cases 1, 2 and 3 described above (Figure 28, Figure 29 and Figure 32, respectively).

We examine the performance in terms of q-q plots. Figure 36a shows q-q plots of the sorted hourly-averaged modelled vs. sorted measured methane concentrations for Ironbark (left) and Burncluith (right) obtained using the emissions from the inversion Case 1 in which effectively no prior is used. Comparing these plots to the corresponding q-q plots obtained using the bottom-up inventory emissions (the faint points, which are the same as in Figure 20), it is apparent that while the Case 1 emissions overestimate methane concentrations at both sites for the upper concentration range, the modelled methane at Ironbark is much better described than that in Figure 20. At Burncluith, the magnitude of overestimation is as large as the magnitude of underestimation in Figure 20.

As is clear from Figure 36b based on the Case 2 inversion emissions, specification of a prior, although rather crude, improves performance of the inversion, particularly at Burncluith. Overall this case represents a large improvement over Figure 20 based on the bottom-up inventory emissions. The Case 3 inversion with a further refined prior improves the emission estimates further as evident from Figure 36c, particularly for Ironbark. Overall, apart from the 3-4 data outliers at the top of the distribution, Case 3 provides the best comparison of the modelled methane with the measurements and hence represents the area-wide emissions as derived from the methane measurements from the two monitoring sites. The underestimation seen in Figure 20 is almost removed. Thus Figure 32, representing Case 3 (i.e. Gaussian prior PDFs with mean values across the domain the same as the bottom-up inventory emissions with corresponding standard deviations of 3% of the mean values) is our best inferred emission distribution.

Obviously there remain some model-data differences. The reasons for this include a coarse distribution of 11 x 11 point sources to represent the domain-wide emissions, differences between the modelled and observed meteorology, the limited amount of information available in terms of the number of sites, their locations and the quantity of data.

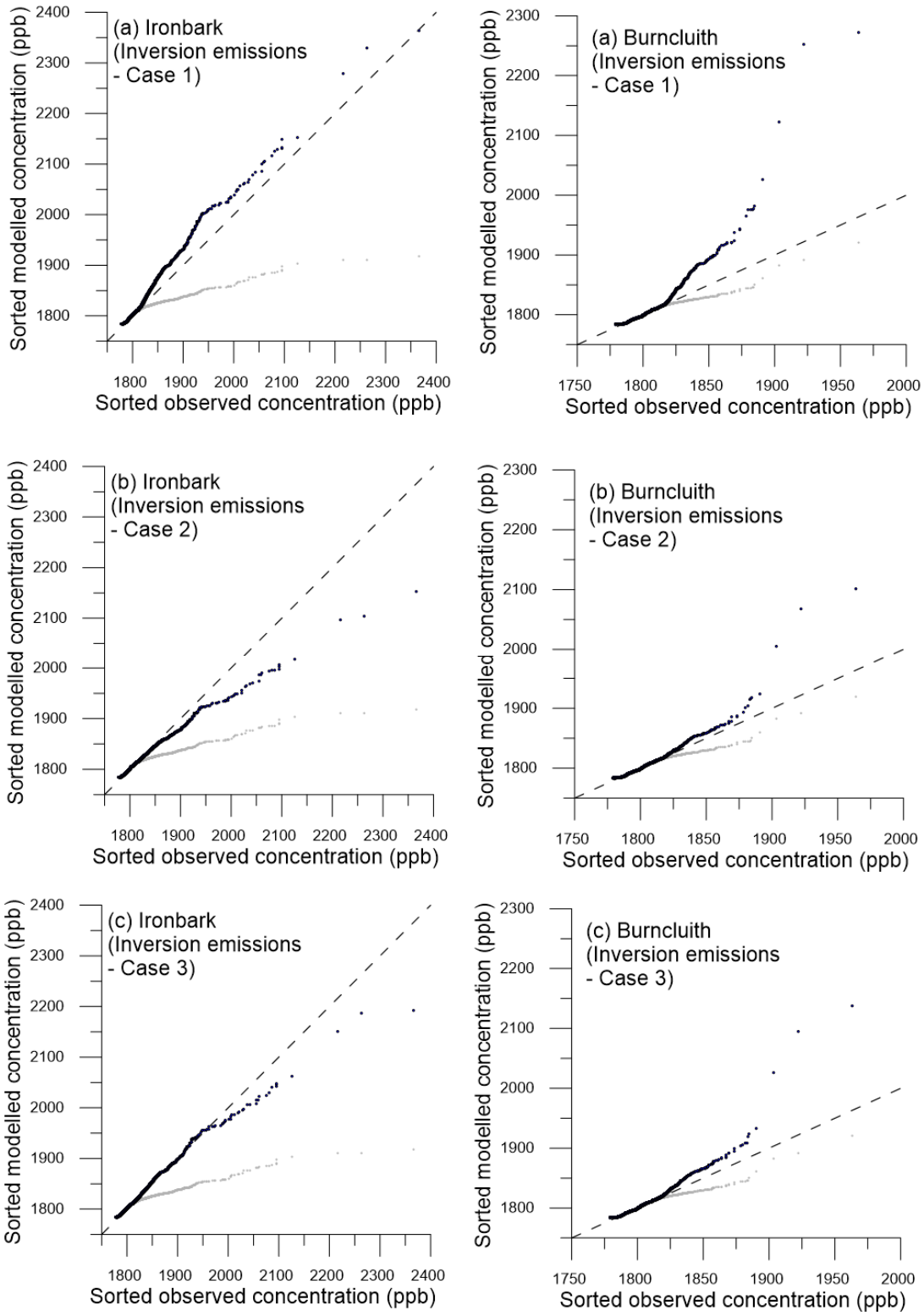

Figure 36. Quantile-quantile (q-q) plots of the sorted hourly-averaged modelled vs. sorted measured methane concentrations at the Ironbark (left) and Burncluith (right) sites in the Surat Basin. The modelled concentrations are produced from the emissions from (a) Case 1 inversion (i.e. with an even prior within a broad range of possible emission rates), (b) Case 2 inversion (i.e. with an even prior with a Gaussian uncertainty of 10%), and (c) Case 3 inversion (i.e. with a bottom-up emission inventory prior with a Gaussian uncertainty of 3%). The faint points are the original forward model results from Figure 20 based on the bottom-up inventory emissions. The dashed line is the line of perfect agreement.

5.6.4 Observed and modelled methane time series

The modelled and observed methane concentration time series can also be compared. This enables a direct visualisation of the magnitude of temporal variability in concentration, and the shape and size of its fluctuations. As an example, Figure 37 shows the hourly averaged methane concentration time series at Ironbark for the months of November 2015 and May 2016. All observations are plotted (i.e. all hours and all wind speed conditions). For both months, although TAPM using the inventory emissions (light blue line) is able to simulate the timings of the occurrence of a number of observed peaks (magenta line), it underestimates the magnitudes of these peaks. In contrast, TAPM using the top-down inverse emissions (dark blue line) is able to describe the magnitude of these peaks much better. The peaks in May are more frequent and of larger magnitude than in November.

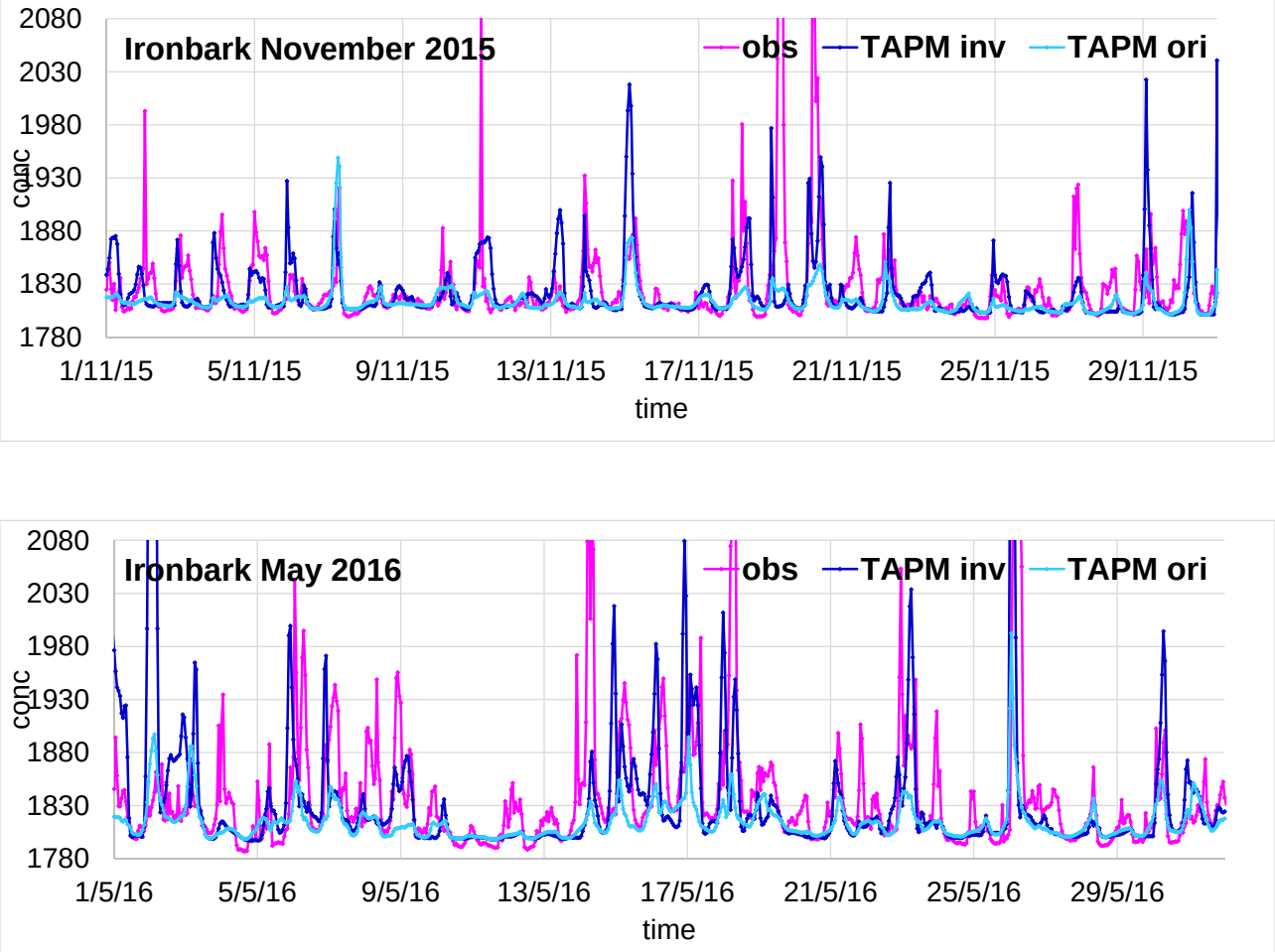

Figure 37. Hourly averaged methane concentration at Ironbark for the months of November 2015 (top) and May 2016 (bottom). Magenta lines are observations, light blue lines are forward TAPM results using the original bottom-up inventory emissions, dark blue lines are forward TAPM results using the inverse emissions from the Case 3 top-down inversion.

Figure 38 is an example time series plot for Burncluith for two months. Only those observed methane concentrations are plotted for which the observed CO concentration was less than 10 ppb above the background value (the CO filter was discussed earlier). All other observations are

plotted (i.e. all hours and all wind speed conditions). Similar to the case of Ironbark, the model with inverse emissions yields a better simulation of the observed peaks than the inventory emissions for both May and November 2016. The measurements suggest that Burncluith has more frequent cases of peaks in methane than Ironbark which are related to a higher proportion of low wind conditions coupled with the possibility of local, intermittent sources in the vicinity of the monitoring stations which are not (or cannot be) accounted for in the model. Although the impact of some of these sources is filtered out by the CO filter, the filter is based statistically and does not eliminate all occurrences of local, non-accounted for emissions (i.e. biomass burning) contributing to the observed methane.

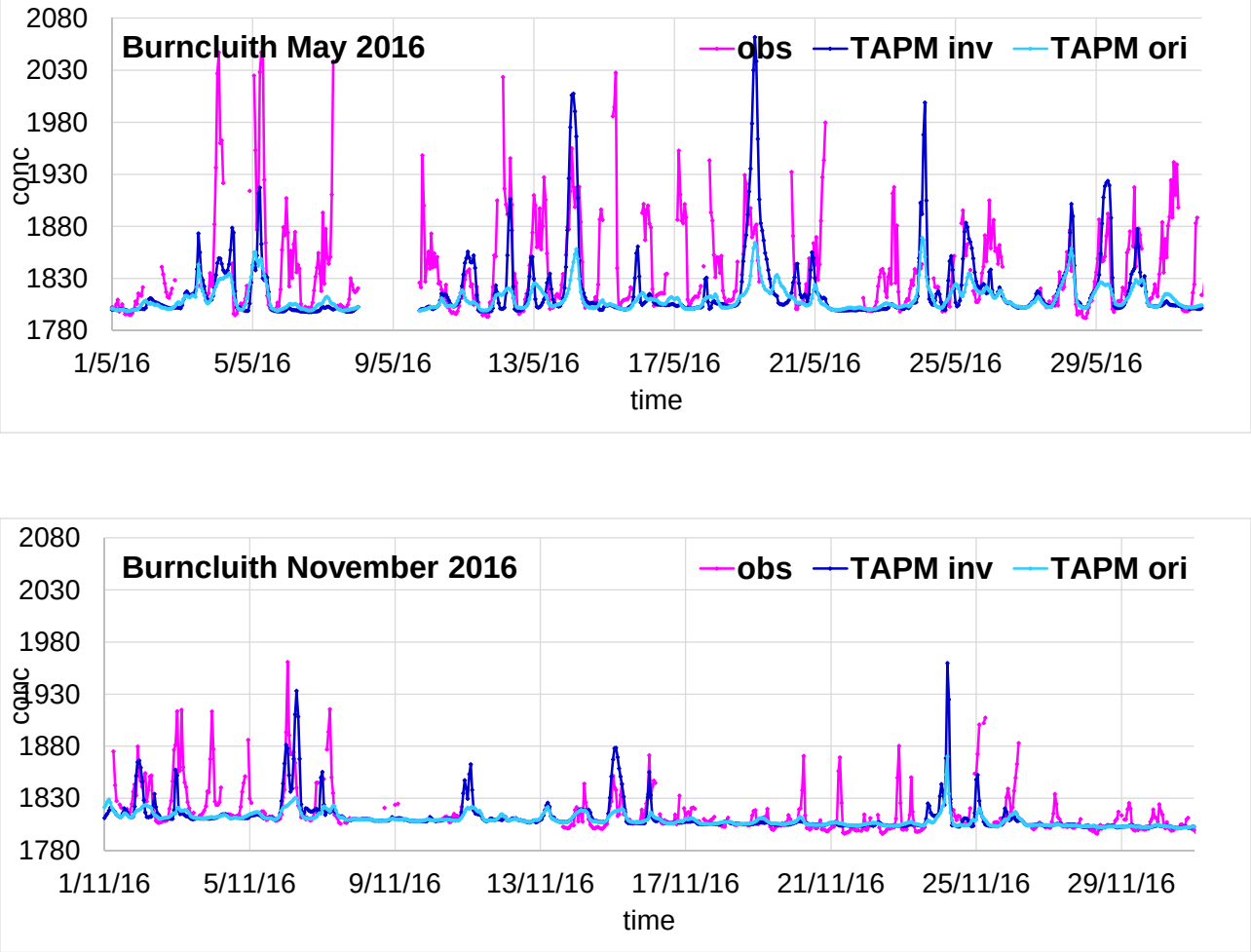

Figure 38. Hourly averaged methane concentration at Burncluith for the months of May 2016 (top) and November 2016 (bottom). Magenta lines are observations, light blue lines are forward TAPM results using the original bottom-up inventory emissions, dark blue lines are forward TAPM results using the inverse emissions from the Case 3 top-down inversion.

5.6.5 Subdomain emissions

The domain-wide emissions obtained from Cases 1, 2 and 3 are: 162.1 x 10^6, 142.6 x 10^6 and 165.8 x 10^6 kg yr^{-1}, respectively, which are lower by 6.4%, 17.7% and 4.2% compared to the bottom-up inventory total emission of 173.163 x 10^6 kg yr^{-1}. Despite the bottom-up inventory emissions being higher (in terms of the total) they yield modelled methane concentrations at Ironbark and

Burncluith that are lower than those obtained using the inverse emission estimates in TAPM. The reason for this is that compared to the bottom-up emission inventory, the inverse methodology generally infers larger emissions closer to the monitoring stations and lower in other areas of the domain, with the domain-wide total being lower. (As was mentioned earlier, one reason for lower emissions in some of the farther subregions of the domain under consideration could be the limitation that the two monitoring sites cannot adequately sample these subregions.) The emissions close to the monitoring sites impact the concentrations at these sites the most because of their larger magnitudes and shorter transport distances. These nearby emissions obtained from the inverse methodology represent the measurements better than the bottom-up inventory emissions.

It is thus instructive to determine and compare estimated emissions from a subdomain area that covers the middle of the domain and encompasses the two monitoring stations. These are the areas that influence the monitoring stations the most, are better sampled and contain some of the highest emission rates. Figure 39 shows the subset of sources (solid circles, covering an area of approximately 155 km x 155 km) considered for aggregating emission rates.

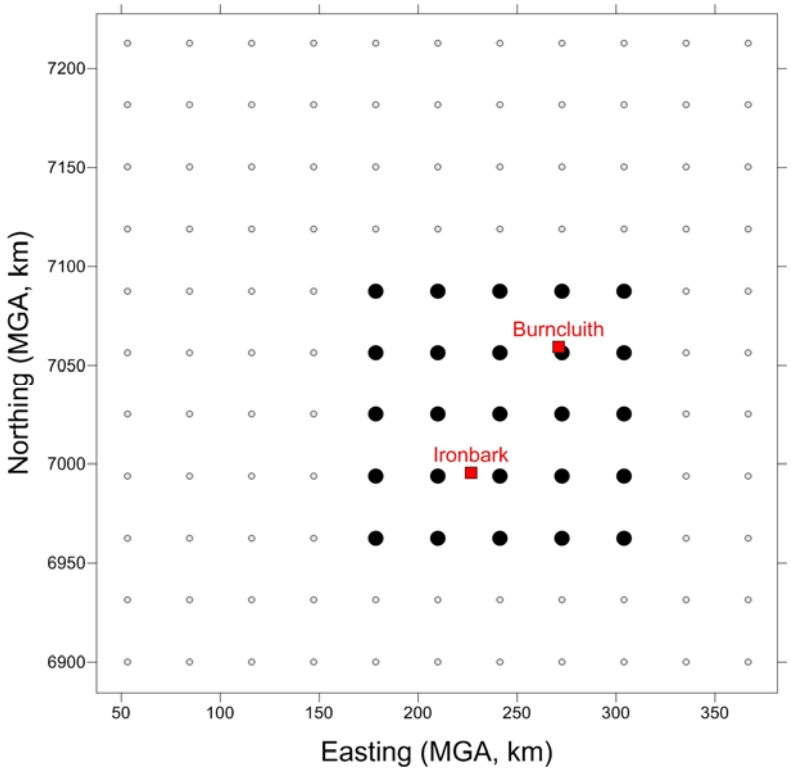

Figure 39. A subset of sources (solid circles) considered for aggregating emission rates. The monitoring site locations are also shown.

The bottom-up inventory emission for the subdomain shown in Figure 39 is 47.67 x 10^6 kg yr^{-1} whereas that obtained using the inversion (Case 3) is 62.66 x 10^6 kg yr^{-1} which is about 30% higher than the inventory emissions. Increasing the bottom-up emissions in the subdomain by 30% would lead to a better representation of the observed methane levels. The total emission represented by the inventory for this source subregion is dominated by feedlots + poultry + piggeries (30%),

followed by cattle grazing (28%) and CSG processing (27%) sectors. These source sectors have uncertainties in their bottom-up emissions rates (Appendix B). Further, emissions from a number of potential methane sources (land clearing, biomass burning, wetlands, ground water wells, and fuel usage and material handling associated with mining activities) are not included in the bottom-up inventory.

On the other hand, all types of methane sources are represented in the model-inferred emission estimates. The inverse methodology does not differentiate between sectors for a given source location, only total emissions are calculated, and therefore, inferred emissions from component sectors are not calculated. Without source discrimination (for example, by using tracers such as the methane isotopic signature) it is not possible to identify which, if any, of the main sources sectors may be under represented by the inventory.

5.6.6 Discussion and limitations

We were able to infer the methane source distribution across a wide region of the Surat Basin by using the available methane concentrations measured during July 2015 – December 2016 at both Ironbark and Burncluith by using these data in a Bayesian inverse modelling setup. By considering two spatially separate stations (instead of one) with precise, well calibrated and continuous concentration data increases the sample size and improves source triangulation, thus strengthening the quality of source determination. Selection of the data for suitable dispersion conditions and filtering to remove the unwanted effects of nearby cow emissions and combustion sources proved beneficial in determining the main regional sources.

The Case 3 inversion provides the best emission estimates, which is evident from its performance in describing the methane measurements from Ironbark and Burncluith (this obviously assumes that the modelled regional meteorology governing plume transport is representative of the true meteorology of the area). The inverse modelling suggests that some source regions between Ironbark and Burncluith have relatively high emission rates compared to the inventory emissions. The inferred emissions imply less intense sources than the emission inventory estimates east of Ironbark close to the domain boundary.

There are various assumptions and parameter uncertainties in the modelling, which include the assumption that all sources emit at constant rate throughout the selected period. Modelled meteorology is an approximation of the real-world meteorology, and differences between the two would cause differences in plume transport, reducing prediction accuracy. We have considered 121 point source locations for source inference. Other source configurations (e.g. area source) could also be considered with further model development.

The 121 source configuration is limited in terms of the number and type of sources (i.e. point sources). But such a configuration is required due to the limitation on the amount of information available (i.e. only two monitoring stations). The point source setup is sensitive to prior emission rate specification, especially its uncertainty. The inverse modelling needs to be developed further to be able to handle other source types such as area and line sources.

Stronger priors provide a better-constrained source estimate and the bottom-up emission inventory proved useful as a prior. However, even a prior with no information from the inventory gave reasonable source distributions and total emission across the full domain, which were

broadly consistent with the independent bottom-up emissions inventory. Given the large size of the domain considered, there was a limit as to how effectively only two stations could sample sources from the whole domain. Additional stations would have been useful to cover the domain better.

The inverse methodology also showed that even a Gaussian prior with a uniform mean throughout the domain could yield emission estimates that describe the methane measurements better than the inventory emissions.

Some potential sources including biomass burning and wetlands are not accounted for in the emissions inventory and forward modelling. The influence of biomass burning, which impacts Burncluith more than Ironbark, is partly filtered out via discarding of the high CO events. Wetlands emissions have no standardised methodology for reporting and they are not given in the Australian National Greenhouse Gas Inventory. There is limited wetland extent in the region of interest (Lehner and Döll, 2004; DES, Queensland, 2018; land use and terrain databases in TAPM) and modelled emissions from this part of Australian appear negligible, at least at limited resolution (Zhu et al., 2015). Wetland emissions would however likely be included in the total methane emissions inferred by the inverse modelling.

Ground seeps and river seeps identified and quantified in earlier CSIRO surveys (Day et al., 2013; 2014; 2015) were included in the bottom-up emission inventory for our model analysis. Methane seeps in the Condamine River are a well quantified and conspicuous source that have received much attention. However, they are a relatively minor emission compared to the other methane sources in the region and our modelling implies that they would not have a large detectable influence on methane concentrations at either of our monitoring stations. Although identified ground seeps were included, it is possible that there are other seeps in the region which are not accounted for in the emission inventory. If sustained and significant in magnitude, these would be included in the inverse model derived emissions, though it wouldn't be possible to discriminate them from other methane sources.

The modelling results presented here provide a useful demonstration of the capability and potential of the Bayesian inference coupled with the calculation of the source-receptor relationship using the backward dispersion approach for source estimation at regional scale.

6 Summary and conclusions

The results presented in this report demonstrate an approach to infer regional emissions of methane across the Surat Basin, using a combination of methane concentration measurements, plume transport modelling, and a Bayesian inference technique. To our knowledge, this study is the first to infer regional emissions of methane in Australia in this way.

An analysis and modelling of methane concentration data from the Ironbark and Burncluith monitoring stations in the Surat Basin was undertaken. The study used concurrent measurements from a period July 2015 – December 2016, which also included meteorological measurements. The two stations were sited based on earlier modelling work (Day et al., 2015) so as to sample potential emission source areas located in the proximity of and between the two sites, which were approximately 80 km apart. Given the emphasis on regional scale emission modelling, intermittent elevated methane measurements due to cattle in the close proximity of the two stations, particularly at Burncluith, were filtered out (Etheridge et al., 2017).

A gridded "bottom-up" methane emissions inventory for the region (≈ 350 km x 350 km) was constructed with various sector contributions (Katestone, 2018), with the largest contribution being from cattle grazing (54%) followed by feedlots (24%) and CSG processing (8.4%) and the total emissions being approximately 173 x 10^6 kg yr^{-1}. This bottom-up emission inventory was further processed and used in CSIRO's regional scale meteorological and air pollution model, TAPM, which is a forward dispersion model and calculates ambient concentration given emission rates. A methodology was devised to estimate hourly varying regional background concentration of methane and this was added to the hourly mean modelled methane for comparison with the data.

The performance of the model for near-surface wind speed and direction, which is a controlling parameter for plume dispersion, was found to be good except that the model had difficulty in simulating nocturnal low winds, particularly at Burncluith, which is a well-known problem with meteorological models. Consequently, a day time filter (1000-1700 h) and a nighttime filter (1800-0900 h with wind speed greater than 3 m s^{-1}) were applied to select the methane measurements for modelling purposes. Additionally, hours with high CO concentration (> 10 ppb above the background) were also filtered out. These hours represent local biomass burning events that are not accounted for in the inventory.

The forward TAPM dispersion modelling using the bottom-up methane emission inventory provided a credible simulation of the observed methane concentration distributions (unpaired in time) at Ironbark and Burncluith, except that the model underestimated approximately the top 15% of the concentrations. The likely reasons for this underestimation include underestimation of emissions from sources close to the monitoring sites, potential presence of time-varying, intermittent or additional sources that are not accounted for in the bottom-up emission inventory, and errors in modelled meteorology and transport.

The forward modelling also showed that the top three contributors to the overall averaged modelled methane at both Ironbark and Burncluith are Grazing cattle, Feedlot + Poultry +

Piggeries, and CSG Processing. These are also the top three contributors to the highest 5% of the modelled concentrations at Burncluith but in contrast these at Ironbark are CSG Processing, Feedlot + Poultry + Piggeries, and Grazing cattle.

A regional inverse model that computes emissions using ambient concentration measurements was formulated for the Surat Basin. It is based on the Bayesian inference approach, coupled with TAPM in a backward meteorological and dispersion mode for the calculation of the required source-receptor relationship. The inverse model was first tested for a 'synthetic' case in which modelled concentrations were treated as ambient concentration measurements. It yielded a stable and consistent solution, giving confidence in the computational techniques.

The extension and application of the inverse model for estimating methane emissions in the Surat Basin using the filtered measurements from Ironbark and Burncluith led to the following conclusions:

Even when we do not specify any prior (except for some loose bounds on the emission rate), the information contained in just the concentration time series from the two monitoring stations is generally able to constrain the total emissions realistically. However, compared to the bottom-up inventory emissions the estimated emissions are more concentrated in some areas in the middle of the domain and less in the areas further away.

Specifying a prior in the Bayesian inversion is important and the use of a more realistic prior leads to better source estimates. The bottom-up emission inventory proved very effective as a prior. The use of Gaussian prior PDFs with mean values across the domain the same as given by the bottom-up inventory emissions with a standard deviation of 3% of the mean value provided a more consistent source emission estimates.

The domain-wide inverse estimate of methane emission is 166×10^6 kg yr^{-1} which is slightly lower than the total bottom-up inventory emission. However, in a subdomain of approximately 155 km x 155 km covering areas between and immediately around the two stations, the estimated emissions are 30% higher than the bottom-up inventory emissions. These higher emissions describe the methane measurements much better when used in forward modelling than do the bottom-up inventory emissions. Emissions from feedlots, poultry, piggeries, grazing cattle and CSG dominate the emissions inventory in this area. There are also potentially other sources not accounted for in the inventory. For example, where detected and quantified by the ground survey, seeps are included in the emission inventory, but it is possible that not all seeps were detected. The causes of this emission difference within the subdomain could be understood or explained by follow up studies using ground surveys.

The inverse modelling is limited by having only two monitoring stations across a wide area that contains many methane sources. It was shown that Ironbark and Burncluith do not sample some distant areas adequately, particularly those located in the north-west and south-east of the domain. Thus, potential sources in these areas would not have been as well estimated. The modelling makes assumptions about the sources that contribute to the measured concentrations, including that they are steady in time and are all contained within the model domain. It relies on the source-receptor relationship (derived from the transport model with modelled meteorology with its own inherent uncertainty) being accurate across the region. These are typical difficulties of inverse modelling.

The study (both measurements and the emissions inferred from them) does not distinguish between different source sectors. To do source attribution, measurements of tracers specific to source sectors (such as isotopes of methane, $^{13}CH_4$, CH_3D) would be useful (Day et al., 2015), when instrumentation suitable for field deployment becomes available.

Although the use of the inverse emission estimates in forward mode showed an improvement in the prediction of nighttime methane concentrations compared to the bottom-up emission inventory, the model physics still needs improvement to deal with low-wind, stable conditions at night.

Overall, the strategy of siting two long-term monitoring stations based on the meteorology of the area and the known source distribution of interest worked well. Two measurements stations were adequate for sampling source areas between and around them. The bottom-up emission inventory informed by the ground-based measurements in the inverse modelling gave results that were realistic in both their total and distribution.

References

Alvarez, R. A., Zavala-Araiza, D., Lyon, D. R., et al., Assessment of methane emissions from the U.S. oil and gas supply chain. Science 10.1126/science.aar7204, 2018.

Bandeira, J. M., Coelho, M. C., Sa, M. E., Tavares, R., Borrego, C. Impact of land use on urban mobility patterns, emissions and air quality in a Portuguese medium-sized city. Science of the Total Environment 409, 1154–1163, 2011.

Brandt, A. R., Heath, G. A., Kort, E. A., O'Sullivan, F. Methane leaks from North American natural gas systems, Science, 343(6172), 733–735, 2014.

CSIRO, 2004. Meteorological and Dispersion Modelling Using TAPM for Wagerup: Phase 1: Meteorology, Report to Alcoa World Alumina Australia, 103 pp (https://www.alcoa.com/australia/en/pdf/WAG_AG_phase1_report_20041202pt1.pdf), 2004.

DES (Department of Environment and Science), Queensland, Wetland Info, extracted June 2018 https://wetlandinfo.ehp.qld.gov.au/wetlands/facts-maps/get-mapping-help/wetland-maps/#wetlandmaps

Day, S., Dell 'Amico, M., Etheridge, D., Ong, C., Rodger, A., Sherman, B. et al. Characterisation of Regional Fluxes of Methane in the Surat Basin, Queensland. Phase 1: A Review and Analysis of Literature on Methane Detection and Flux Determination. CSIRO Australia report, 2013.

Day, S., Dell'Amico, M., Fry, R., Javanmard Tousi, H. Field Measurements of Fugitive Emissions from Equipment and Well Casings in Australian Coal Seam Gas Production Facilities. CSIRO Australia report, 2014.

Day, S., Ong, C., Rodger, A., Etheridge, D., Fry, R., Dell'Amico, M., Sestak, S., Williams, D., Loh, Z., and Barrett, D. Characterisation of Regional Fluxes of Methane in the Surat Basin, Queensland: Phase 2: A Pilot Study to Detect and Quantify Methane Sources. Australia report, 2015.

Day, S., Tibbett, A., Sestak, S., Knight, C., Marvig, P., McGarry, S., Weir, S., White, S., Armand, S., van Holst, J., Fry, R., Dell'Amico, M., Halliburton, B., Azzi, M. Methane and Volatile Organic Compound Emissions in New South Wales. CSIRO Australia report, 2016.

Day, S., Luhar, A., Etheridge, D., Hibberd, M., Thatcher, M., Loh, Z., Noonan, J., Marvig, P., Weir, S., Halliburton, B., Improving Methods for Quantifying Fugitive Emissions from Open-Cut Coal Mining. ACARP Project C24017 report, CSIRO Australia, 80 pp., 2017.

Emmerson, K., Reisen, F., Luhar, A., Williamson, G., Cope, M. Air Quality Modelling of Smoke Exposure from the Hazelwood Mine Fire. CSIRO Australia report, 45 pp., http://hazelwoodhealthstudy.org.au/wp-content/uploads/2017/01/Hazelwood_AirQualityModelling_December2016_Final.pdf, 2016.

Etheridge, D. M., Day, S., Hibberd, M. F., Luhar, A., Spencer, D. A., Loh, Z. M., Zegelin, S., Krummel, P. B., van Gorsel, E., Thornton, D. P., Gregory, R. L., Ong, C., and Barrett, D. Characterisation of Regional Fluxes of Methane in the Surat Basin, Queensland - Milestone 3.1 GISERA Greenhouse Gas Research – Phase 3. CSIRO Australia report, 2016.

Etheridge, D., Luhar, A., Loh, Z., Noonan, J., Spencer, D. A., Day, S., Hibberd, M., Zegelin, S., Kitchen, M., Thornton, D., Gregory, R., Krummel, P., Halliburton, B., Barrett, D. Characterisation of Regional Fluxes of Methane in the Surat Basin, Queensland. Interim report on Task 3: Broad scale application of methane detection, and Task 4: Methane emissions enhanced modelling, CSIRO, Australia, 2017.

Feitz, A., Schroder, I., Phillips, F., et al. The Ginninderra CH_4 and CO_2 release experiment: An evaluation of gas detection and quantification techniques. International Journal of Greenhouse Gas Control 70, 202–224, 2018.

Humphries, R., Jenkins, C., Leuning, R., Zegelin, S., Griffith, D., Caldow, C., Berko, H., Feitz, A. Atmospheric tomography: A Bayesian inversion technique for determining the rate and location of fugitive emissions. Environmental Science and Technology, 46, 1739–1746, 2012.

Hurley, P. J., Physick, W. L., Luhar A. K. TAPM: a practical approach to prognostic meteorological and air pollution modelling. Environmental Modelling and Software, 20, 737–752, 2005. Hurley, P., Edwards, M., Luhar, A. TAPM V4. Part 2: Summary of Some Verification Studies. CSIRO Marine and Atmospheric Research Paper No. 28. 31 pp (https://www.cmar.csiro.au/research/tapm/docs/tapm_v4_technical_paper_part2.pdf), 2008.

IPCC: Climate Change 2014: Mitigation of Climate Change. Contribution of Working Group III to the Fifth Assessment Report of the Intergovernmental Panel on Climate Change, edited by: Edenhofer, O., Pichs-Madruga, R., Sokona, Y., Farahani, E., Kadner, S., Seyboth, K., Adler, A., Baum, I., Brunner, S., Eickemeier, P., Kriemann, B., Savolainen, J., Schlömer, S., von Stechow, C., Zwickel, T., and Minx, J. C., Cambridge University Press, Cambridge, UK, 2014.

Jaynes, E. T. Probability Theory: The Logic of Science, Cambridge University Press, Cambridge, UK, 753 pp., 2003.

Katestone, 2018. Surat Basin Methane Inventory 2015 – Summary Report. Prepared by Katestone Environmental for CSIRO, 2018.

Lafleur, D., Forcey, T., Saddler, H., and Sandiford, M. A review of current and future methane emissions from Australian unconventional oil and gas production. Melbourne Energy Institute, University of Melbourne, 89 pp. 2016.

Lehner, B., and Döll, P., Development and validation of a global database of lakes, reservoirs and wetlands. Journal of Hydrology, 296, 1-22, 2004.

Luhar, A. K., Hurley, P. J. Evaluation of TAPM, a prognostic meteorological and air pollution model, using urban and rural point-source data. Atmospheric Environment 37, 2795–2810, 2003.

Luhar, A. K., Mitchell, R. M., Meyer, C. P., Qin, Y., Campbell, S., Gras, J. L., Parry, D. Biomass burning emissions over northern Australia constrained by aerosol measurements: II–Model

validation, and impacts on air quality and radiative forcing. Atmospheric Environment 42, 1647–1664, 2008.

Luhar, A. K., Hurley, P. J., Rayner, K. N. Modelling near-surface low winds over land under stable conditions: sensitivity tests, flux-gradient relationships, and stability parameters. Boundary-Layer Meteorology 130, 249–274, 2009.

Luhar, A. K., Hurley, P. J. Application of a coupled prognostic model to turbulence and dispersion in light-wind stable conditions, with an analytical correction to vertically resolve concentrations near the surface. Atmospheric Environment 51, 56–66, 2012.

Luhar, A. K., Etheridge, D. M., Leuning, R., Loh, Z. M., Jenkins, C. R., Yee, E. Locating and quantifying greenhouse gas emissions at a geological CO_2 storage site using atmospheric modeling and measurements. Journal of Geophysical Research: Atmospheres 119, 10959–10979, 2014.

MacFarling Meure, C. M., Etheridge, D. M., Trudinger, C. M., Steele, L. P., Langenfelds, R. L., van Ommen, T. D., Smith, A., Elkins, J. W. Law Dome CO_2, CH_4 and N_2O ice core records extended to 2000 years BP. Geophysical research letters, 33, L14810, doi:14810.11029/12006GL026152, 2006.

Meinshausen, M., Vogel, E., Nauels, A., Lorbacher, K., Meinshausen, N., Etheridge, D., Fraser, P., Trudinger, C., Krummel, P., Canadell, P., Law, R., Rubino, M., Montzka, S., Rayner, P., Beyerle, U., Daniel, J., Enting, I., O'Doherty, S., Prinn, R., Reinmann, S., Velders, G., Vollmer, M., Weiss, R., Historical greenhouse gas concentrations for climate modelling (CMIP6), Geosci. Model Dev., 10, 2057-2116, https://doi.org/10.5194/gmd-10-2057-2017, 2017.

Michalak, A. M., Hirsch A., Bruhwiler L., Gurney, K. R., Peters, W., Pieter P. Tans, P. P. Maximum likelihood estimation of covariance parameters for Bayesian atmospheric trace gas surface flux inversions. Journal of Geophysical Research: Atmospheres 110, D24107, doi: 10.1029/2005JD005970, 2005.

Paumier, J. O., Perry, S. G., Burns, D. J. CTDMPLUS: a dispersion model for sources near complex topography. Part II: performance characteristics. Journal of Applied Meteorology 31, 646–660, 1992.

Pétron, G., Frost, G., Miller, B. R., Hirsch, A. I., Montzka, S. A., Karion, A., Trainer, M., Sweeney, C., Andrews, A. E., Miller, L., Kofler, J., Bar-Ilan, A., Dlugokencky, E.J., Patrick, L., Moore Jr., C.T., Ryerson, T.B., Siso, C., Kolodzey, W., Lang, P.M., Conway, T., Novelli, P., Masarie, K., Hall, B., Guenther, D., Kitzis, D., Miller, J., Welsh, D., Wolfe, D., Neff, W., Tans, P. Hydrocarbon emissions characterization in the Colorado Front Range: A pilot study. Journal of Geophysical Research-Atmospheres, 117. D04304, 2012.

Rao, K. S. Source estimation methods for atmospheric dispersion. Atmospheric Environment 41, 6964–6973, 2007.

Rayner, P., Utembe, S. Modelling the Airborne Dispersion of Pollutants from Coal Seam Gas Extraction. Reports commissioned by the NSW Chief Scientist & Engineer for the Independent Review of Coal Seam Gas Activities in NSW. Available at http://www.chiefscientist.nsw.gov.au/coal-seam-gas-review/csg-backgroundpapers, 2014.

Saddler, H., Gotham, K. Review of methods for the estimation of greenhouse gas emissions from diffuse sources associated with unconventional gas fields, Pitt and Sherry, Australia, 2013.

Saunois, M., et al. The global methane budget: 2000–2012, Earth Syst. Sci. Data, 8, 697–751, doi:10.5194/essd-2016-25, 2016.

Schneising, O., Burrows, J. P., Dickerson, R. R., Buchwitz, M., Reuter, M., Bovensmann, H. Remote sensing of fugitive methane emissions from oil and gas production in North American tight geologic formations, Earth's Future, 2, 548–558, doi:10.1002/2014EF000265, 2014.

Sherman, B. S., Ford, P. W., Kernke, M. Condamine River coal seam gas emissions: final report. CSIRO Australia, 2014

Tarantola, A. Inverse Problem Theory and Methods for Model Parameter Estimation. Society for Industrial and Applied Mathematics, Philadelphia, 342 p., 2005.

Thoning, K. W., Tans, P. P., Komhyr, W. D. Atmospheric Carbon Dioxide at Mauna Loa Observatory: 2. Analysis of the NOAA GMCC Data, 1974-1985. Journal of Geophysical Research: Atmospheres 94 (D6), 8549–8565, 1989.

Venkatram, A., Brode, R., Cimorelli, A., Lee, R., Paine, R., Perry, S., Peters, W., Weil, J., Wilson, R.: 2001. A complex terrain dispersion model for regulatory applications. Atmospheric Environment 35, 4211–4221.

Willmott, C. J.: On the validation of models, Phys. Geography, 2, 184–194, 1981.

Yee, E., and T. K. Flesch. Inference of emission rates from multiple sources using Bayesian probability theory, Journal of Environmental Monitoring, 12, 622–634, 2010.

Zawar-Reza, P., Sturman, A. Application of airshed modelling to the implementation of the New Zealand National Environmental Standards for air quality. Atmospheric Environment 42, 8785–8794, 2008.

Zhu, Q., Peng, C., Chen, H., Fang, X., Liu, J., Jiang, H., Yang, Y., Yang, G. Global natural wetland methane emissions. Global Ecology and Biogeography, 24: 959-972. doi:10.1111/geb.12307, 2015.

Ziehn, T., Nickless, A., Rayner, P. J., Law, R. M., Roff, G., Fraser, P. Greenhouse gas network design using backward Lagrangian particle dispersion modelling – Part 1: Methodology and Australian test case. Atmospheric Chemistry and Physics 14, 9363–9378, 2014.

Appendix A Modelled contributions by various emissions inventory source categories

To investigate the sources of the modelled concentration that might be detected at Burncluith Figure A.1 and Figure A.2 show TAPM concentration roses at Burncluith for each tracer in the bottom-up emissions inventory as well as the total concentration for comparison (Figure A.1 top left). TAPM models most of the concentration signals occurring at Burncluith to be due to Tracer 1 (Grazing cattle) under all wind conditions, while concentration signals due to the other tracers occur less frequently. Modelled concentrations due to Tracer 2 (Feedlot + Poultry + Piggeries) occur at Burncluith under a northeasterly wind and in larger concentrations when the wind is in the south-westerly sector. Concentrations due to Tracer 3 (CSG Processing) occur at Burncluith under predominantly south-westerly winds, while those due to Tracer 4 (CSG Production) also occur when the wind is from the south-west but with a much smaller modelled concentration, mostly less than 2 ppb. Modelled concentrations due to Tracer 5 (Mining) occur at Burncluith when the wind is southerly to south-easterly, and when the wind is westerly to south-southwesterly. Tracer 6 (River seeps) has modelled concentrations predominantly occurring at Burncluith under south-southwesterly to southwesterly winds similar to concentrations due to Tracer 7 (Wastewater treatment + Domestic wood heating + Motor vehicles). TAPM concentrations due to Tracer 8 (Landfill + Ground seeps) also occur at Burncluith under predominantly south to south-westerly winds while those due to Tracer 9 (Power stations) occur under predominantly south to south-southeasterly winds. The largest modelled concentrations and those that occur most frequently at Burncluith are due to Tracers 1, 2 and 3.

Figure A.3 and Figure A.4 show TAPM concentration roses at Ironbark for each tracer as well as the total concentration for comparison (Figure A.3 top left). TAPM models most of the concentration occurring at Ironbark to be due to Tracer 1 (Grazing cattle), Tracer 2 (Feedlot + Poultry + Piggeries) and Tracer 3 (CSG Processing), while concentrations due to the other tracers occur less frequently. Modelled concentrations at Ironbark due to Tracer 1 (Grazing cattle) occur under all wind conditions, while those due to Tracer 2 (Feedlot + Poultry + Piggeries) occur predominantly when the winds are in the north-east sector with much smaller frequency and values from winds in the south-west sector. Concentrations due to Tracer 3 (CSG Processing) are modelled at Ironbark to occur under winds predominantly from the north-east sector as are those due to Tracer 4 (CSG Production) but with much less modelled concentration. Tracer 5 (Mining) has modelled concentrations when the wind is predominantly in the north-east sector, while those due to Tracer 6 (River seeps) occur at Ironbark under north-northeasterly to northeasterly winds. Modelled concentrations due to Tracer 7 (Wastewater treatment + Domestic wood heating + Motor vehicles) occur at Ironbark at very small values when the wind is easterly, those due to Tracer 8 (Landfill + Ground seeps) occur at Ironbark when the modelled wind is in the north-east sector and those due to Tracer 9 (Power stations) occur under east to east-northeasterly winds. The largest modelled concentrations that occur at Ironbark are due to Tracers 1, 2, 3 and 5.

At Ironbark the modelled wind is most frequently from the north-east sector and the concentrations for all tracers are mostly associated with winds from the north-east. Modelled winds at Burncluith, like those at Ironbark, are generally from the north-east sector but the concentrations for all tracers except for Tracers 1 and 2 are mostly observed when the wind is from the south-west. Tracer 1 is observed at Burncluith from all wind directions but in larger concentrations from the north-east, while Tracer 2 has the largest concentrations when the wind is from the south-west and also registers concentrations when the winds are from the north-east.

Modelled total and tracer concentration roses for Burncluith and Ironbark during daytime hours, 1000-1700, are shown in Figure A.5 and Figure A.6, respectively, while those for nighttime, 1800-0900, are shown in Figure A.7 and A.8, respectively - note that tracer results are not shown when the values are very small. TAPM concentration roses during the nighttime are similar to those for all hours, while during the daytime the concentration values are less than those for all hours at both sites. Generally, during the daytime, concentrations due to Tracer 1 (Grazing cattle) are observed at both sites under all wind directions but not all the time. Concentrations due to Tracer 2 (Feedlot + Poultry + Piggeries) and Tracer 3 (CSG Processing) are modelled to occur at Burncluith when the winds are south-westerly and at Ironbark when the winds are north-easterly, but not at all times.

TAPM output used in the inverse run is CO filtered at Burncluith and has nighttime data removed from both sites at times when the observed site wind speed is < 3 ms^{-1}. Nighttime low wind speeds are associated with a strongly stable nighttime boundary layer in which concentrations are often intensified during the night due to the reduced mixing height and still conditions. Many models struggle to reproduce these low wind speeds and the corresponding increase in concentration. Therefore this filter removes low nighttime wind speed data and hence larger nighttime concentrations of CH_4. The CO filter was primarily applied at Burncluith to remove large CO values most likely associated with bushfires north of Burncluith in the Barakula forest as these are not included as sources in TAPM runs.

The observed CH_4 roses under these conditions are shown in Figure A.9 for all times, daytime (1000 – 1700) and nighttime (1800 – 0900), while the corresponding TAPM concentration roses including those for various tracers are shown in Figures A.10 – A.14. Figure A.9 shows that the observed CH_4 roses at Ironbark with the wind speed filter are very similar to those without the filter (Figure 16), which is expected since Ironbark does not have large frequencies of light nighttime winds. Observed daytime CH_4 roses at Burncluith are also similar to those without the CO filter, although there is less frequent wind from the north and hence less frequent CH_4 observations. The nighttime observed filtered CH_4 rose at Burncluith is quite different to that without the filters (Figure 18), the predominant wind direction is easterly to east-northeasterly, followed by south-southwesterly to west southwesterly – a greater easterly component and southerly component than the unfiltered observations. The CH_4 concentration values are also not as large as those for the unfiltered observations. Figure A.9 also shows the all times observed CH_4 rose with both filters included, concentrations are much less than those for the unfiltered observations and the frequency of CH_4 from the north is reduced.

TAPM concentration roses for the filtered data tracers are shown for Burncluith in Figures A.10 – A.12 for all times, daytime and nighttime, respectively and for Ironbark in Figures A.13 and A.14 for all times and nighttime, respectively. Mostly they show similar results at Ironbark for filtered

and unfiltered data except the magnitude of the concentrations is somewhat reduced in the filtered data. Burncluith, however has much reduced concentrations for the all times, in particular when the wind is in the north-east sector, predominantly due to the nighttime filter.

Generally, the TAPM concentration roses and the observed CH_4 roses are broadly similar, Burncluith shows the largest difference between modelled and observed, unfiltered CH_4 data is observed at Burncluith to come from the north-east sector with greater concentrations than modelled. Filtering reduces this difference.

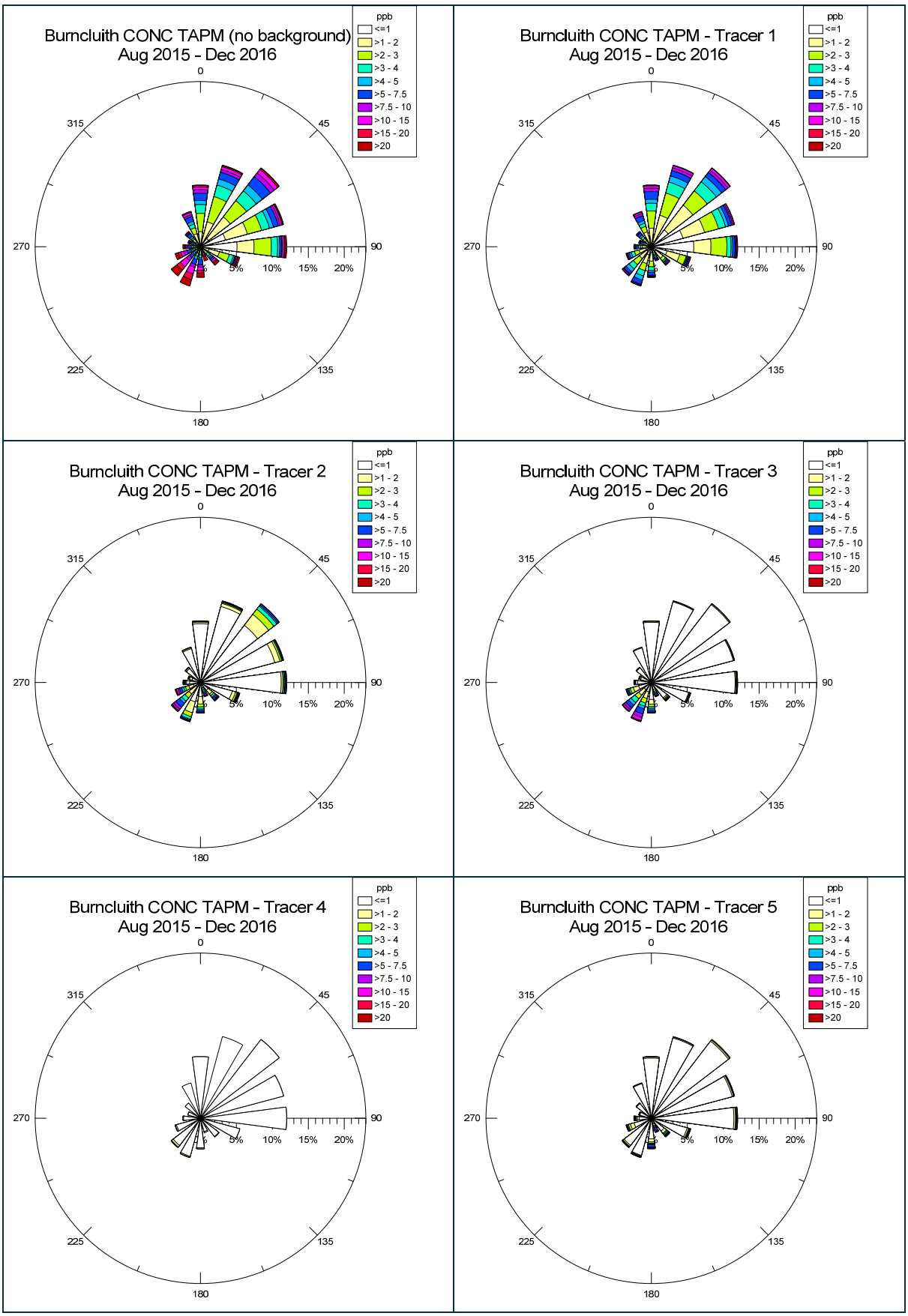

Figure A.1 Modelled methane concentration roses for Burncluith for each tracer (August 2015 to December 2016).

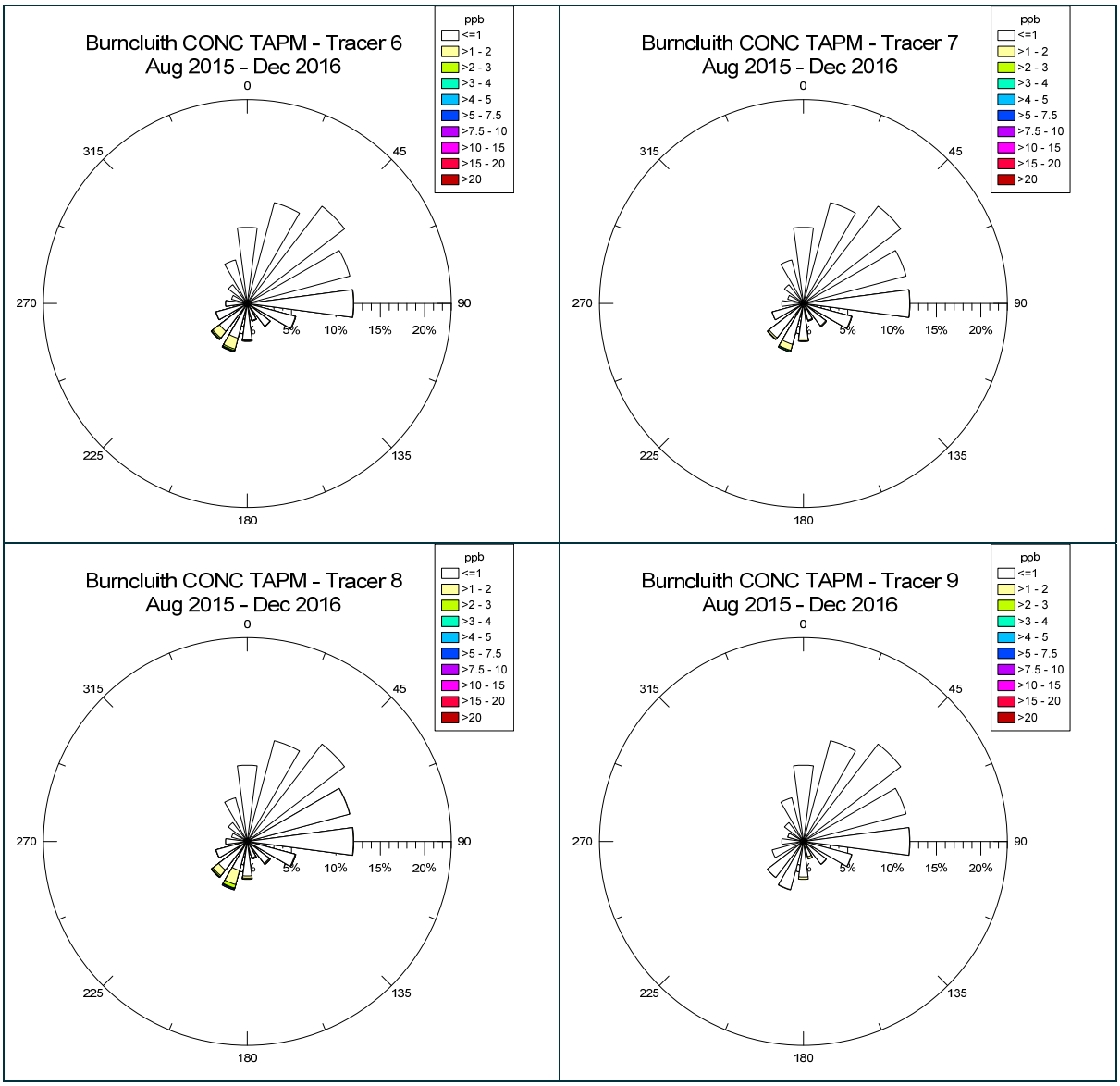

Figure A.2 Modelled methane concentration roses for Burncluith for each tracer (August 2015 to December 2016).

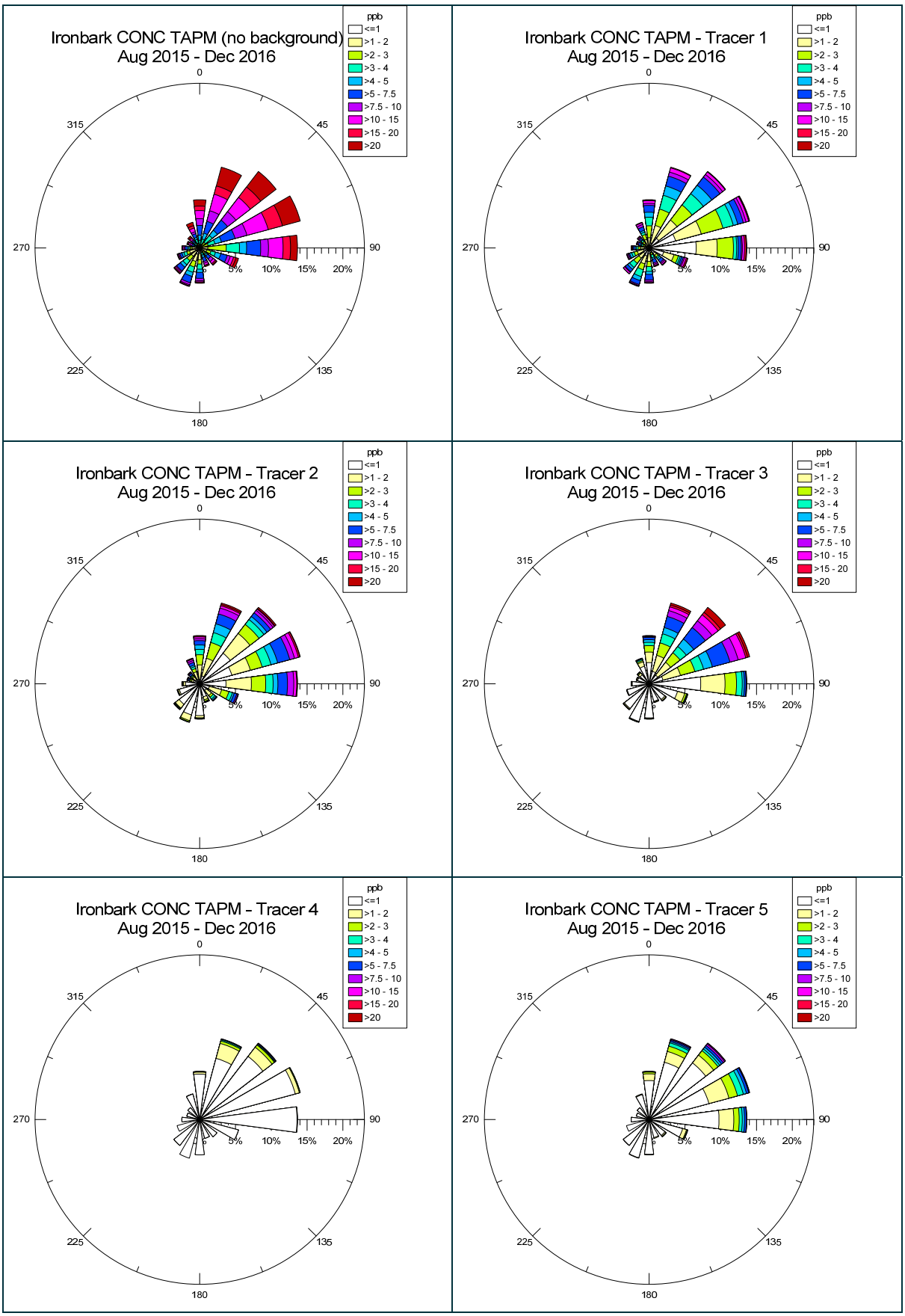

Figure A.3 Modelled methane concentration roses for Ironbark for each tracer (August 2015 to December 2016).

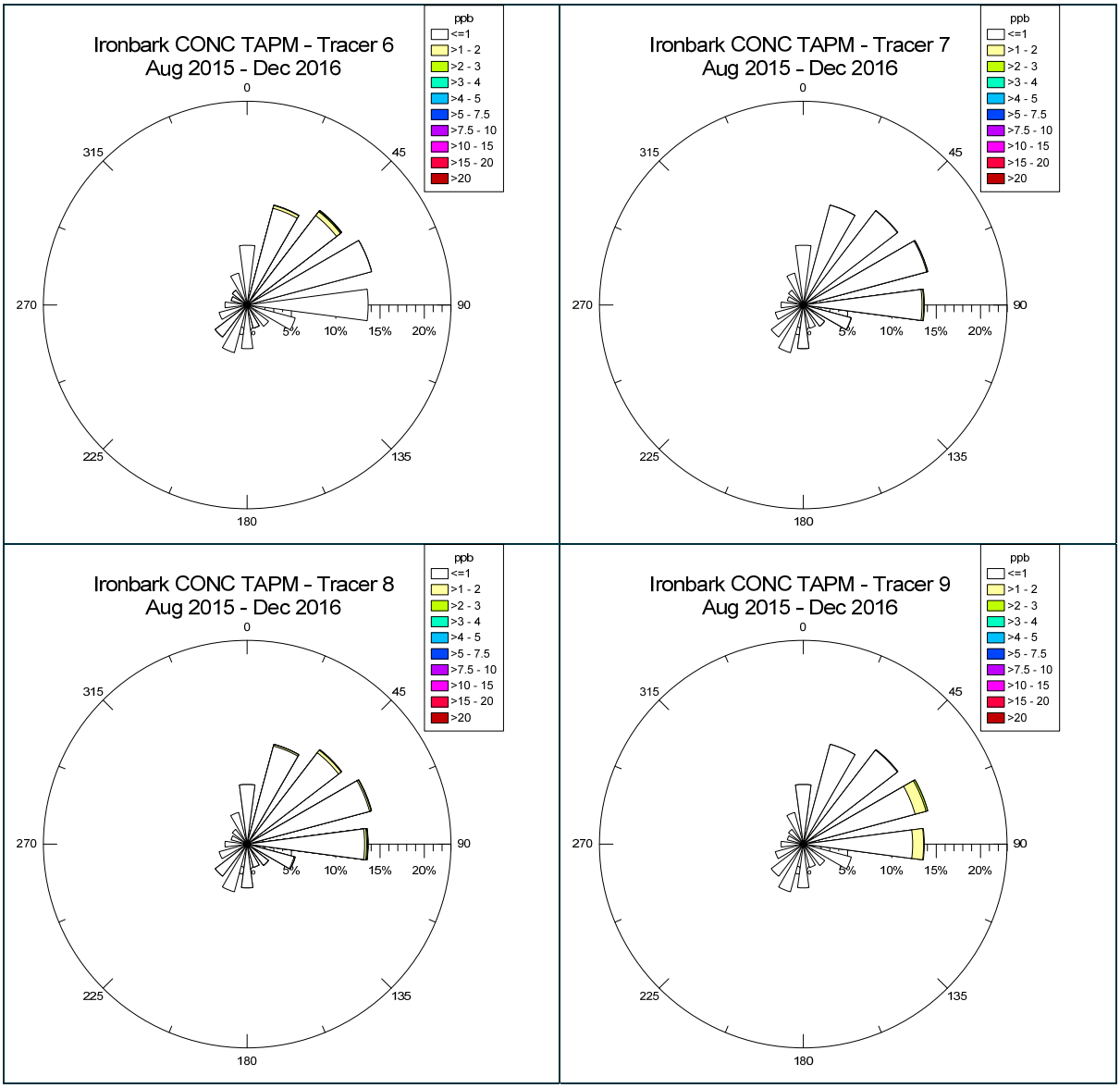

Figure A.4 Modelled methane concentration roses for Ironbark for each tracer (August 2015 to December 2016).

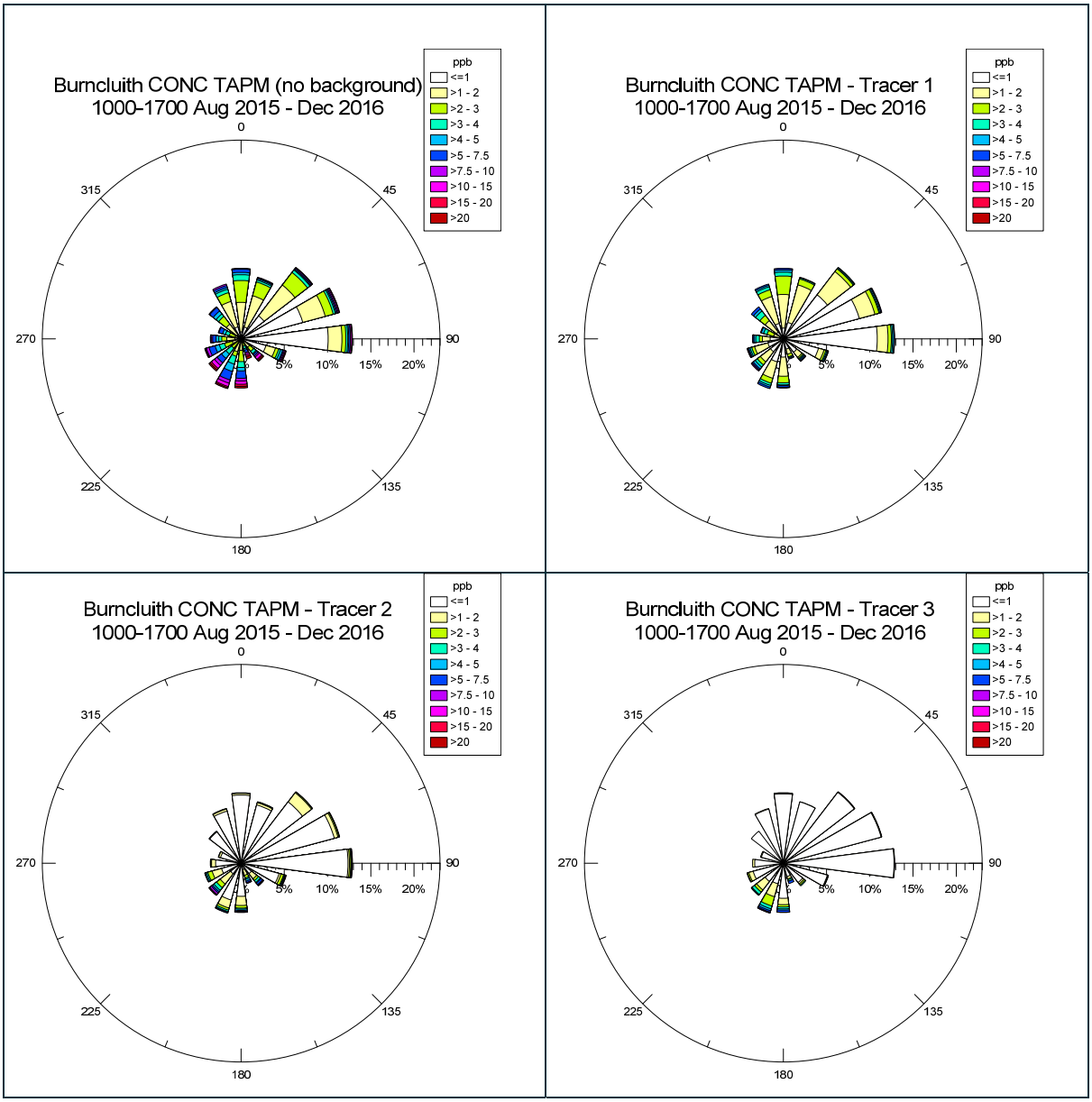

Figure A.5 Modelled methane concentration roses for Burncluith for each tracer for daytime hours only (1000 – 1700 h) (August 2015 to December 2016).

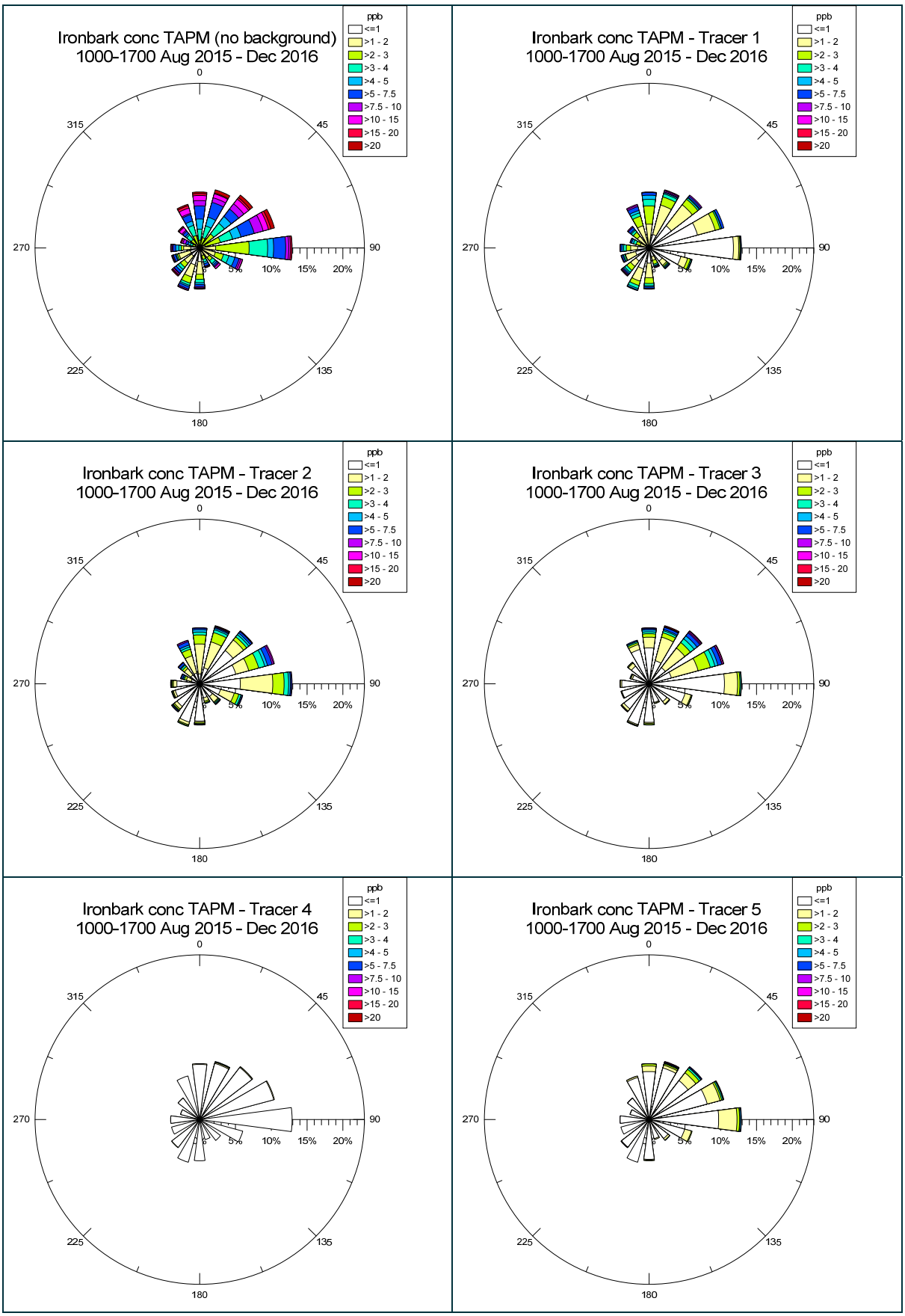

Figure A.6 Modelled methane concentration roses for Ironbark for each tracer for daytime hours only (1000 – 1700 h) (August 2015 to December 2016).

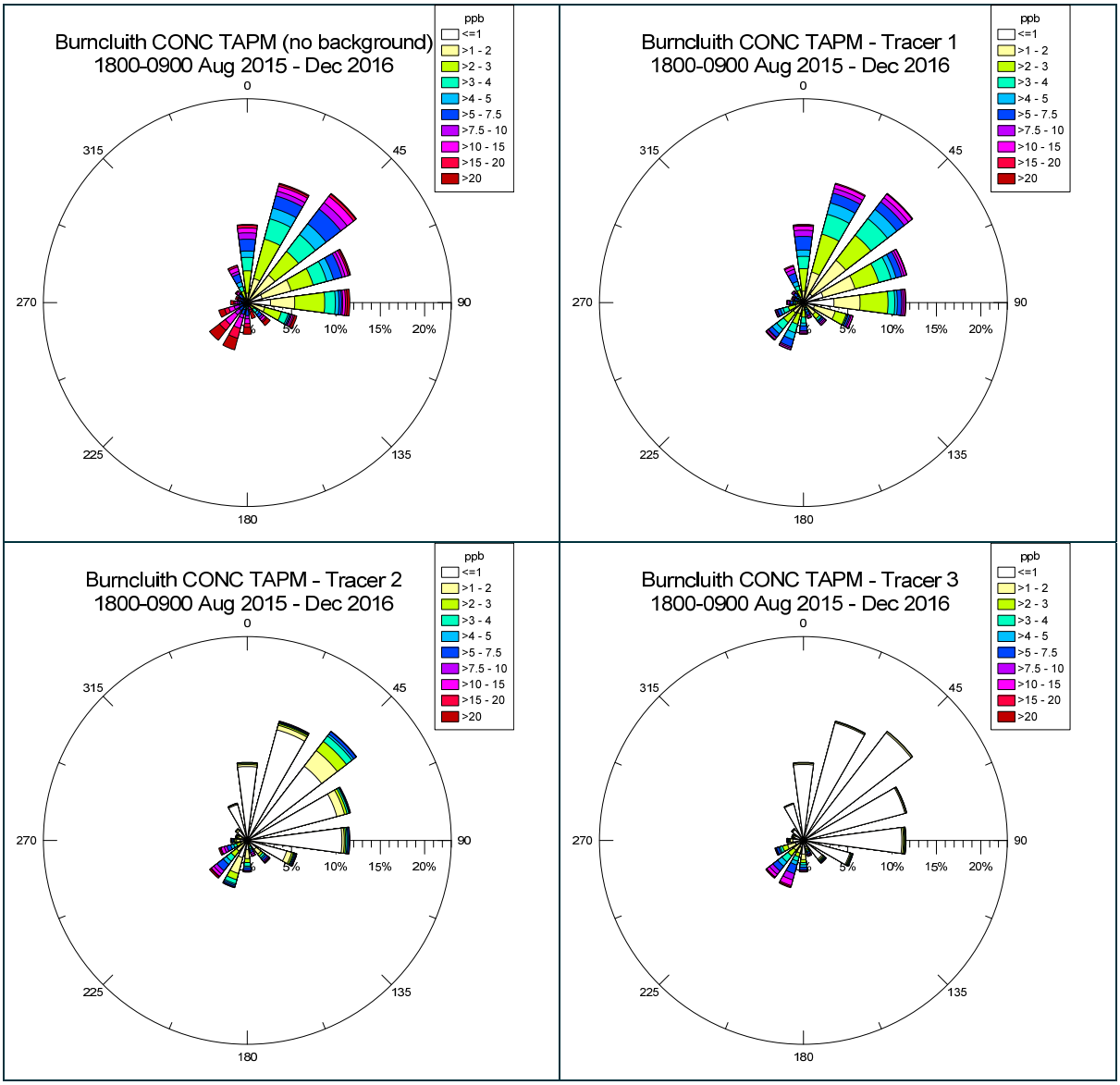

Figure A.7 Modelled methane concentration roses for Burncluith for each tracer for nighttime hours only (1800 – 0900 h) (August 2015 to December 2016).

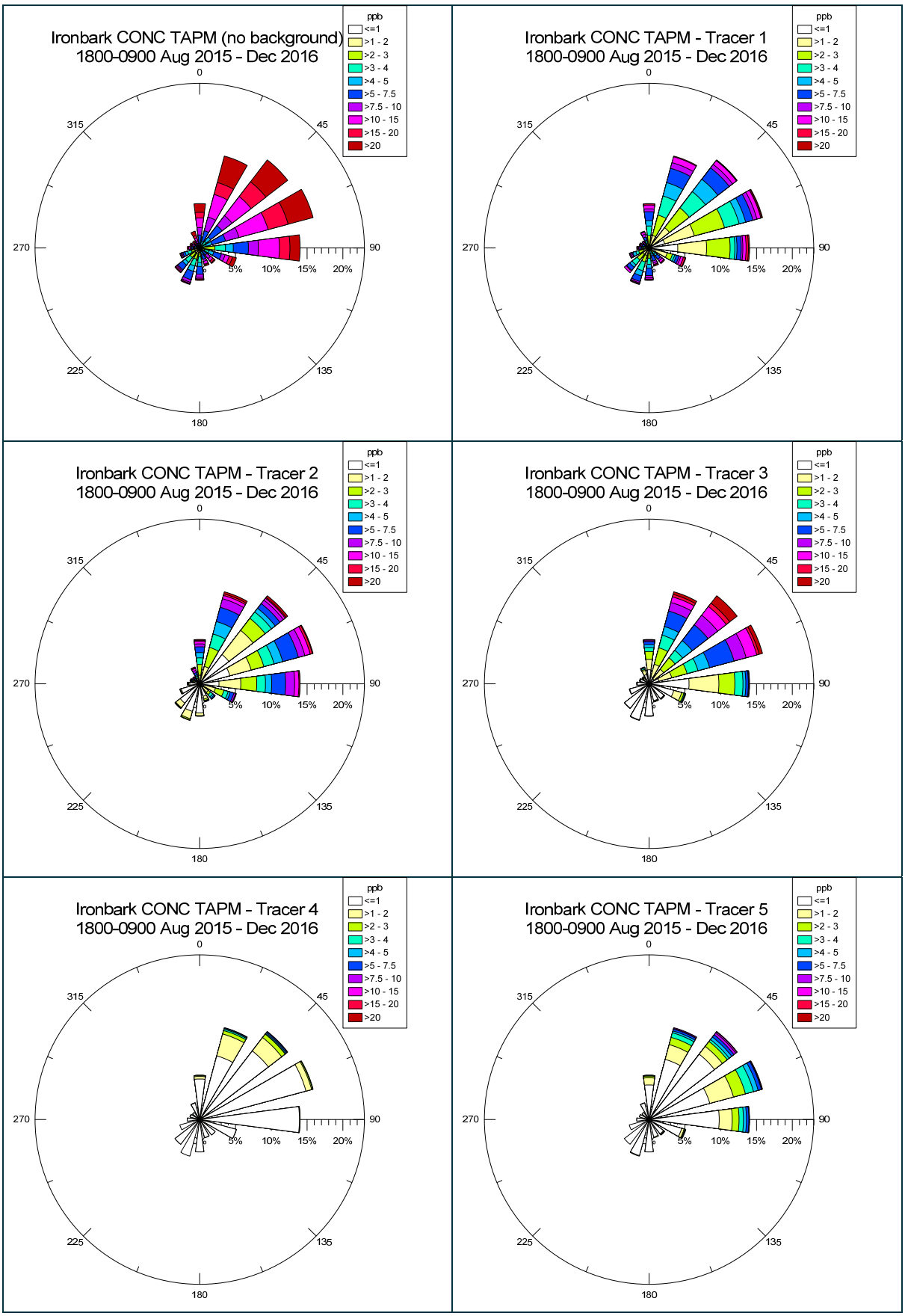

Figure A.8 Modelled methane concentration roses for Ironbark for each tracer for nighttime hours only (1800 – 0900 h) (August 2015 to December 2016).

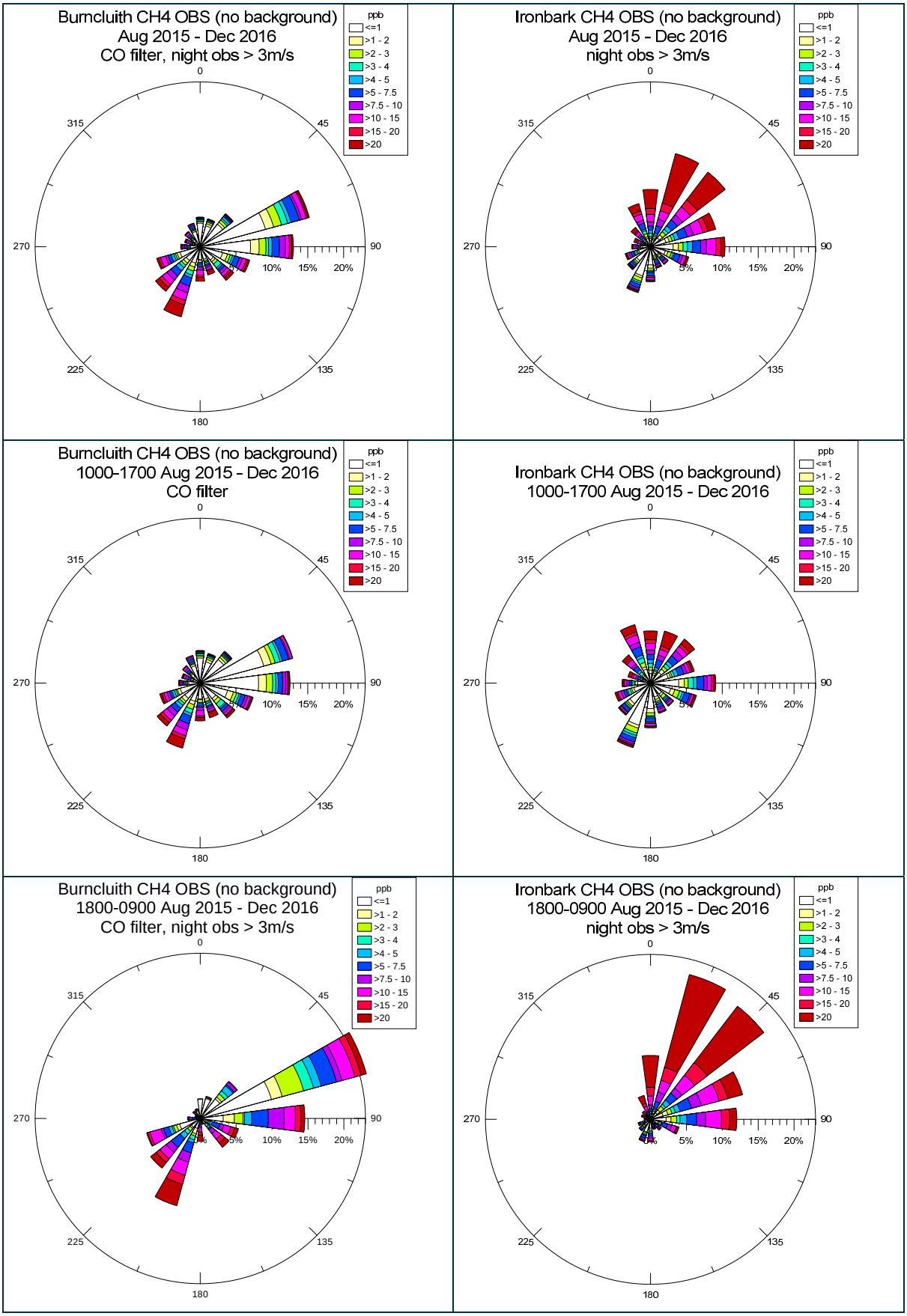

Figure A.9 Observed CH_4 roses for Burncluith and Ironbark, with the wind speed filtered at night to only include times when the observed wind speed is > 3 ms^{-1} and the CO filter applied to Burncluith data. All times, daytime (1000 - 1700) and nighttime (1800 – 0900) are shown. (August 2015 to December 2016).

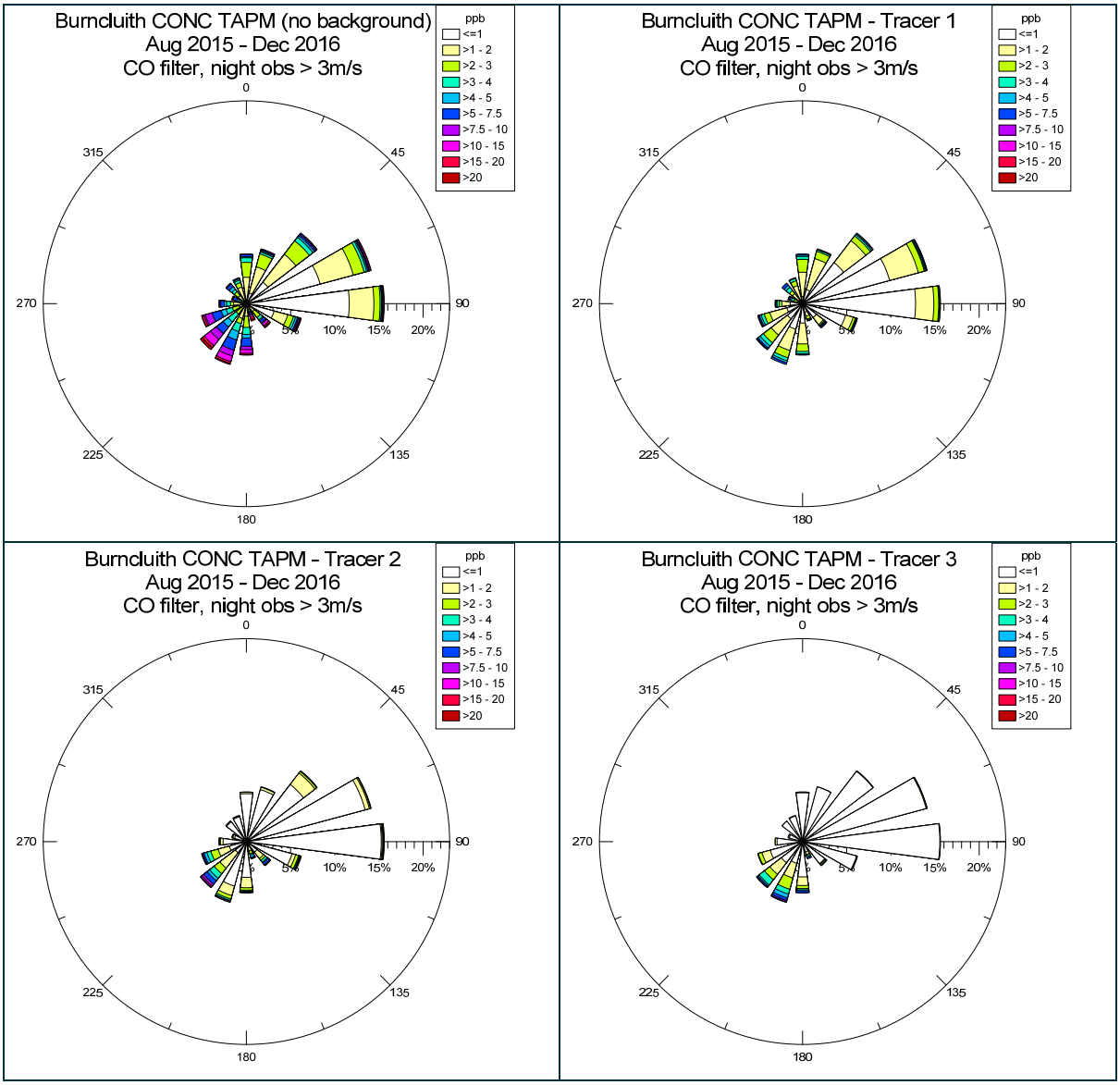

Figure A.10 Modelled methane concentration roses for Burncluith for each tracer, with the CO filter applied and the wind speed filtered at night to only include times when the wind speed is > 3 ms^{-1} (August 2015 to December 2016).

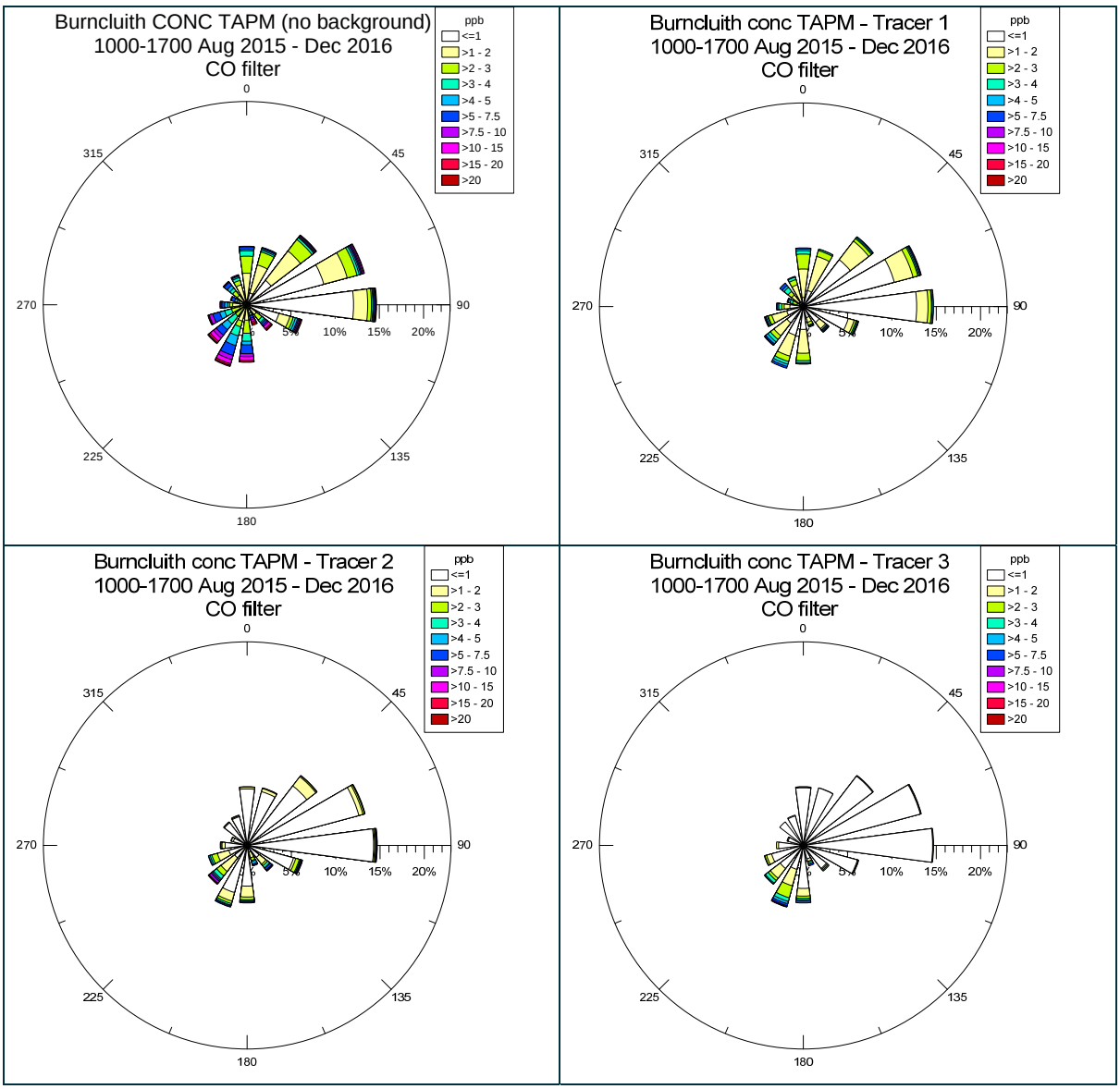

Figure A.11 Modelled methane concentration roses for Burncluith for each tracer for daytime hours only (1000 – 1700 h), with the CO filter applied (August 2015 to December 2016).

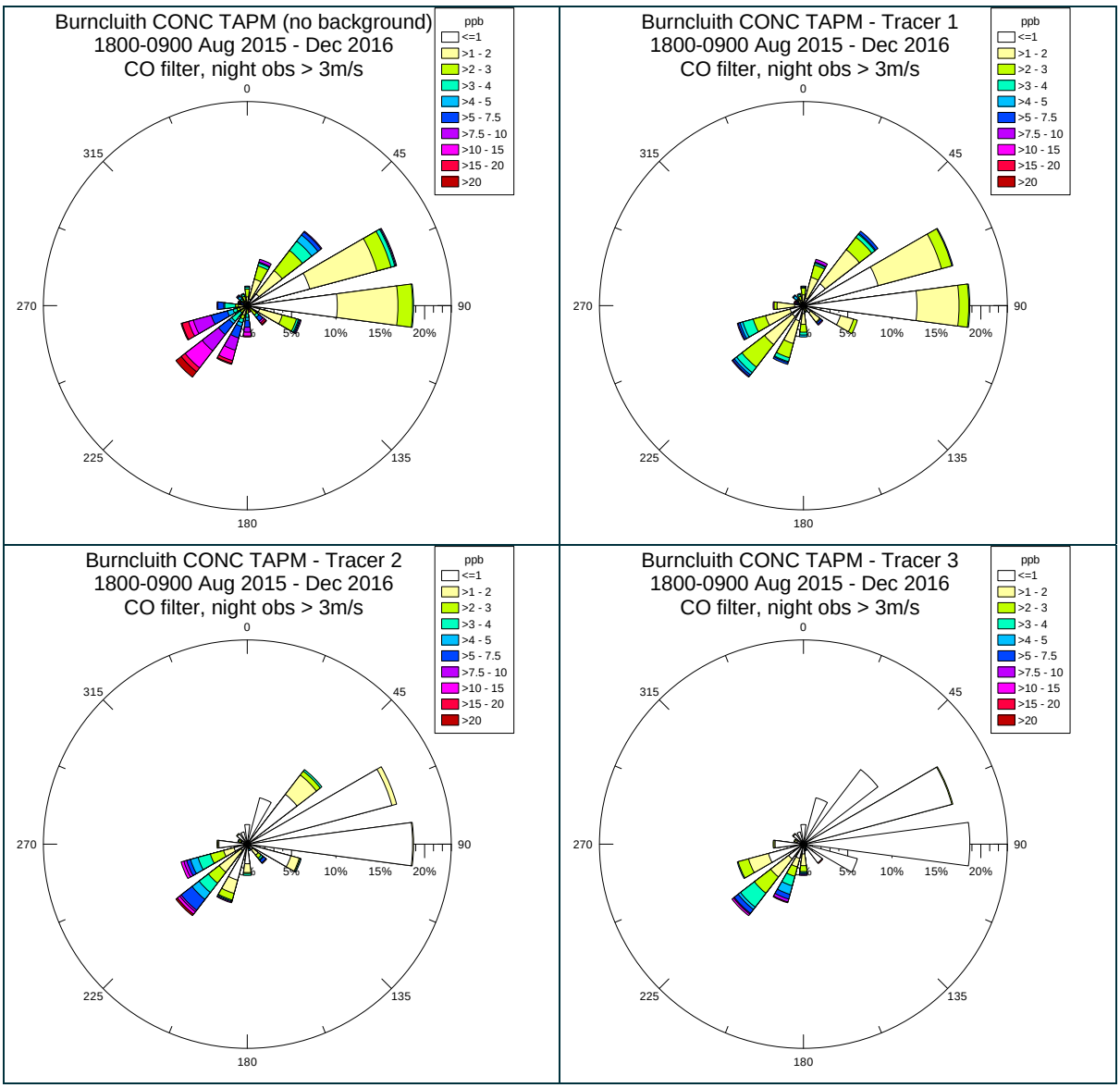

Figure A.12 Modelled methane concentration roses for Burncluith for each tracer for nighttime hours only (1800 – 0900 h), with the CO filter applied and the wind speed filtered at night to only include times when the wind speed is > 3 ms^{-1} (August 2015 to December 2016).

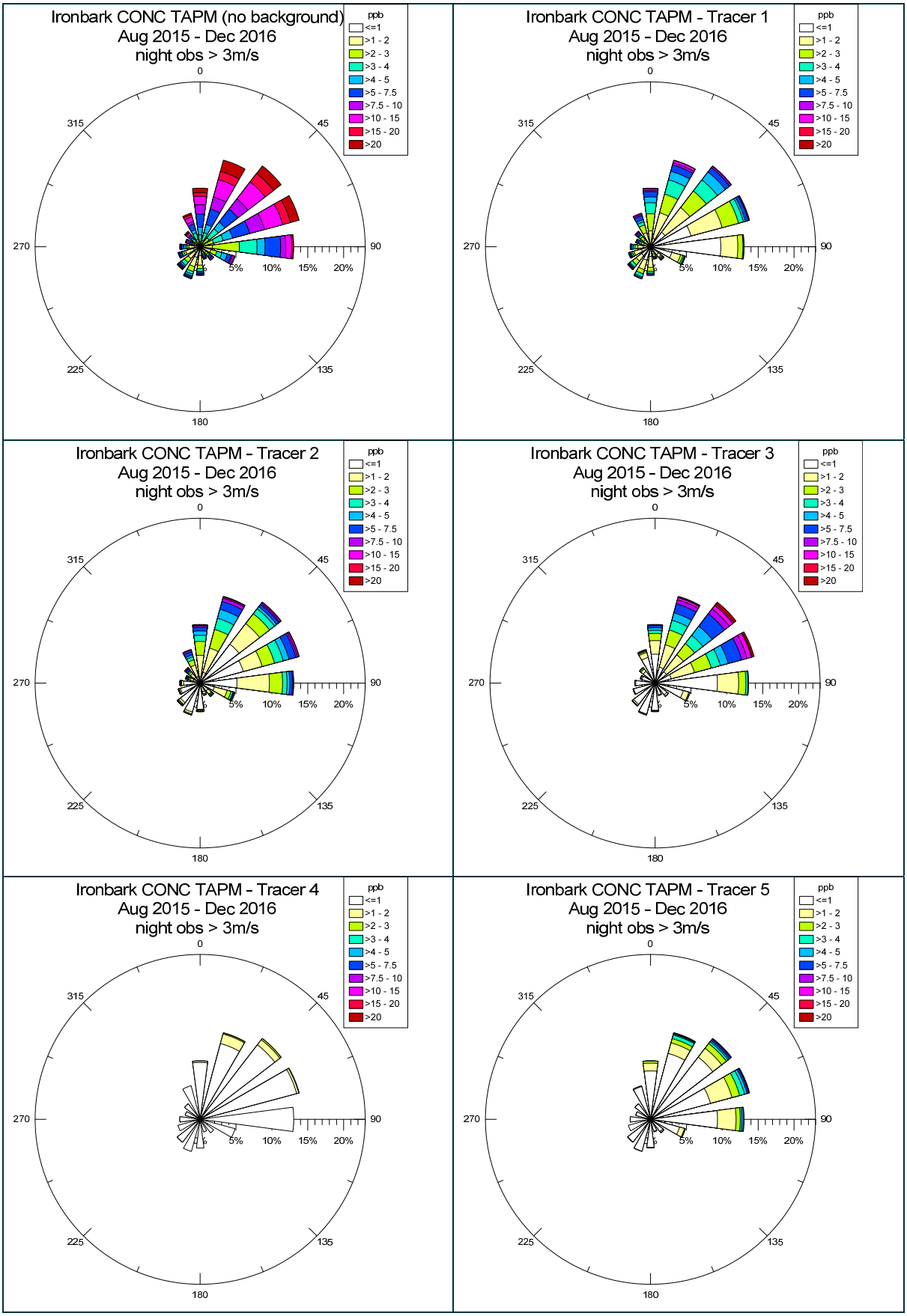

Figure A.13 Modelled methane concentration roses for Ironbark for each tracer ,with the wind speed filtered at night to only include times when the wind speed is > 3 ms^{-1} (August 2015 to December 2016).

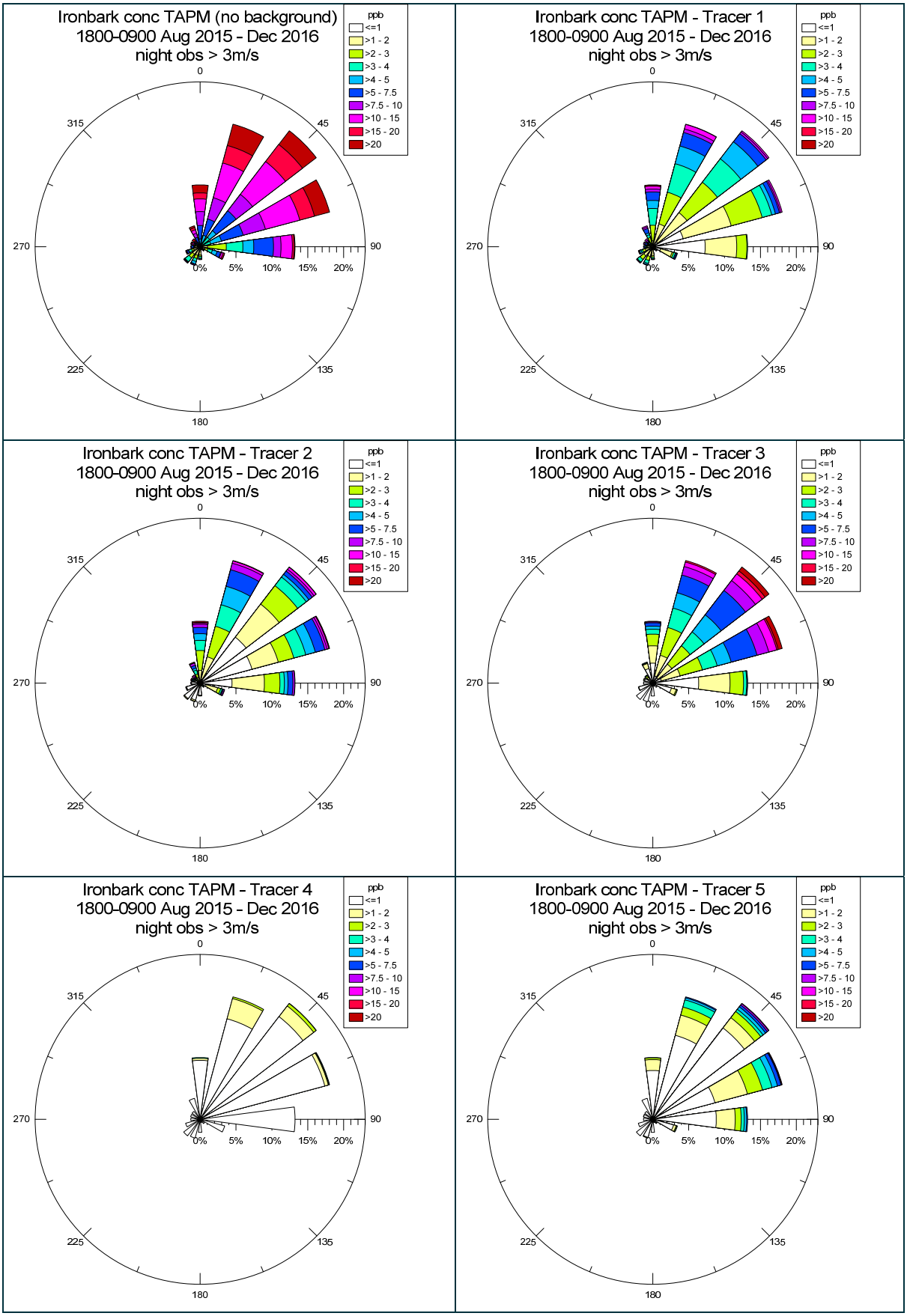

Figure A.14 Modelled methane concentration roses for Ironbark for each tracer for nighttime hours only (1800 – 0900 h), with the wind speed filtered at night to only include times when the wind speed is > 3 ms^{-1} (August 2015 to December 2016).

Appendix B Surat Basin Methane Inventory

katestone
www.katestone.com.au

Surat Basin Methane Inventory 2015 - Summary Report

Prepared for:

CSIRO

August 2018

Prepared by:

Katestone Environmental Pty Ltd
ABN 92 097 270 276
Ground Floor, 16 Marie Street | PO Box 2217
Milton, Brisbane, Queensland, 4064, Australia

www.katestone.com.au
us@katestone.com.au
Ph +61 7 3369 3699
Fax +61 7 3369 1966

katestone
www.katestone.com.au

Document Control

Deliverable #:	D15193-18
Title:	Surat Basin Methane Inventory 2015 - Summary Report
Version:	1.0
Client:	CSIRO
Document reference:	D15193-18 Surat Basin Methane Emissions Inventory Summary Report.docx
Prepared by:	Natalie Shaw, Lisa Smith, Tania Haigh, Michael Burchill
Reviewed by:	Simon Welchman
Approved by:	 Simon Welchman 17/08/2018

Disclaimer

http://katestone.com.au/disclaimer/

Contents

Tables

Figures

Glossary

Term	Definition
kg	kilograms
kg/year	kilograms per year
kL	kilolitre
km	kilometre
km/h	kilometre per hour
m	metre
m^2	square metres
MWh	megawatt hour
SCU	standard cattle unit
$tCO_{2\text{-}e}$	tonnes carbon dioxide equivalent
yr	year
Nomenclature	**Definition**
CH_4	methane
CO_2	carbon dioxide
Abbreviations	**Definition**
AADT	Annual Average Daily Traffic
ABS	Australian Bureau of Statistics
ADR	Australian Design Rules
AEMO	Australian Energy Market Operator
ANZSIC	Australian and New Zealand Standard Industrial Classification
ASGS	Australian Statistical Geography Standard
CSG	Coal Seam Gas
CSIRO	Commonwealth Scientific and Industrial Research Organisation
DAF	Department of Agriculture and Fisheries
NRM	Department of Natural Resources and Mines
DTMR	Department of Transport and Main Roads
EF	Emission Factor
ER	Emission Rate
LDV	Light Duty Vehicles
NPI	National Pollutant Inventory
NSW	New South Wales
NSW EPA	NSW Environment Protection Authority
NSW EPA GMR	NSW Environment Protection Authority Greater Metropolitan Region
PD	Property Development
VKT	Vehicle Kilometres Travelled

1. INTRODUCTION

The Surat Basin is a geological region in central Queensland that has seen large scale development of coal seam gas (CSG) extraction and processing operations in the past five years. The main driver of CSG development in the Surat Basin is the recent technology advancement in unconventional gas (CSG) extraction techniques and specifically advanced drilling capabilities. This technology advancement has made unconventional gas extraction projects commercially viable and, coupled with the extensive CSG resources in Surat Basin, has led to large scale development.

The Commonwealth Scientific and Industrial Research Organisation (CSIRO) commissioned Katestone Environmental Pty Ltd (Katestone) to develop an inventory of activities that generate emissions of methane within the Surat Basin and quantify their associated annual emission rates (Surat Basin Methane Inventory).

The Surat Basin Methane Inventory was provided to CSIRO as a series of datafiles. This report provides a summary of the activities that generate methane emissions and describes the methodologies that were used to generate the Surat Basin Methane Inventory.

1.1 Project background

The datafiles provided to CSIRO for the Surat Basin Methane Inventory include the following industry sectors and activities:

- Large industry (power stations, coal mines, coal seam gas processing and production)
- Agriculture (feedlots, grazing cattle, piggeries and poultry farms)
- Domestic wood heating
- Motor vehicles
- Miscellaneous sources (landfills, sewage treatment plants, river seeps and geological seeps).

1.2 Study area

The study area for the Surat Basin Methane Inventory was defined by CSIRO. It extends from Toowoomba in the southeast to Emerald in the northwest. The study area is 344 km by 345 km and is shown in Figure 1. The study area was divided into a network of evenly-spaced grid cells each 1 km by 1 km.

1.3 Scope of works

The scope of works includes the following elements:

- Identification and mapping of sources in the Surat Basin with emissions of methane for the year 2015
- Quantification of annual methane emission rates from each identified source for 2015
- Provision of a methane emissions dataset for each source type in a format suitable for use by CSIRO
- Provision of a summary report detailing all the methods and sources used to create the inventory.

1.4 Exclusions and missing data

The scope of works does not include methane emissions from the following activities:

- Land clearing
- Biomass burning
- Wetlands
- Registered ground water wells
- Fuel usage and material handling associated with mining activities. Methane emissions from these aspects of mining operations are expected to be minimal and significantly less than the aspects of mining that have been quantified, namely: open cut coal mining and coal off gassing.

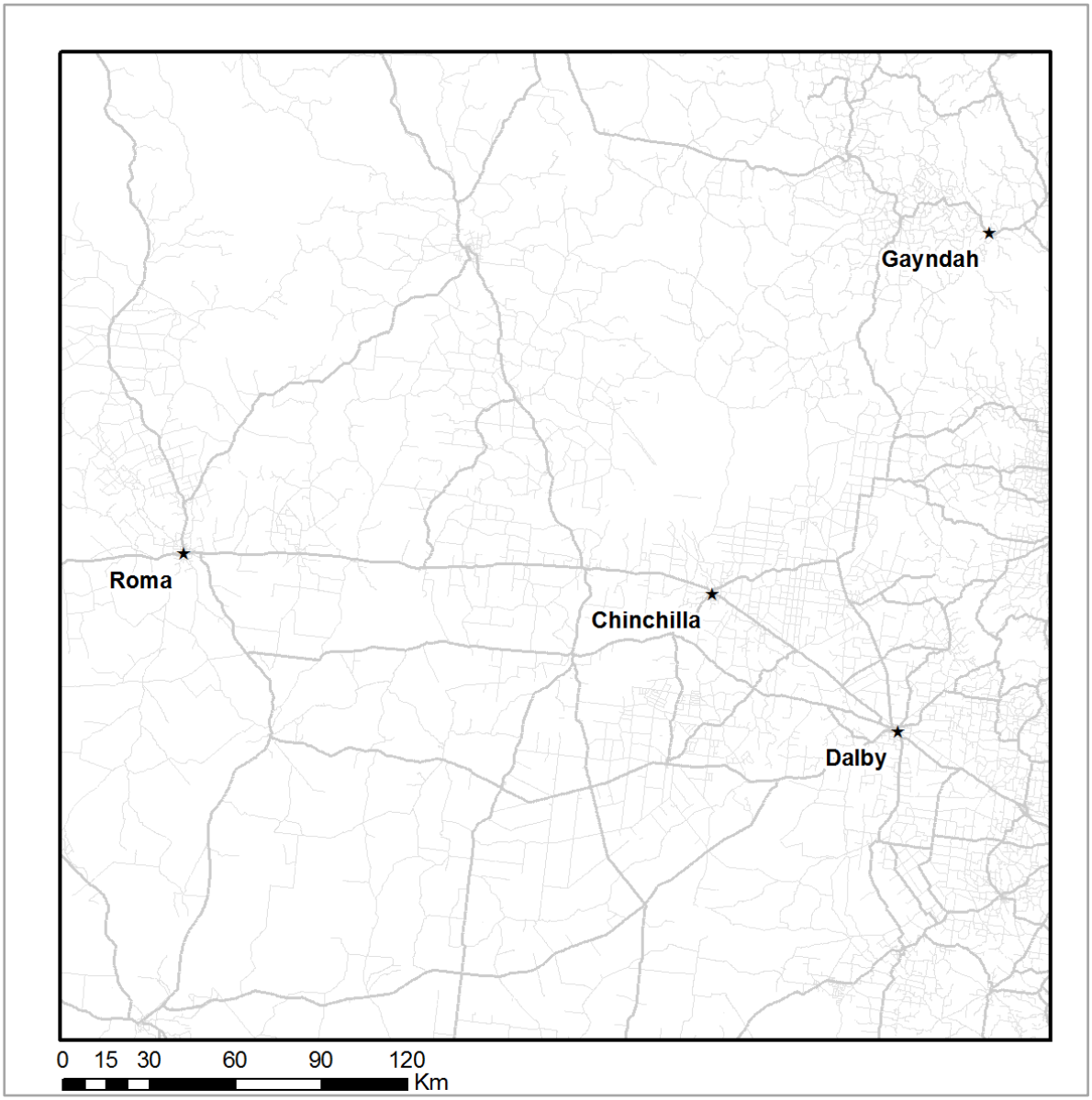

Figure 1 Surat Basin Methane Inventory Study Area

2. SUMMARY OF THE SURAT BASIN METHANE INVENTORY

A summary of total methane emissions from the industry sectors and sources included in the Surat Basin Inventory is presented in Table 1 and shown in Figure 2. Emission rates of methane aggregated by each 1 km by 1 km grid cell across the study area is presented in Figure 3. A detailed breakdown of the Surat Basin Methane Inventory by industry sector or source, including a description of the methane emissions calculation methodology, is provided in the following sections.

Table 1 Surat Basin Methane Inventory (kg/year) by industry sector or source

Industry sector or source		Methane emissions (kg/year)
Agriculture	Feedlot	42,270,444
	Grazing cattle	92,991,979
	Poultry	96,699
	Piggeries	2,358,892
Coal seam gas	Processing	14,610,306
	Production	1,918,532
Domestic wood heating		280,324
Landfill		1,905,644
Mining	Coal extraction	14,424,564
Motor vehicles		24,071
Power stations		640,070
Seeps	Ground seeps	127,714
	River seeps	375,909
Wastewater treatment		1,137,905
Total		**173,163,053**

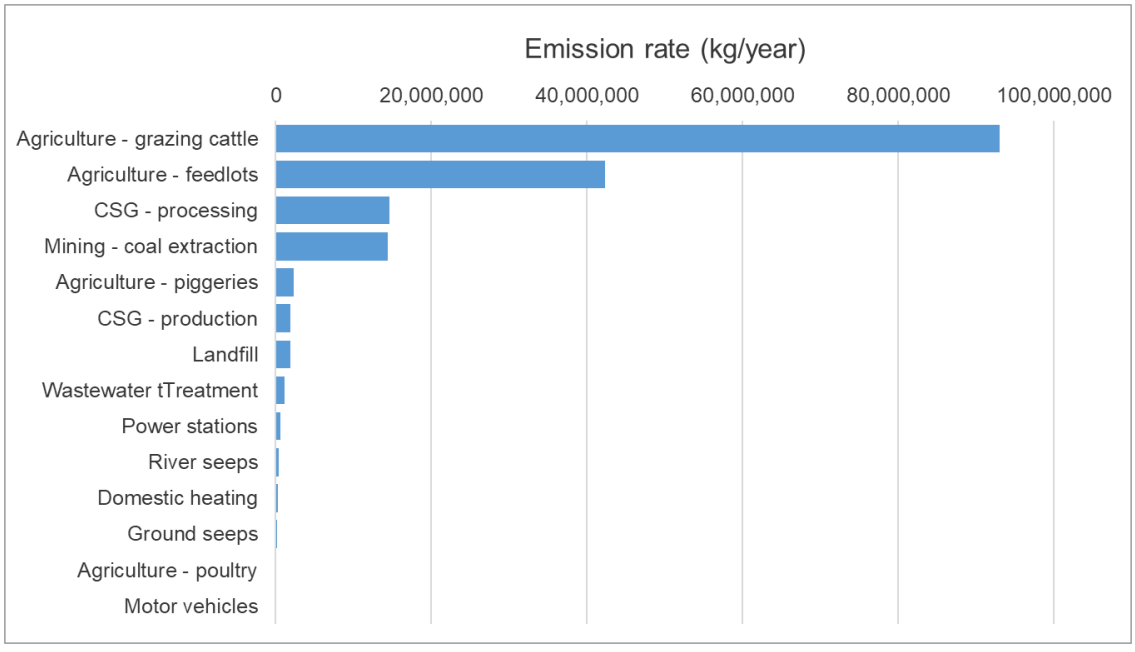

Figure 2 Surat Basin Methane Inventory by industry sector or source (kg/year)

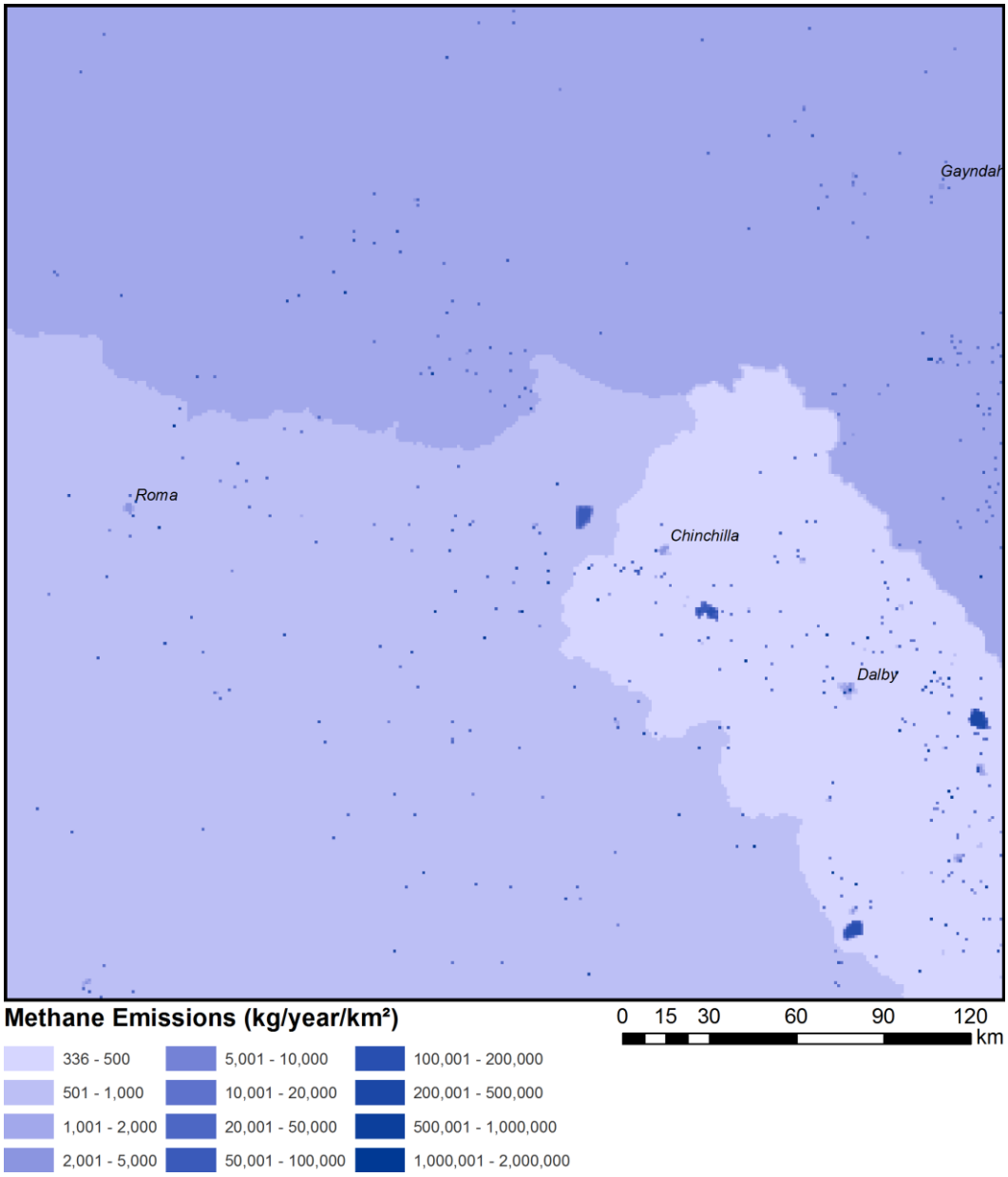

Figure 3 **Spatial distribution of the Surat Basin Methane Inventory**

3. AGRICULTURE

3.1 Overview

This chapter details the agricultural activities included in the Surat Basin Methane Inventory and summarises their associated emission rates of methane. The methods used to calculate methane emissions, the data sources and assumptions are provided.

3.2 Emission sources

There are 235 beef cattle feedlots, 1,086,059 grazing cattle, 114 piggeries and 18 poultry farms in the study area for which methane emissions have been estimated for 2015.

The locations of the agricultural facilities (feedlots, poultry farms and piggeries) included in the Surat Basin Methane Inventory are shown in Figure 4. The National Resource Management (NRM) region boundaries within the study area are also shown in Figure 4 (blue lines).

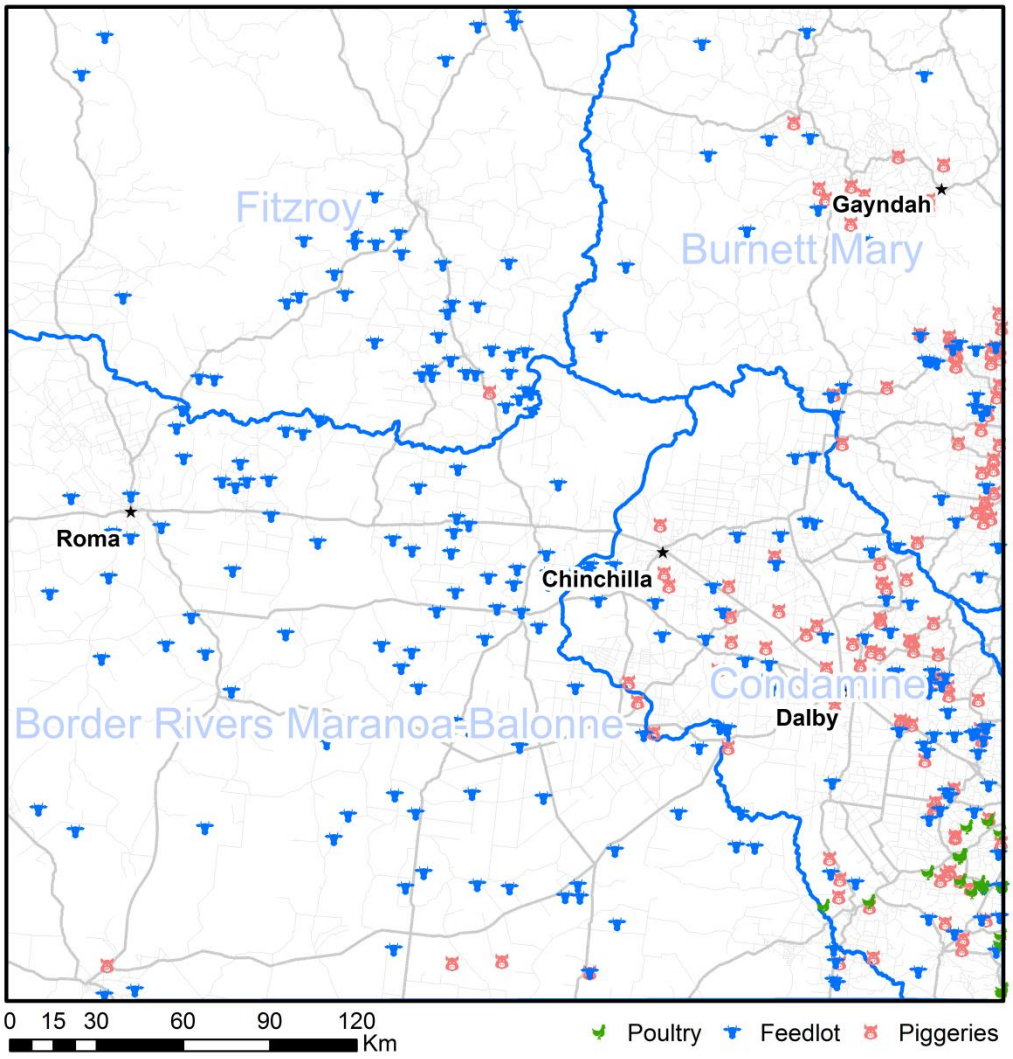

Figure 4 Agricultural facilities included in the Surat Basin Methane Inventory

3.3 Methodology

3.3.1 Information

3.3.1.1 Feedlots

The following information was used to calculate methane emissions from cattle feedlots:

- National Pollutant Inventory (NPI) data for the 2014/15 reporting year for facilities in the study area with the ANZSIC description "Beef Cattle Feedlots (Specialised)".
- Queensland Government datasets including:
    - Lot and plan boundaries contained in the *Property boundaries Queensland* cadastral dataset
    - Locations and standard cattle unit (SCU) numbers contained in NRM regions (Department of Agriculture and Fisheries (DAF)).
- Methane emission factor for enteric fermentation and manure management for non-dairy cattle from the Food and Agriculture Organization (FAO) of the United Nations (FAOSTAT, 2016). A total emission factor of 62 kg CH_4/SCU was used, which combines the two key methane sources at a feedlot (Table 2).

Table 2 Methane emission factors for non-dairy cattle (FAOSTAT, 2016)

Emissions Source	Methane emission factor (kg CH_4/SCU)
Enteric Fermentation	60
Manure Management	2

3.3.1.2 Grazing cattle

The following information was used to calculate methane emissions for grazing cattle:

- Total cattle livestock information and total area used mainly for grazing based on agricultural commodities for Australia for 2014-15 (ABS, 2015a) and Land Management and Farming in Australia for 2014-15 (ABS, 2015b).
- Digital Boundaries for NRM Regions for 2016 (DEE, 2016) in the study area.
- Methane emission factor for grazing cattle of 0.23 kg CH_4/animal/day based on direct measurements (Harper et al., 1999).

3.3.1.3 Poultry farms

The following information was used to calculate methane emissions from poultry farms:

- NPI for the 2014/15 reporting year for facilities in the study area with the ANZSIC description "Poultry farming (Eggs)" and “Poultry Farming (Meat).” There were three records returned for the filter "Poultry farming (Eggs)." There were no records returned for “Poultry Farming (Meat).”
- NRM’s and DAF’s (Department of Agriculture and Fisheries) datasets including:
    - Lot and plan boundaries contained in the *Property boundaries Queensland* cadastral dataset
    - Locations and bird numbers contained in the *Agricultural land audit - current poultry farms - Queensland* dataset.
- Approvals documentation publicly available via council’s PD (Property Development) online services.
- Google Earth imagery to determine approximate floor areas of some poultry farm sheds.
- Distribution of broiler chickens and layer chickens for Australia (Table 3) from the FAO (FAOSTAT, 2016).
- Methane emission factor for manure management (Table 4) for broiler chickens and layer chickens from the FAO (FAOSTAT, 2016). Emission factor for unknown poultry farm types derived from combined emissions for broiler and layer chickens, using a weighted average based on population distribution.
- Stocking densities for different farm types (Table 5) based on industry literature (Sustainable Table, 2015; Queensland Government, 2013) and industry experience.

Table 3 Distribution of birds by poultry farm type for Australia (FAOSTAT, 2016)

Parameter	Number of birds by Farm Type	
	Broiler	Layer
Count	83,052,847	14,447,153
Percentage	85.2%	14.8%

Table 4 Methane emission factors for various poultry farm types (FAOSTAT, 2016)

Emission source	Methane emission factor by farm type (kg CH_4/bird)		
	Broiler	Layer	Default – Unknown Type
Manure Management	0.02	0.03	0.0215[1]

Table notes:
[1] Emission factor for unknown poultry farm types based on scaling based on distribution of bird types in Australia

Table 5 Poultry farm stocking densities

Farm type	Stocking density (birds/m^2)	Information Source
Meat chicken	18	Assumed, based on highest stocking density for Post 1 January 2001 cages for laying or breeding fowls from the Model Code of Practice for the Welfare of Animals, Domestic Poultry 4th Edition (CSIRO, 2002)
Breeder	14	Assumed, based on highest stocking density for Australian Egg Corporation Assured standard (11-14) (Sustainable Table, 2015)
Layer	14	Highest stocking density for Australian Egg Corporation Assured standard (11-14) (Sustainable Table, 2015)
Barn layer	9	Maximum stocking density for RSPCA Approved Farming standard (Sustainable Table, 2015)

3.3.1.4 Piggeries

The following information was used to calculate methane emissions from piggeries:

- Emissions of ammonia reported to the NPI for the 2014/15 reporting year for facilities in the study area with the ANZSIC description "Pig Farming".
- The NPI reporting threshold of 10,000 kg/year of ammonia emissions for facilities that do not report to the NPI.
- NRM's and DAF's datasets including:
    - Lot and plan boundaries contained in the *Property boundaries Queensland* cadastral dataset
    - Locations of piggeries contained in the *Agricultural land audit - current piggeries - Queensland* dataset.
- Distribution of breeding swine and market swine for Australia (Table 6) from the FAO (FAOSTAT, 2016).
- Methane emission factor for enteric fermentation and manure management (Table 7) for breeding swine and market swine from the FAO (FAOSTAT, 2016). A total emission factor of 15.6 kg CH_4/SPU (standard pig unit) (default type) was used, which combines the two key methane sources at a piggery.

Table 6 Distribution of pig types for Australia (FAOSTAT, 2016)

Parameter	Number of pigs by pig type	
	Breeding	Market
Count	230,800	2,077,200
Percentage	10%	90%

Table 7 Emission factors used to calculate emissions from piggeries

Farm type	Methane emission factor (kg CH_4/head)		
	Breeding	Market	Default – Unknown Type
Enteric Fermentation	1.5	1.5	1.5
Manure Management	24	13	14.1

3.3.2 Data checks

The calculation of the methane emissions for agriculture involved obtaining information from a range of sources (as described in Section 3.3.1). To ensure that activities were not double counted, a number of checks were conducted.

3.3.2.1 Feedlots

Several feedlots were contained in both the NPI and DAF datasets. To avoid double counting of feedlot emissions, the following checks were conducted:

- Lot and plan numbers were identified for all feedlots in both datasets.
- For each feedlot in the NPI dataset, the nearest feedlot in the DAF's dataset was identified.
- Any feedlots with matching plan numbers were considered to be the same. The coordinates of the feedlots identified to be within both datasets varied by no more than 70 m.

3.3.2.2 Poultry farms

Locations of poultry farms contained in the NPI and DAF datasets were overlaid on aerial imagery to identify farms that were contained in both datasets. The checks found that the three poultry farms that reported to the NPI were also found in the DAF dataset.

3.3.2.3 Piggeries

Some piggeries, but not all, were contained in both the NPI and DAF datasets. To avoid double counting, the following steps were taken:

- Lot and plan numbers were identified for all piggeries in both datasets.
- For each piggery in the NPI dataset, the nearest piggery in the DAF dataset was identified.
- Any piggeries with matching lot or plan numbers in both datasets were considered to be the same.

3.3.3 Calculation methodology

3.3.3.1 Feedlots

There were 217 cattle feedlots identified in DAF dataset and 19 cattle feedlots that reported to the NPI during the 2014/15 period within the study area, resulting in a total number of 236 cattle feedlots.

For the 19 cattle feedlots that reported to the NPI, the number of cattle was estimated based on the reported ammonia emissions for 2014/15 and the emission factor for ammonia of 67.3 kg NH_3/SCU (Katestone, 2016).

The 217 cattle feedlots identified in the DAF dataset included information on the operating capacity (maximum SCU) for each feedlot. Methane emissions from a cattle feedlot are directly dependent on the number of cattle. Therefore, the emission factor of 62 kg CH_4/SCU was multiplied by the operating capacity (SCU) to estimate total emissions for each facility. In equation form methane emissions due to feedlot cattle were calculated as:

$$CH_4\_ER = FeedlotCattle \times CH_4\_EF$$

where:

CH_4_ER	Methane emissions (kg/year)
FeedlotCattle	Feedlot capacity in SCU (registered operating capacity)
CH_4_EF	Methane emission factor of 62 kg/SCU/year

3.3.3.2 Grazing cattle

The total number of grazing cattle in each NRM region are available within the NRM dataset. The percentage of each NRM region that intersects the study area was calculated using GIS and the equivalent number of grazing cattle for each NRM region in the study area was calculated as:

$$Cattle_{NRM\_Dom} = Cattle_{NRM} \times \frac{Area_{NRM\_Dom}}{Area_{NRM}}$$

where:

$Cattle_{NRM\_Dom}$	Number of cattle livestock within the NRM region within the study area
$Cattle_{NRM}$	Number of cattle livestock within the entire NRM region
$Area_{NRM\_Dom}$	Area of NRM region within the study domain
$Area_{NRM}$	Area of the entire NRM region

The number of grazing cattle within the study area were calculated as the difference between the total cattle livestock in the NRM region and the total number of feedlot livestock. There is no detailed information on the type of livestock, therefore each head of cattle is assumed to be equivalent to 1 SCU.

In equation form:

$$GrazCattle_{NRM\_Dom} = Cattle_{NRM\_Dom} - FeedlotCattle_{NRM\_Dom}$$

where:

$GrazCattle_{NRM\_Dom}$	Number of grazing cattle livestock within the NRM region within the study area
$Cattle_{NRM\_Dom}$	Number of cattle livestock within the NRM region within the study area
$FeedlotCattle_{NRM\_Dom}$	Feedlot cattle livestock within the NRM region within the study area

Methane emissions due to grazing cattle were calculated as:

$$CH_4\_ER = GrazCattle_{NRM\_Dom} \times CH_4\_EF$$

where:

CH_4_ER	Methane emissions (kg/year)
$GrazCattle_{NRA\_Dom}$	Number of grazing cattle livestock within the NRM region within the study area
CH_4_EF	Methane emission factor of 83.95 kg/SCU/year (equivalent to 0.23 kg/SCU/day).

3.3.3.3 Poultry farms

The DAF dataset identified 12 poultry farms within the study area.

The comparison of the NPI database and DAF dataset indicated that all poultry farms that reported to the NPI were found in the DAF dataset.

The capacity of each poultry farm was determined from publicly available approval documents, where available. Where no publicly available data could be found, capacity was estimated from the area of poultry sheds evident in aerial imagery and stocking densities presented in Table 5.

The DAF dataset reported poultry farm capacity as a range. In these cases, a mid-point was selected. For example, for poultry farms with a reported capacity of 1,000 – 200,000, emissions were calculated using a capacity of 100,000.

The type of poultry farm was determined from approval documents or publicly available information, where available. Where no information could be found, the default emission factors were used.

For poultry farms of unknown type, a stocking density for breeder farms of 14 birds/m2 was used as required to calculate poultry farm capacity.

Methane emissions due to poultry were calculated as:

$$CH_4\_ER = Poultry \times CH_4\_EF$$

where:

CH_4_ER	Methane emissions (kg/year)
Poultry	Poultry population
CH_4_EF	Methane emission factor (kg/bird/year) for bird type summarised in Table 4.

3.3.3.4 Piggeries

The DAF dataset included 114 piggeries within the study area. Six of these facilities reported to the NPI during the 2014/15 period.

For facilities that reported to the NPI, piggery capacity was estimated based on the reported ammonia emissions for 2014/15 and the ammonia emission factor of 6.8 kg NH_3/SPU (Katestone, 2016). Where piggeries did not report to the NPI, the capacity was estimated as the number of pigs that would produce ammonia emissions equal to 70% of the reporting threshold of 10,000 kg NH_3/year.

There is no detailed information on specific farm types. Therefore, the default factor of 15.6 kg CH_4/SPU, estimated using pig population distribution (Table 6) and emission factors for enteric formation and manure management (Table 7), was used.

Methane emissions due to piggeries were calculated as:

$$CH_4\_ER = Pigs \times CH_4\_EF$$

where:

CH_4_ER	Methane emissions (kg/year)
Pigs	Piggery capacity
CH_4_EF	Methane emission factor (kg/bird/year) of 15.6 kg/SPU

3.4 Emission rates

Total methane emissions from agriculture (feedlots, grazing cattle, poultry farms and piggeries) included in the Surat Basin Methane Inventory are summarised in Table 8.

Table 8 Total methane emissions (kg/year) due to agriculture

Source Type	Methane emissions (kg/year)
Feedlots	42,270,444
Grazing Cattle	92,991,979
Poultry farms	96,699
Piggeries	2,358,892

4. COAL MINING

4.1 Overview

This chapter details the coal mines included in the Surat Basin Methane Inventory and summarises their associated emissions of methane. The methods used to calculate emissions, data sources and assumptions are provided.

4.2 Emission sources

Four coal mines within the study area were identified as in operation during 2015. Table 9 details Run-of-mine (ROM) tonnages for each mine for 2014/15 (DNRM, 2016) and Figure 5 shows the mine locations.

Table 9 ROM coal tonnages for Surat Basin mines

Coal Mine	ROM Coal (Gross Raw Feed) Million tonnes (Mt)
Cameby Downs Coal Mine	1.75
Kogan Creek Mine	2.66
New Acland Open Cut Coal Mine	10.14
Commodore Coal Mine	3.48

Mining activities that may result in methane emission include:

- Extraction of coal
- Coal exploration
- Material handling
- Combustion of fuel.

There is no emission factor for methane emissions associated with coal exploration. Therefore, emissions of methane from this activity could not be quantified and have been excluded for the inventory. Notwithstanding this, methane emissions associated with coal exploration are likely to be relatively small.

There is also no publicly available information regarding material handling and fuel usage at the coal mines identified in the study area. Emissions of methane from these activities are expected to be relatively small compared to extraction of coal, consequently, emissions of methane from these sources have been excluded from the inventory.

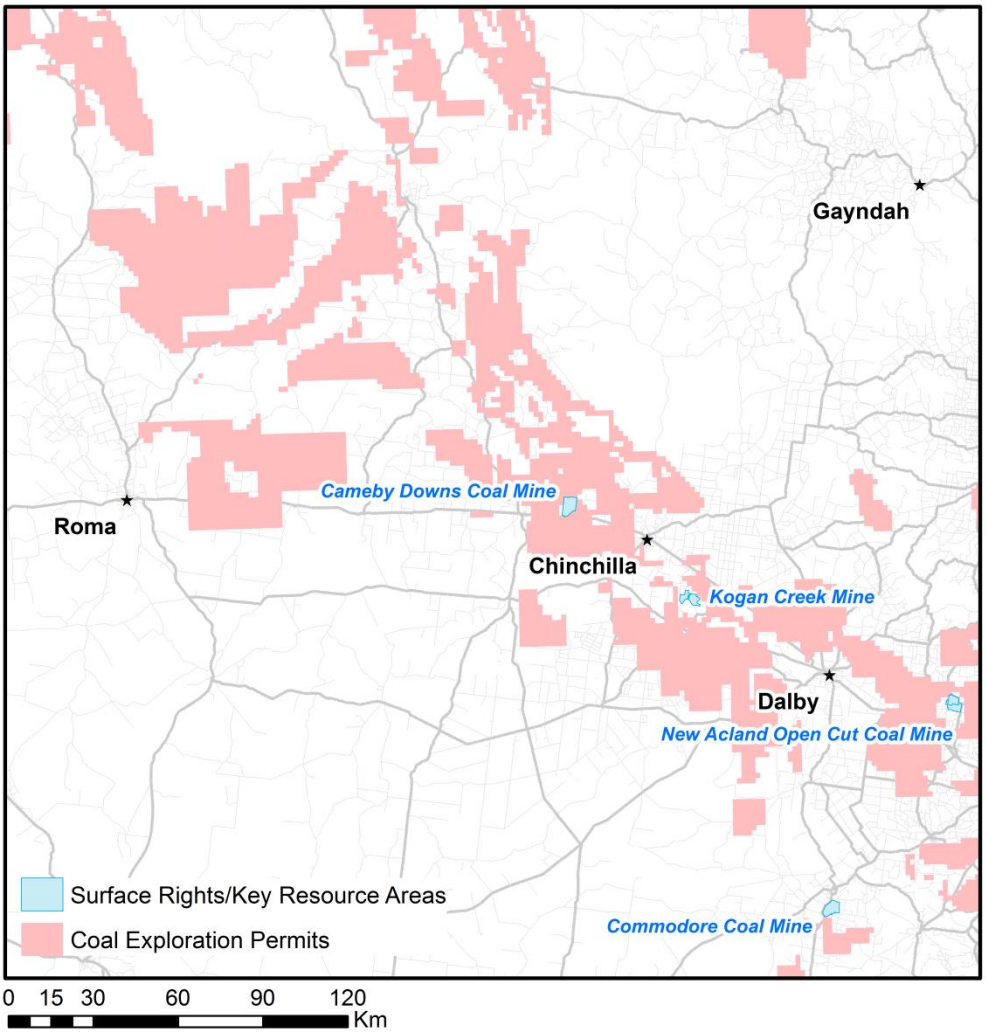

Figure 5 **Coal mines included in the Surat Basin Methane Inventory**

4.3 Methodology

4.3.1 Information

The following information was used to estimate methane emissions from coal mining:

- Run of mine (ROM) (gross raw output) coal tonnages for 2014/15 (Department of Natural Resources and Mines (DNRM) - *Queensland coal production by individual mine*, May 2016).
- DNRM Mining lease surface areas.
- Fugitive methane emission factor for extraction of coal in Queensland of 0.020 tonnes CO_2-e / tonne raw coal (DoE, 2016).
- Methane GWP of 25 (DoE, 2016).

4.3.2 Calculation methodology

4.3.2.1 Coal extraction

Methane emissions from extraction of coal were calculated as:

$$CH_4\_ER = Coal \times CH_4\_EF$$

where:

CH_4_ER Methane emissions (kg/year)

Coal Amount of run-of-mine coal (kg/year)

CH_4_EF Methane emission factor of 0.8 kg/tonne coal/year (equivalent to 0.020 tonnes CO_2-e/tonne coal)

Methane emissions were allocated uniformly across the mining lease areas associated with each mine as identified from the DNRM dataset.

4.4 Emission rates

Methane emissions from coal mining activities included in the Surat Basin Methane Inventory are summarised in Table 10.

Table 10 Total methane emissions (kg/year) due to coal mining

Source Type	Cameby Downs Coal Mine	Kogan Creek Coal Mine	New Acland Open Cut Coal Mine	Commodore Coal Mine
Coal extraction	1,397,990	2,128,364	8,115,158	2,783,052

5. COAL SEAM GAS ACTIVITIES

5.1 Overview

This chapter details the coal seam gas (CSG) activities that were considered by the Surat Basin Methane Inventory. The methods used to calculate emissions, data sources and assumptions are provided.

5.2 Emission sources

CSG is primarily composed of methane. CSG production and processing can lead to the release of methane into the atmosphere. Methane emission from CSG operations can occur for a number of reasons, with some sources emitting continuously while others are more intermittent in nature. A summary of the emission sources considered in this inventory is provided in Table 11.

Table 11 Summary of methane emission sources from CSG operations

	Emission source		Intermittent	Continuous
Production emissions	Wellhead emissions	Wellhead control equipment		X
		Separators		X
		Maintenance	X	
		Leaks	X	
	Combustion emissions	Well head pumps		X
		Flaring	X	
		Diesel used in vehicles	X	
		Backup generators	X	
	Pipeline emissions	Pipeline control equipment		X
		High point vents on produced water pipelines	X	
Processing emissions	Processing facility emissions	Compressor venting		X
		Control equipment		X
		Gas conditioning units including dehydrators		X
	Combustion emissions	Plant compressors		X
		Flaring	X	
		Diesel used in vehicles	X	
		Backup generators	X	
	Produced water	Collection and storage of produced water	X	

The CSG operators active in the study area are as follows:

- Origin
- QGC
- Arrow
- Santos
- APT Petroleum Pipelines (Kogan North Processing Facility).

Table 12 provides a summary of the operations.

Table 12 Summary of gas field operations

Number of Operators	Number of Gas Fields	Number of Wells^	Number of Processing Facilities
Five	16	4628	16
Table note: ^Number of wells estimated based on Queensland Government CSG production data			

Methane emissions due to two of the five operators have not been included in the inventory due to insufficient detail being available at the time of this report. Based on published Queensland government CSG production data, it has been determined that these operators account for approximately 1.5% of emissions associated with CSG activities. This is small compared to the overall uncertainty associated with the estimated methane emissions from CSG operations (see Section 13). As a result, omission of these small operators from the inventory is unlikely to affect the reliability of the CSG methane inventory.

Figure 6 provides a summary of the location and scale of operations considered by the study.

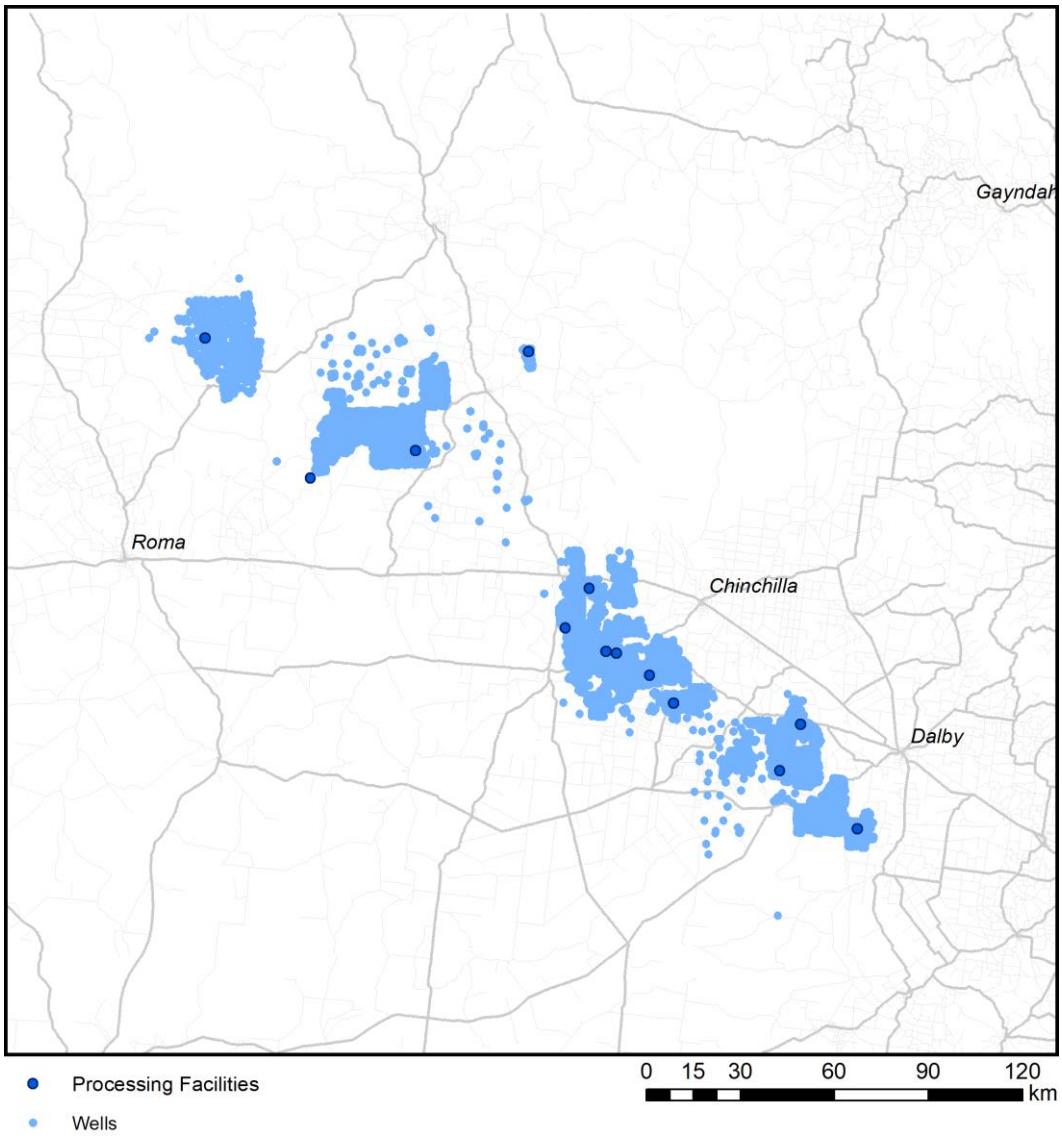

Figure 6 CSG operations in the Surat Basin

5.3 Methodology

The methane emissions resulting from CSG activities in the Surat Basin have been estimated in consultation with the relevant operators.

5.3.1 Information

Information sources used in the assessment include:

- Location of CSG well and processing facilities based on data available through DNRM.
- Methane emissions data and calculations provided by operators.

Where possible, all information provided by operators has been subject to a comprehensive review process. This has included consideration of the calculation methods and emission factors as well as the magnitude and intensity of methane emissions associated with production and processing activities.

5.3.2 Calculation methodology

The calculation methods used to estimate methane emissions from CSG activities are consistent with the NGER program. Methane is classified as a GHG under the NGER program and is quantified and reported in terms of carbon dioxide equivalents (CO_2-e). CO_2-e is calculated by multiplying the mass rate of methane by its Global Warming Potential (GWP), which for methane (GWP_{CH4}) is 25. It provides an indication of the contribution of methane to global warming relative to CO_2 (where CO_2 GWP=1). In simple terms the quantity of methane emissions can be calculated by dividing the quantity of methane emissions estimated in CO_2-e by the GWP for methane:

tonnes **CH_4 =** tonnes **CO_2-e** / **25**

The general equations used to estimate methane emissions from CSG activities are described in the following sections.

5.3.2.1 Combustion

Emissions due to combustion of CSG (including flaring) and diesel were calculated based on the following equation:

$$E_{CH_4} = Q_i \times EC_i \times EF_{CH_4}/GWP_{CH_4}$$

Where:

E_{CH_4}	Emissions of methane in kilograms due to the combustion of fuel type (*i*).
Q_i	Quantity of fuel type (*i*) combusted measured in cubic metres (CSG combustion), tonnes (CSG flaring), kilolitres (diesel) or gigajoules (energy content is not applied in this instance).
EC_i	Energy content of fuel type (*i*) measures in gigajoules per cubic metre (CSG) or gigajoules per kiloliter (diesel).
EF_{CH_4}	Emission factor for methane (CH_4) measured in kilograms CO_2-e/gigajoule (CSG combustion and diesel), tonnes CO_2-e/tonnes of gas flared (CSG flaring).
GWP_{CH_4}	Global Warming Potential (GWP) of methane, equals 25.

Table 13 Emission factors and energy content for methane emissions from combustion and flaring of CSG

Emission source	Energy content	Units	Emission factor***	Units
Coal seam methane (combustion)*	$37.7x10^{-3}$	GJ/m^3	0.2	$kgCO_2e/GJ$
Unprocessed natural gas (flaring)**	-	-	0.1	tCO_2e/t gas flared
Diesel*	38.6	GJ/kL	0.1	kgCO2e/GJ
Table note: *Source: *National Greenhouse and Energy Reporting (Measurement) Determination 2008, Schedule 1* **Source: *National Greenhouse and Energy Reporting (Measurement) Determination 2008, Section 3.85* ***Emission factors listed are for a Method 1 estimation of emissions				

5.3.2.2 Fugitive emissions - Venting of CSG

Estimates of the quantities of gas vented are based on methods prescribed by the Compendium of Greenhouse Gas Emissions Methodologies for the Oil and Natural Gas Industry (API Compendium) (API, 2009). Emissions estimated based on the direct measurement of gas released is the preferred and sometimes only available method; however, if this information is unavailable industry standard factors can be applied. Table 14 provides a list of the relevant sections of the API Compendium.

Table 14 Summary of API Compendium venting emissions calculation methodologies

Emissions process	API Compendium section
Gas treatment processes	Section 5.1
Cold process vents	Section 5.3
Other venting sources—gas driven pneumatic devices	Section 5.6.1
Other venting sources—gas driven chemical injection pumps	Section 5.6.2
Other venting sources—coal seam exploratory drilling, well testing and mud degassing	Section 5.6.3 and 5.6.6
Non-routine activities—production related non-routine emissions	Section 5.7.1 or 5.7.2
Non-routine activities—gas processing related non-routine emissions	Section 5.7.1 or 5.7.3

5.3.2.3 Fugitive emissions – other than venting or flaring

Fugitive methane emissions, other than emissions that are vented of flared (also referred to as leaks), include emissions from (NGER Determination 2008, Section 3.70):

- *a gas wellhead through to the inlet of gas processing plants; and*
- *a gas wellhead through to the tie-in points on gas transmission systems, if processing of natural gas is not required; and*
- *gas processing plants; and*
- *well servicing; and*

- *gas gathering; and*
- *gas processing and associated waste water disposal.*

Fugitive methane emissions other than emission that are vented or flared have been calculated based on the following equation:

$$E_{CH_4} = Q \times EF_{CH_4}/GWP_{CH_4}$$

E_{CH_4}	Emissions of methane other than emissions that are vented or flared from production and processing of natural gas in kilograms.
Q	the total quantity of natural gas that passes through the natural gas. production and processing measured in tonnes.
EF_{CH_4}	1.2 x 10^{-3}, which is the emission factor for methane from general leaks in the natural gas production and processing, measured in CO_2-e tonnes per tonne of natural gas that passes through the natural gas production and processing.
GWP_{CH_4}	Global Warming Potential (GWP) of methane, equals 25.

5.4 Emission Rates

Methane emissions associated with CSG activities have been estimated based on the data provided together with supplementary calculations using the methodology described above. Table 15 provides a summary of methane emissions from CSG activities in the Surat Basin.

Table 15 Total methane emissions (kg/year) due to CSG activities

Activity	Methane emissions (kg/year)
Gas consumed for combustion	197,603
Diesel combustion	4,384
Flaring	1,309,137
Venting	14,499,257
Fugitive emissions	518,456
TOTAL	**16,528,838**

6. LANDFILLS

6.1 Overview

This chapter details the landfills that were included in the Surat Basin Methane Inventory and summarises their estimated methane emissions. The methods used to calculate emissions, data sources and assumptions are provided.

6.2 Emission sources

There are 41 landfills in the Surat Basin Methane Inventory study area for which methane emissions have been calculated, as shown in Figure 7.

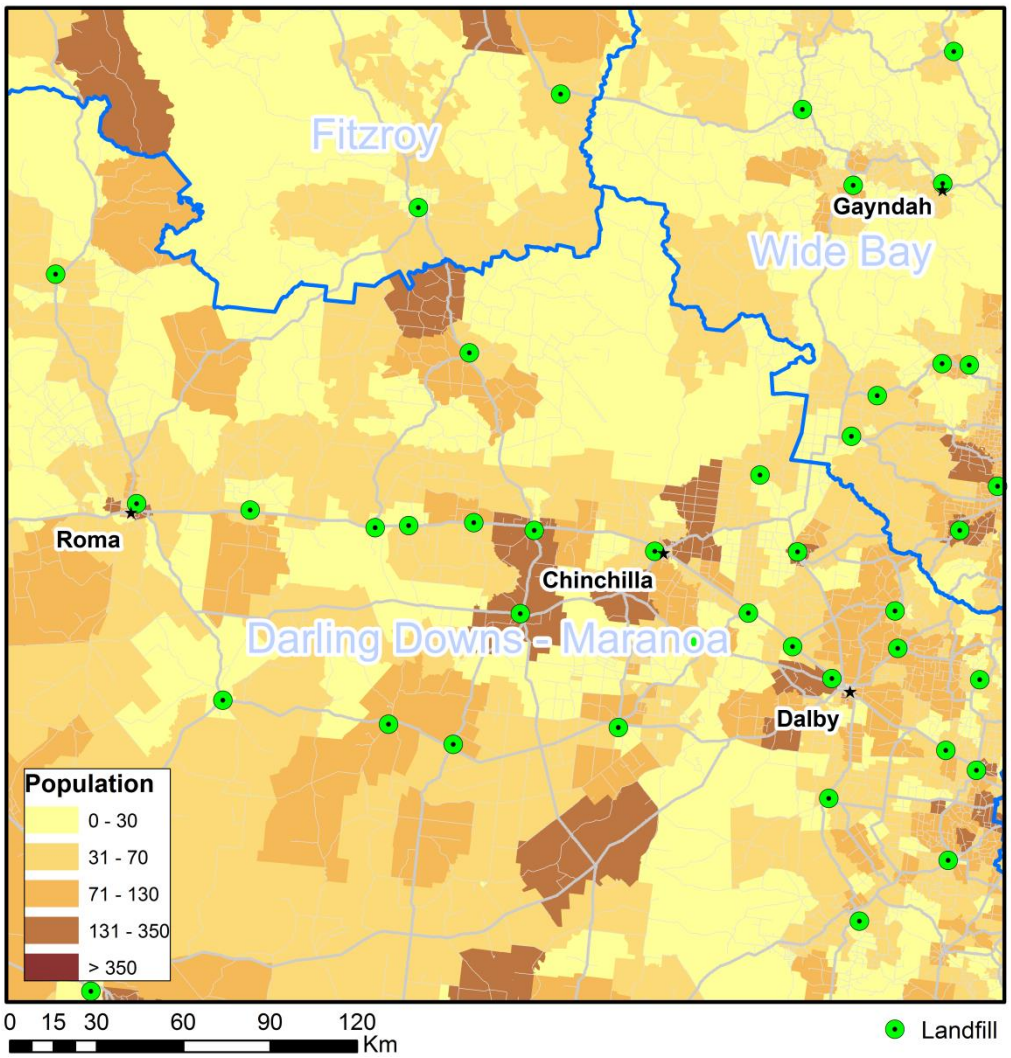

Figure 7 Location of landfills in the study area

6.3 Methodology

6.3.1 Information

The following information was used to generate the methane emissions for landfills in the study area:

- Locations of landfills was based on contact details and site information for public waste and recycling facilities in Queensland (EHP, 2016)
- Population data for 2011 (ASGS, 2011) from residential mesh blocks, approximately 30-60 dwellings designed to be small enough to aggregate accurately to a wide range of spatial units
- Statistical Area Level 4 (SA4) ASGS digital boundaries (ASGS,2011)
- Queensland regional waste per person estimate (DERM, 2011)
- Methane fraction of landfill gas (50%) and emission factor for municipal solid disposed to landfill of 1.4 tonnes CO_2-e/tonne waste (DoE, 2016)
- Methane GWP of 25 (DoE, 2016).

6.3.2 Calculation methodology

Locations of each landfill in the study area were identified from the EHP (2016) dataset. Population data for the study area was sourced from ASGS (2011) for residential mesh blocks.

The total waste per mesh block was calculated using the estimated waste per person for Queensland, detailed in Table 16.

Table 16 Waste per person estimate for Queensland (DERM, 2011)

Region	Waste per person disposed to landfill (tonnes waste / person)
Darling Downs - Maranoa	1
Fitzroy	0.51
Wide Bay	0.28
Toowoomba[1]	1
Table note: [1] The Toowoomba region is not defined in the DERM study. Estimated waste per person for this region based on the adjacent Darling Downs – Maranoa region.	

In equation form:

$$Waste_{mb} = Pop_{mb} \times WasteFactor_{reg}$$

where:

$Waste_{mb}$ Total waste per mesh block (tonnes waste)

Pop_{mb} Population per mesh block (count)

$WasteFactor_{reg}$ Waste Factor for the region

Distances between the mesh block and landfill facilities were calculated using GIS. Mesh blocks were then assigned to the nearest landfill facility. Total waste processed at each facility was then calculated.

In equation form:

$$Waste_{fac} = \sum_{mb=1}^{n} Waste_{mb}$$

where:

$Waste_{fac}$ Total waste per facility (tonnes waste)

$Waste_{mb}$ Total waste per mesh block (tonnes waste)

n Number of mesh blocks assigned to facility

The population and total waste calculated for each region are summarised in Table 17.

Table 17 Population and total waste calculated for each region

Region	Population	Waste (tonnes)
Darling Downs - Maranoa	63,891	63,891
Fitzroy	1,504	767
Wide Bay	11,656	3,264
Toowoomba	137	137
Total	**77,188**	**68,059**

6.4 Emission rates

Methane emissions due to landfills included the Surat Basin Methane Inventory are summarised in Table 18.

Table 18 Total methane emissions (kg/year) due to landfills

Landfill Area	Methane emissions (kg/year)
Darling Downs - Maranoa	1,788,948
Fitzroy	21,477
Wide Bay	91,383
Toowoomba	3,836
Total	**1,905,644**

7. POWER STATIONS

7.1 Overview

This chapter details the power stations that were included in the Surat Basin Methane Inventory. The methods used to calculate emissions, data sources and assumptions are provided.

7.2 Emission sources

There are eight power stations in the study area for which methane emissions have been calculated. The power stations detailed in Table 19 and Figure 8 are:

- Braemar 1 Power Station
- Braemar 2 Power Station
- Condamine Power Station
- Daandine Power Station
- Darling Downs Power Station
- Roma Power Station
- Kogan Power Station
- Millmerran Power Station.

Methane emissions from the above power stations are related to the combustion of coal or natural gas.

Table 19 Power stations in Surat Basin Methane Inventory

Power Station	Easting (WGS-84, m)	Northing (WGS-84, m)	Latitude	Longitude	Type
Braemar 1	292,235	6,999,150	-27.1145	150.9041	Gas, open cycle turbines
Braemar 2	292,352	6,999,341	-27.1128	150.9053	Gas, open cycle turbines
Condamine	228,319	7,047,429	-26.6680	150.2703	Gas, combined cycle turbines
Daandine	295,724	7,002,098	-27.0884	150.9397	Gas, reciprocating engines
Darling Downs	291,352	6,999,208	-27.1138	150.8952	Gas, combined cycle turbines
Roma	85,549	7,053,625	-26.5775	148.8404	Gas, open cycle turbines
Kogan	276,249	7,020,300	-26.9212	150.7467	Coal
Millmerran	330,698	6,905,504	-27.9648	151.2788	Coal

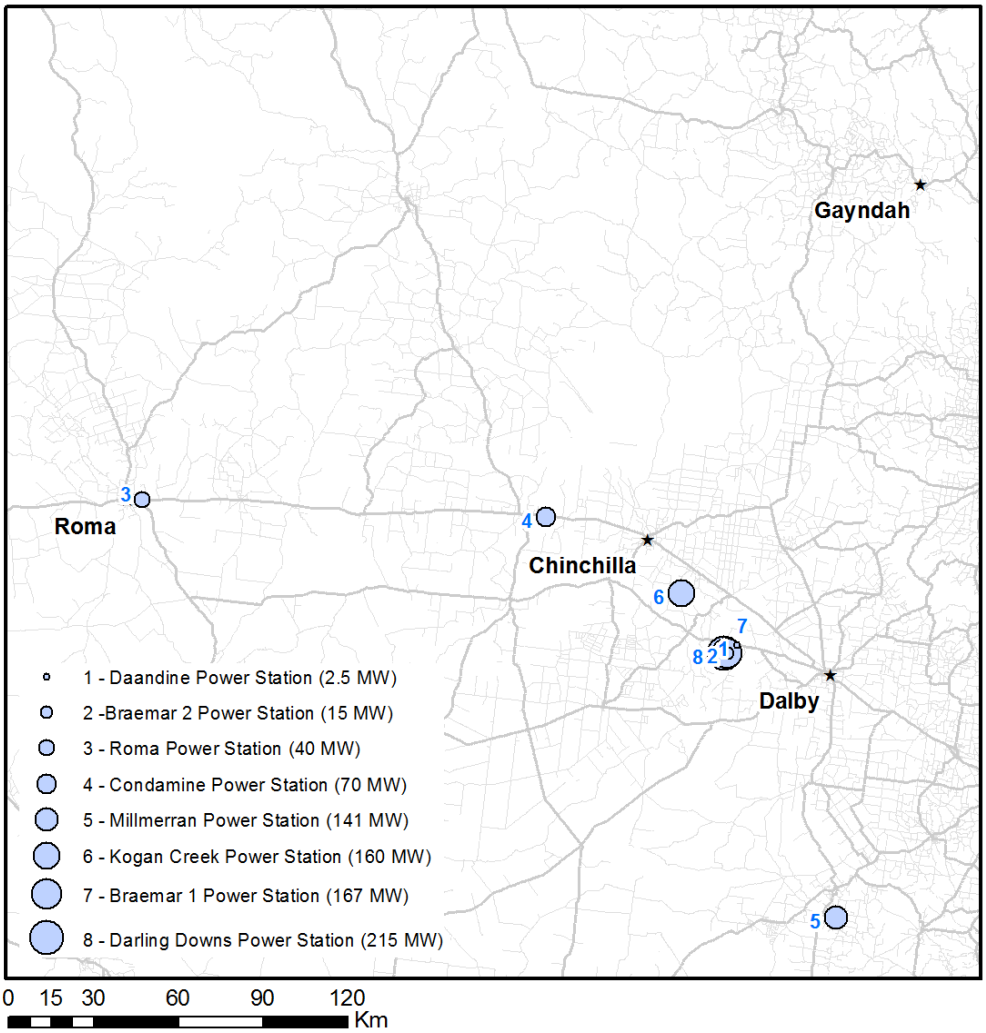

Figure 8 **Power stations included in the Surat Basin Methane Inventory**

7.3 Methodology

7.3.1 Information

The following information was used to generate the power stations methane emissions:

- Actual electricity generation for each power station from the Australian Energy Market Operator (AEMO) for 2015 at 5-minute intervals
- Emission intensity information from the Clean Energy Regulator for 2015/2016 National Greenhouse and Energy Reporting year
- National Greenhouse Accounts Factors (DoE, 2016)
    - Emission and energy content factors - gaseous fuels
    - Emission and energy content factors – solid fuels and certain coal-based products
- Methane GWP of 25 (DoE, 2016).

- Stack characteristics sourced from *Australia Pacific LNG Project Volume 5: Attachments Attachment 28: Air Quality Impact Assessment – Gas Fields* (Katestone, 2010b).

Emission intensity for each power station changes with load. However, this detailed information was not available. Therefore, it was assumed that the emission intensity remained constant throughout the year.

7.3.2 Calculation methodology

Methane emissions from the power stations were calculated as follows:

$$CH_4\_ER = MWh \times EI \times CH_4\_EF$$

where:

CH4_ER Methane emission rate in g/s

MWh Megawatt hours per 5 minutes

EI Emission intensity in tonnes / MWh

CH4_EF Emission factor for methane derived from CO2-e emission factors and GWP for methane

Table 20 details total electricity generation and intensity data used for 2015.

Table 20 Total electricity generation (MWh) for each power station for 2015

Power Station	2015 MWh	Intensity data (t/MWh)[1]
Braemar 1	1,600,121	0.57
Braemar 2	1,944,877	0.59
Condamine	527,140	0.44
Daandine	236,520	0.52
Darling Downs	4,373,193	0.41
Roma	118,572	0.65
Kogan	5,764,719	0.83
Millmerran	6,983,105	0.81
Table note: 1 Emission intensity data is based on 2014/2015 NGER reporting period		

7.4 Emission rates

Methane emissions due to power stations included in the Surat Basin Methane Inventory are summarised in Table 21.

Table 21 Total methane emissions (kg/year) due to power stations

Power Station	Methane emissions (kg/year)
Braemar 1	141,324
Braemar 2	177,800
Condamine	18,004
Daandine	18,888
Darling Downs	139,182
Roma	5,983
Kogan	63,634
Millmerran	75,255

8. WASTEWATER TREATMENT FACILITIES

8.1 Overview

This chapter details the wastewater treatment facilities that were included in the Surat Basin Methane Inventory and summarises the estimated methane emissions. The methods used to calculate emissions, data sources and assumptions are provided.

8.2 Emission sources

There are 20 wastewater treatment facilities in the Surat Basin study area for which methane emissions have been calculated.

The location of the wastewater treatment facilities in the study area are shown in Figure 9.

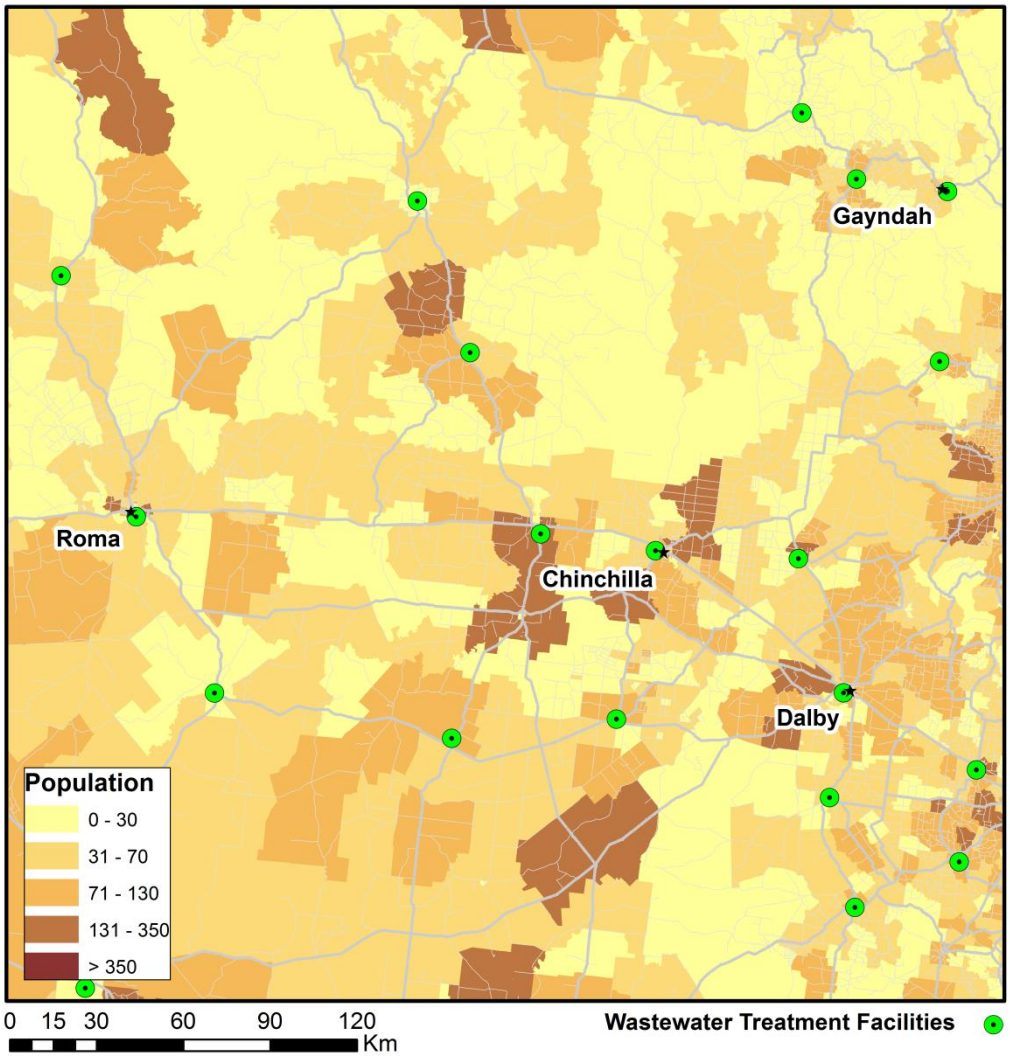

Figure 9 Wastewater treatment facilities in the study area

8.3 Methodology

8.3.1 Information

The following information was used to generate the wastewater treatment facility methane emissions:

- Locations of wastewater treatment facilities based on national database (Geoscience Australia, 2012)
- Population data for 2011 (ASGS, 2011) from residential mesh blocks, approximately 30-60 dwellings designed to be small enough to aggregate accurately to a wide range of spatial units
- Wastewater per person estimate of 0.0585 tonnes wastewater/person (DoE, 2016)
- Methane emission factor of 6.3 tonnes CO_2-e/tonne waste (DoE, 2016)
- Methane GWP of 25 (DoE, 2016).

8.3.2 Calculation methodology

The location of each wastewater treatment facility in the study area was identified from the Geoscience Australia (2012) dataset. Population data within the study area were sourced from ASGS (2011), consistent with population data used in the development of the landfill and motor vehicle methane inventory.

The total wastewater per mesh block was calculated using the estimated wastewater factor of 0.0585 tonnes wastewater/person (DoE, 2016).

In equation form:

$$Wastewater_{mb} = Pop_{mb} \times WasteFactor$$

where:

$Wastewater_{mb}$	Total wastewater per mesh block (tonnes waste)
Pop_{mb}	Population per mesh block (count)
WasteFactor	Waste Factor for the region (0.0585 tonnes wastewater/person (DoE, 2016))

Distances between the mesh block and wastewater treatment facilities were calculated using GIS. Mesh blocks were then assigned to the nearest facility. Total wastewater treated at each facility was then calculated.

In equation form:

$$Wastewater_{fac} = \sum_{mb=1}^{n} Wastewater_{mb}$$

where:

$Wastewater_{fac}$	Total wastewater per facility (tonnes waste)
$Wastewater_{mb}$	Total wastewater per mesh block (tonnes waste)
n	Number of mesh blocks assigned to facility

The population and total wastewater treated in the study area is summarised in Table 22.

Table 22 Population and total wastewater treated in the study area

Source	Population	Wastewater treated (tonnes)
Wastewater Treatment Facility	77,188	4,515

Further assumptions used in estimating emissions include:

- All wastewater assumed to be sludge treated at each facility
- Chemical oxygen demand (COD) of sludge removed from each facility assumed to be zero, resulting in the most conservative estimate of methane emissions
- Direct discharge to open waters does not occur
- No capture of methane.

8.4 Emission rates

Methane emissions from wastewater treatment facilities included in the Surat Basin Methane inventory are summarised in Table 23.

Table 23 Total methane emissions (kg/year) due to wastewater treatment facilities

Source	Methane emissions (kg/year)
Wastewater treatment facilities	1,137,905

9. RIVER SEEPS

9.1 Overview

This chapter summarises the methane emissions due to river seeps included in the Surat Basin Methane Inventory. The methods used to calculate emissions, data sources and assumptions are provided.

9.2 Information

The emissions of methane from river seeps in the study area is based on advice from Stuart Day from CSIRO who advised that a total methane flux of 1000L/min should be used for the four main seeps in the Condamine River.

The location of river seeps in the study area are shown in Figure 10 and correspond to locations provided by CSIRO in the file “Condamine River Seeps.kmz”.

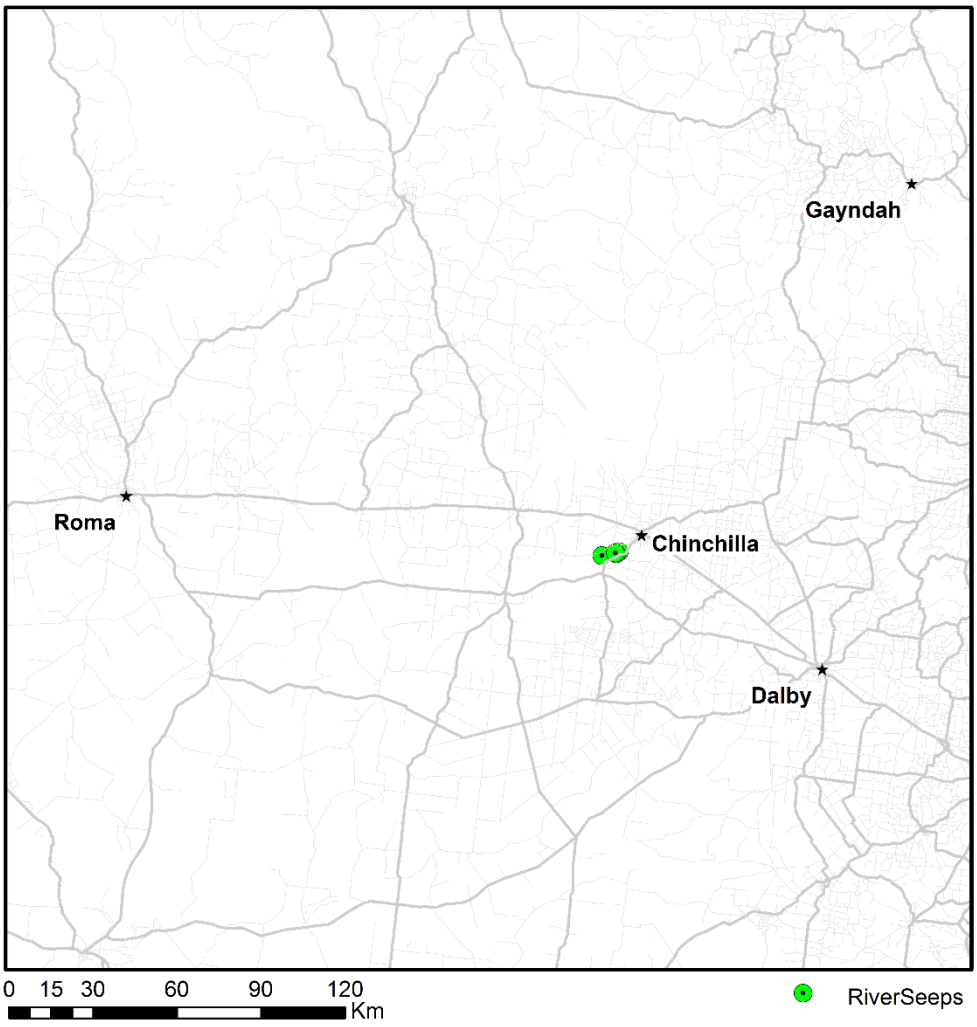

Figure 10 Location of river seeps included in the Surat Basin Methane Inventory

9.3 Calculation methodology

The emission rate of methane from river seeps was calculated using the following formula:

$$CH_4\_ER = \frac{methane\ flux\ x\ density}{n_{sites}\ x\ 60}$$

Where:

CH_4_ER	Emission rate of methane g/s
Methane flux	Methane flux in L/min (1000)
n_{sites}	Number of sites giving methane flux (4 sites)
density	Density of methane (0.716 g/L)

9.4 Emission rates

Methane emissions due to river seeps included in the Surat Basin Methane Inventory are summarised in Table 24.

Table 24 Total methane emissions (kg/year) due to river seeps

Source	Methane emissions (kg/year)
River seeps	375,909

10. GROUND SEEPS

10.1 Overview

This chapter summarises the methane emissions due to ground seeps included in the Surat Basin Methane Inventory. The methods used to calculate emissions, data sources and assumptions are provided.

10.2 Information

The emissions of methane from ground seeps in the study area is based on work conducted by CSIRO and reported in the report Characterisation of Regional Fluxes of Methane in the Surat Basin, Queensland, Phase 2: A Pilot Study of Methodology to Detect and Quantify Methane Sources (CSIRO, 2015).

The locations of ground seeps in the study area are shown in Figure 11 and correspond to locations provided in CSIRO (2015).

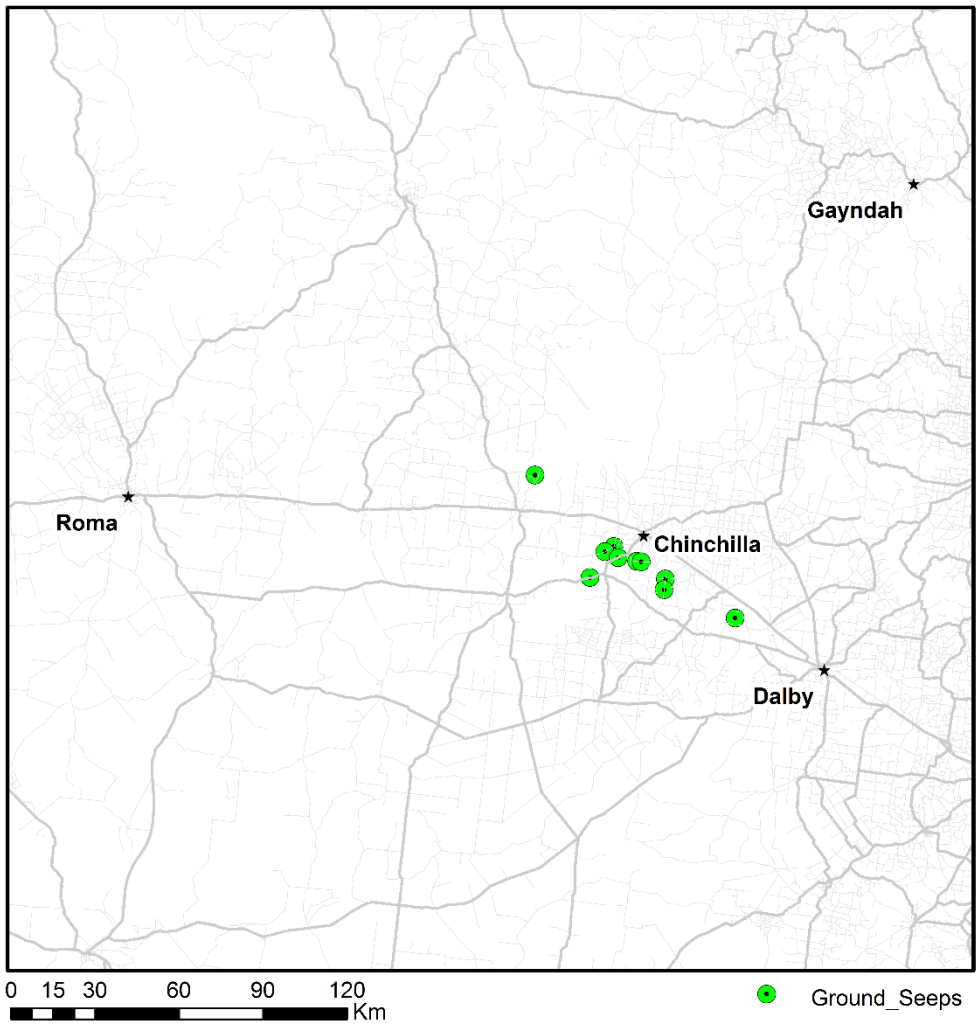

Figure 11 Location of ground seeps in the study area

Table 3.5 of CSIRO (2015) summarised the measured methane emission rate for 10 sites using a combination of measurement methods (traverse and flux chamber). The measured emission rates are reproduced in Table 25. The maximum emission at each site has been used in the Surat Basin Methane Inventory.

Table 25 Summary of emission flux results for ground seeps (Table 3.5 CSIRO, 2015)

Site	Emission rate (kg/day)	
	Traverse	Flux Chamber
Site 1 Jan 2013	48.8	46.6
Site 1 Sept 2013	79.8	na
Site 2	na	102
Site 3	103	61.3
Site 4	na	7.1
Site 5	na	3.7
Site 6	na	51.5
Site 7	na	1.7
Site 8	na	1.0
Site 9	na	0.2
Site 10	0.1	na

10.3 Emission rates

Methane emissions due to ground seeps included in the Surat Basin Methane Inventory are summarised in Table 26.

Table 26 Total methane emissions (kg/year) due to ground seeps

Source	Methane emissions (kg/year)
Ground seeps	127,714

11. DOMESTIC WOOD HEATING

11.1 Overview

This chapter details the domestic wood heating sources included in the Surat Basin Methane Inventory. The methods used to calculate emissions, data sources and assumptions are provided.

11.2 Emission sources

The types of domestic wood heaters included in the Surat Basin Methane Inventory were based on the NSW EPA GMR Inventory 2008 (NSW EPA, 2012a) and include the following:

- Slow combustion heaters with compliance plates
- Slow combustion heaters without compliance plates
- Open fireplaces
- Potbelly stoves.

11.3 Methodology

11.3.1 Information

The following information was used to generate the domestic wood heating methane emissions:

- NSW EPA GMR Inventory 2008 (NSW EPA, 2012a):
    - Emission factors for domestic wood heating
    - Diurnal, weekly and monthly profiles for domestic wood heating.
- Number of dwellings by mesh block based on the 2011 census (ASGS, 2011), presented in Figure 12.

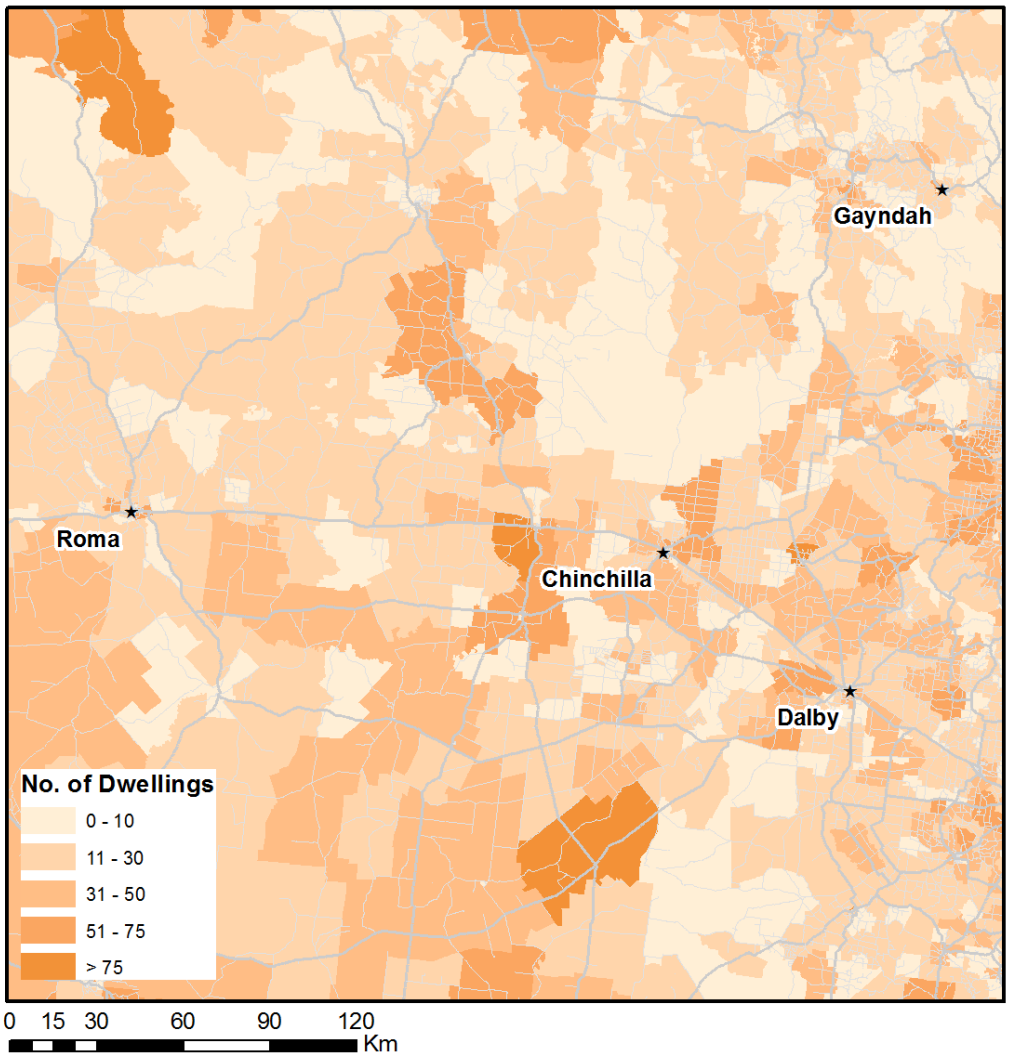

Figure 12 Number of dwellings in the study area (assigned by mesh block)

11.3.2 Calculation methodology

The following approach was taken to assign domestic wood heating methane emissions spatially:

- The average ownership of solid fuel heaters and the average consumption of fuel per heater were taken from the NSW EPA GMR Inventory 2008 and used to determine a consumption factor for each heater type per dwelling
- The consumption factor was then applied to estimate the total annual consumption of fuel within each ABS mesh block
- The estimated consumption rates were assigned to individual grids within the study area.

Diurnal, weekly and monthly profiles were constructed from information presented in the NSW EPA GMR Inventory 2008.

All dwellings in the study area were assumed to fall into the 'Separate house' category.

The methane emission factors for the different types of wood heaters are based on the NSW EPA GMR Inventory 2008 as presented in Table 27.

Table 27 Methane emission factors for solid fuel from the NSW EPA GMR Inventory 2008

Wood Heater Type	Methane emission factor (kg CH_4/tonne of fuel)
Slow combustion heater with compliance plate	14.2
Slow combustion heater without compliance plate	32
Open fireplace	7.2
Potbelly stove	32

11.4 Emission rates

Methane emissions due to wood-fired heaters included in the Surat Basin Methane Inventory are summarised in Table 28.

Table 28 Total methane emissions (kg/year) due to domestic wood heating

Domestic Wood Heater Type	Methane emissions (kg/year)
Slow combustion heater with compliance plate	109,171
Slow combustion heater without compliance plate	108,321
Open fireplace	34,889
Potbelly stove	27,943

12. MOTOR VEHICLES

12.1 Overview

This chapter details the methane emissions from motor vehicles included in the Surat Basin Methane Inventory. The methods used to calculate emissions, data sources and assumptions are provided.

12.2 Emission sources

Roads within the study area that were included in the Surat Basin Methane Inventory are shown in Figure 13. The following scenarios were used to develop methane emissions from motor vehicles in the study area:

- Hot running base emissions
- Speed correction.

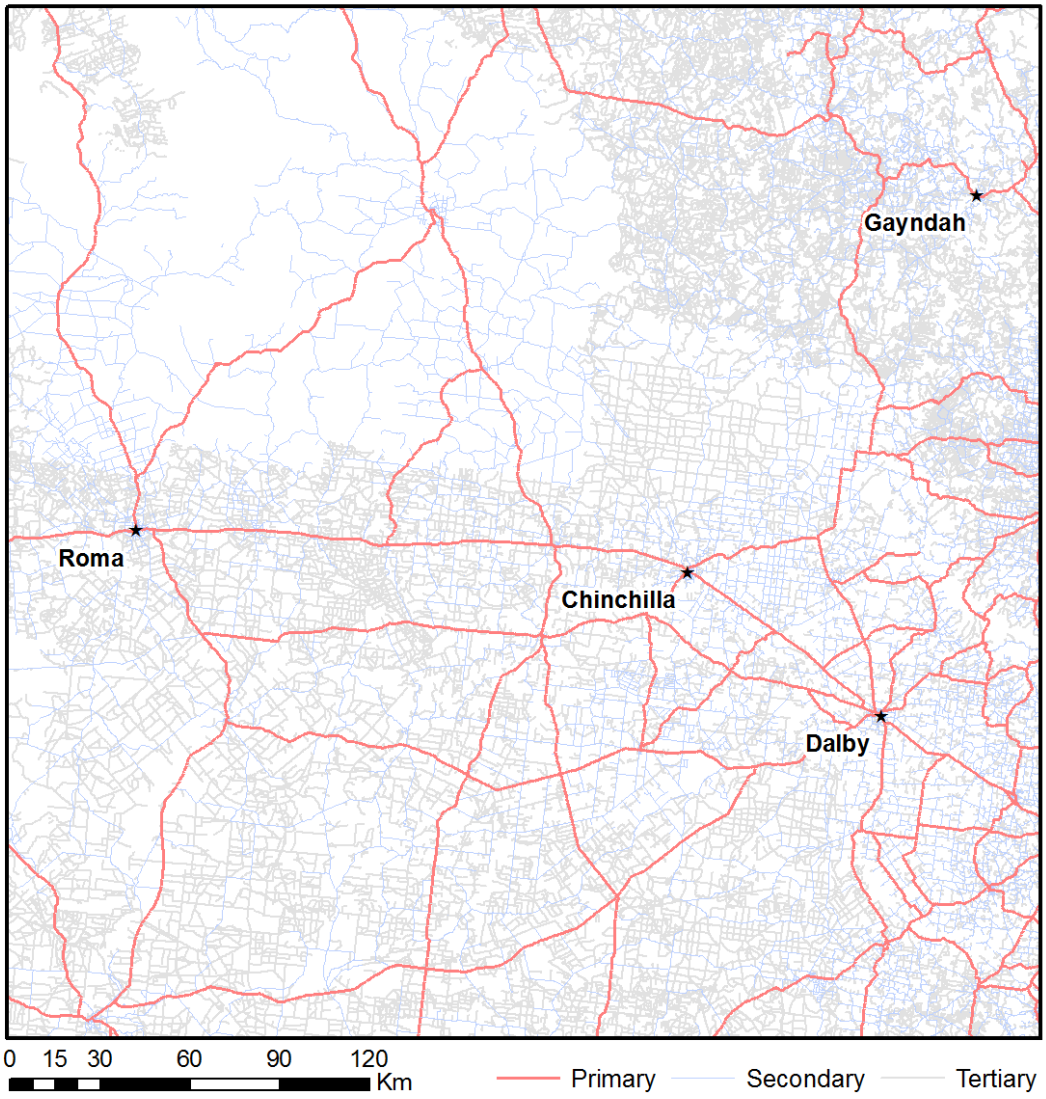

Figure 13 Roads within the study area

12.3 Methodology

12.3.1 Information

The following information was used to generate the motor vehicle inventory:

- NRM, 2010. Attributes and Locations of Queensland Roads
    - DTMR's (Department of Transport and Main Roads) dataset for Annual Average Daily Traffic (AADT) for most of the primary roads (Figure 14).
- Australian Bureau of Statistics:
    - Population and land use data (ASGS, 2011) from residential mesh blocks (Figure 15)
    - Vehicle fleet by age and fuel type from the Motor Vehicle Census (ABS, 2015c).
- NSW EPA GMR Inventory 2008 (NSW EPA, 2012b):
    - Hourly Vehicle Kilometer Travelled (VKT) distribution for average weekday/weekend by vehicle type
    - Hourly average speeds by road type
    - Fleet composite splitting factors by vehicle type and road type
    - Twenty-four-hour VKT weighted average speeds
    - Estimated number of axles for heavy duty fleet
    - Base exhaust hot running emissions by vehicle and fuel type.

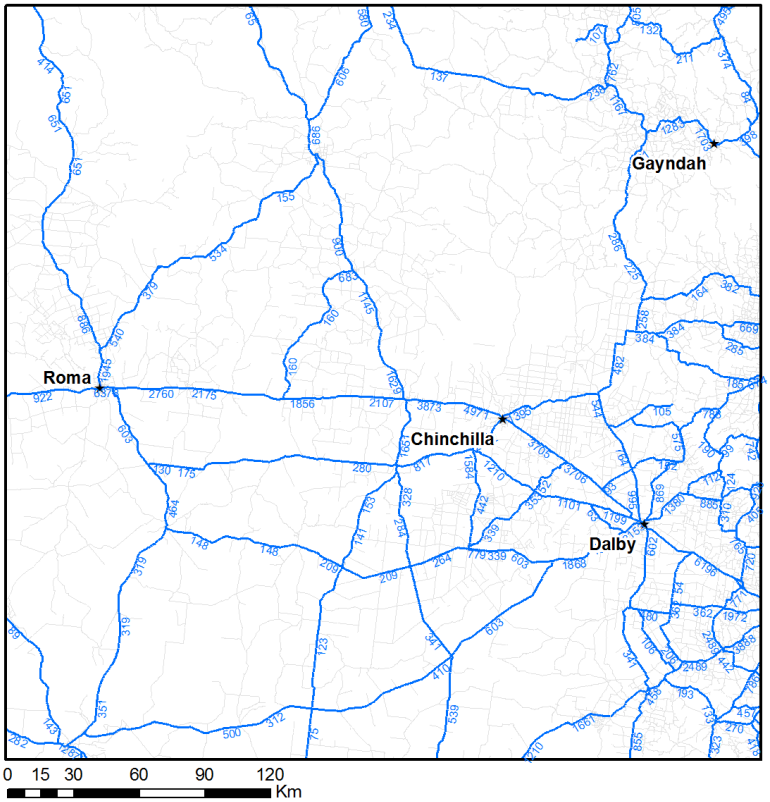

Figure 14 Annual average daily traffic data for primary roads

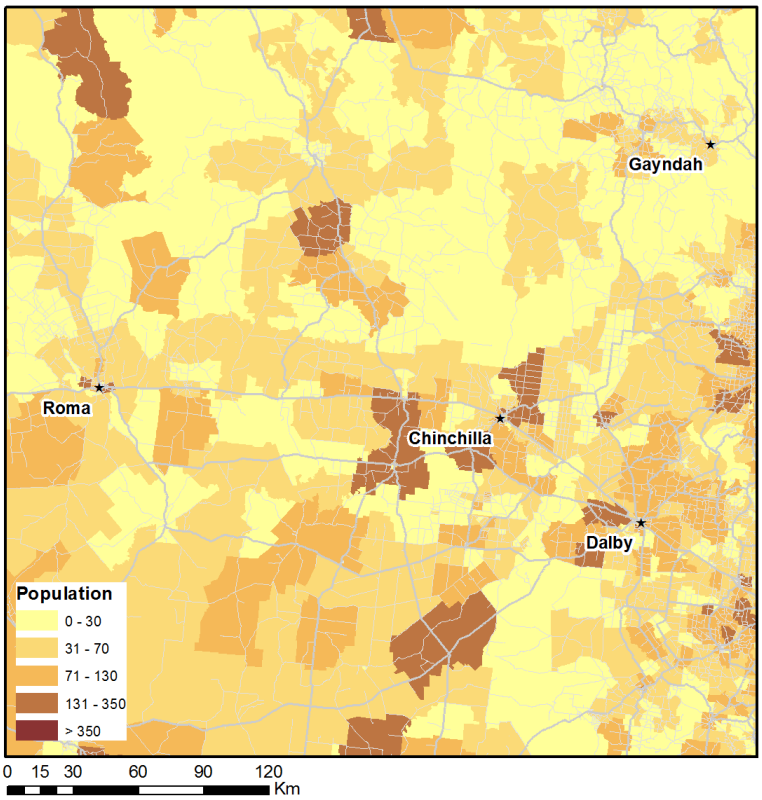

Figure 15 Population data (mesh blocks) in the study area

12.3.1.1 Emission factors

Base hot running exhaust emissions are dependent on vehicle type, age of vehicle and fuel used. Organic compound emission factors for petrol and diesel vehicles, were based on emission factors used in the NSW EPA GMR Inventory 2008 (NSW EPA, 2012b).

12.3.2 Data checks

The following data checks were conducted on the motor vehicle information:

- Continuity of AADT data in segments
- Estimates of AADT were compared with estimated grid emissions
- Missing data were interpolated from existing data
- Overlay of detailed road data with imagery
- Visual comparison and inspection of AADT road geospatial information and detailed road information.

12.3.3 Calculation methodology

Methane emissions attributed to motor vehicles were calculated using the base equation:

$$CH4\_ER = \frac{VKT \times CH4\_EF}{1000}$$

where:

CH_4_ER Emission rate of methane in kg/year

VKT Vehicle kilometres travelled per year

CH_4_EF Emission factor methane in g/VKT.

Methane emission factors were determined for each vehicle type (light vehicles, heavy vehicles, diesel light duty vehicles). Total methane emissions were calculated as the aggregate emission factors for all vehicles in the fleet, proportional to the composition. In equation form, the methane emission factor for a vehicle type was calculated as:

$$EF_{substance,veh\_type} = \sum_{yr\_manufacture=1991}^{2014} \%yr\_manufacture \times EF_{substance,yr\_manufacture}$$

where:

substance substance

veh_type vehicle type (light vehicles, heavy vehicles, diesel light duty vehicles)

$EF_{substance,veh\_type}$ aggregate emission factor for *substance* for vehicle type(g/VKT)

%yr_manufacture % of vehicle type per year of manufacture

$EF_{substance,yr\_manufacture}$ emission factor for *substance* for vehicle manufactured during *yr_manufacture* (g/VKT).

Methane emissions were derived using the speciation of organic compounds in vehicle exhausts by fuel type. Aggregate methane emission factors for each vehicle type are summarised in Table 29. Diesel light duty vehicles are a subset of diesel light vehicles on all road types except for off-road.

Table 29 Aggregate methane emission factors (g/VKT) by vehicle type and road type

Road Type	Petrol		Diesel		
	Light Vehicles	Heavy Vehicles	Light Vehicles	Heavy Vehicles	Light Duty Vehicles
Commercial Highway	1.45E-03	2.93E-02	7.76E-03	4.45E-02	
Commercial Arterial	2.04E-03	4.26E-02	1.18E-02	6.60E-02	
Arterial	1.90E-03	4.02E-02	1.11E-02	6.22E-02	
Local/Residential	2.91E-03	5.84E-02	1.61E-02	9.14E-02	
Tertiary roads	-	-	-	-	1.75E-02

12.4 Emission rates

Methane emissions due to motor vehicles included in the Surat Basin Methane Inventory are summarised in Table 30.

Table 30 Total methane emissions (kg/year) due to motor vehicles

Road Type	Methane emissions (kg/year)		
	Light Vehicles	**Heavy Vehicles**	**Diesel LDV**
Commercial Highway	1,918	13,139	-
Commercial Arterial	1,324	6,829	-
Arterial	83	51	-
Local/Residential	28	17	-
Offroad	-	-	681
Total	**3,354**	**20,036**	**681**

13. UNCERTAINTY

Table 31 provides an indication of the uncertainty associated with the emission source categories defined for the Surat Basin Methane Inventory.

Table 31 Methane Emissions CSG Activities - Uncertainty Estimate

Emission category	Emission source description	Estimated Uncertainty
Agriculture	Feedlots	Moderate (estimate ±10-50%)
	Grazing cattle	High (estimate ±50-100%)
	Poultry farms	Moderate (estimate ±10-50%)
	Piggeries	Moderate (estimate ±10-50%)
Coal mining	Coal extraction	Moderate (estimate ±10-50%)
Landfills	Landfill gas	High (estimate ±50-100%)
Wastewater Treatment Facilities	Off gas	Moderate (estimate ±10-50%)
Power Stations	Combustion emissions	Low (estimate ±0-10%)
River seeps	Fugitive emissions	High (estimate ±50-100%)
Domestic wood heading	Combustion emissions	High (estimate ±50-100%)
Ground seeps	Fugitive emissions	High (estimate ±50-100%)
Motor vehicles	Exhaust emissions	High (estimate ±50-100%)
CSG Activities	Gas consumed for combustion	Low (estimate +/-5%)
	Diesel combustion	Low (estimate +/-10%)
	Flaring	Low (estimate +/-10%)
	Venting	High (estimate +/-50-100%)
	Fugitive emissions	High (estimate +/-50-100%)

14. REFERENCES

AEMO, 2015. *Web Archive Public_DISPATCHSCADA 2010-2015*. Australia Energy Market Operator. Purchased December 2015.

American Petroleum Institute (API), 2009, Compendium of Greenhouse Gas Emissions Methodologies for the Oil and Natural Gas Industry Available at: www.api.org

Australian Bureau of Statistics (ABS), 2015a. Agricultural Commodities. Available at http://www.abs.gov.au/AUSSTATS/abs@.nsf/DetailsPage/7121.02014-15?OpenDocument

Australian Bureau of Statistics (ABS), 2015b. Land Management and Farming in Australia. Available at http://www.abs.gov.au/AUSSTATS/abs@.nsf/DetailsPage/4627.02014-15?OpenDocument

Australian Bureau of Statistics (ABS), 2015c. Motor Vehicle Census - 2015. Available at http://www.abs.gov.au/AUSSTATS/abs@.nsf/Lookup/9309.0Main+Features131%20Jan%202015?OpenDocument.

ASGS,2011. Australian Statistical Geography Standard (ASGS) Volume 1 - Main Structure and Greater Capital City Statistical Areas (cat no. 1270.0.55.001). Available at http://www.ausstats.abs.gov.au/ausstats/subscriber.nsf/0/D3DC26F35A8AF579CA257801000DCD7D/$File/1270055001_july%202011.pdf.

Australian Government Department of the Environment, 2016. National Pollutant Inventory for 2014/15. Available at http://www.npi.gov.au/.

Australian Government Department of the Environment, 2016. Diesel fuel quality standard. Available at https://www.environment.gov.au/topics/environment-protection/fuel-quality/standards/diesel#

Clean Energy Regulator, 2017. National Greenhouse and Energy Reporting Act 2007, Commonwealth of Australia

Clean Energy Regulator, 2016a. National Greenhouse and Energy Reporting (Measurement) Determination 2008. Australian Government.

Clean Energy Regulator, 2016b. National Greenhouse and Energy Reporting Regulations 2008. Australian Government.

CSIRO, 2015, Characterisation of Regional Fluxes of Methane in the Surat Basin, Queensland, Phase 2: A Pilot Study of Methodology to Detect and Quantify Methane Sources, Report for the Gas Industry Social and Environmental Research Alliance (GISERA), Project No GAS1315.

CSIRO, 2002, Model Code of Practice for the Welfare of Animals, Domestic Poultry 4th Edition, SCARM Report 83, Primary Industries Standing Committee, published by CSIRO, 2002.

Department of Agriculture and Fisheries, 2014. *Agricultural land audit - current cattle feedlots – Queensland*. State of Queensland (Department of Agriculture and Fisheries). Published 31 January 2014. Available at http://qldspatial.information.qld.gov.au/catalogue/

Department of Agriculture and Fisheries (DAF), 2014. *Agricultural land audit - current piggeries – Queensland*. State of Queensland (Department of Agriculture and Fisheries). Published 31 January 2014. Available at http://qldspatial.information.qld.gov.au/catalogue/

Department of Agriculture and Fisheries (DAF), 2014. *Agricultural land audit - current poultry farms – Queensland*. State of Queensland (Department of Agriculture and Fisheries). Published 31 January 2014. Available at http://qldspatial.information.qld.gov.au/catalogue/

Department of Agriculture and Fisheries (DAF), 2013. *Property boundaries Queensland*. State of Queensland (Department of Natural Resources and Mines). Published 20 October 2013. Available at http://dds.information.qld.gov.au/dds/.

Department of the Environment and Energy (DEE), 2016. Natural Resource Management (NRM) Regions for 2016. Available at http://www.environment.gov.au/fed/catalog/search/resource/details.page?uuid=%7BAB80DA43-CB00-455D-8A3C-70162EB8D964%7D

Department of Environment and Heritage Protection (EHP), 2016. Contacts for public waste and recycling facilities in Queensland. Available at https://www.ehp.qld.gov.au/waste/facilities/list/.

Department of Environment and Resource Management (DERM), 2011. Waste characterisation Survey Final Report.

Department of Natural Resources and Mines (NRM) 2015. *Key resource areas - resource processing area – Queensland*. State of Queensland (Department of Natural Resources and Mines). Published 17 April 2015. Available at http://qldspatial.information.qld.gov.au/catalogue/

Department of the Environment (DoE), 2016, National Greenhouse Accounts Factors, Australian National Greenhouse Accounts, August 2016, Australian Government Department of the Environment, ISSN: 2202-333X.

Department of Transport and Main Roads (TMR) 2015. *Traffic census 2014 - Queensland*. State of Queensland (Department of Transport and Main Roads). Published 14 May 2015. Available at http://qldspatial.information.qld.gov.au/catalogue/

FAOSTAT, 2016. Food and Agriculture Organization of the United Nations. Available at http://fenix.fao.org/faostat/beta/en/#data/GE

Geoscience Australia, 2012. The Wastewater Treatment Facilities Database. Available at http://www.ga.gov.au/metadata-gateway/metadata/record/74625. Catalogue number 74625.

Harper, L.A, Denmead, O.T., Freney, J.R, Byers, F.M., 1999. Direct Measurements of Methane Emissions from Grazing and Feedlot Cattle.J. Anim. Sci. 1999. 77:1392-1401. Available at https://naldc.nal.usda.gov/download/4072/PDF.

Katestone Environmental, 2016. Surat Basin Air Emissions Inventory 2014 Summary Report, prepared for CSIRO.

New South Wales Environment Protection Authority, 2012a. Air Emissions Inventory for the Greater Metropolitan Region in New South Wales, Technical Report No. 3: 2008 Calendar Year Commercial Emissions, Environment Protection Authority, 59–61 Goulburn Street, Sydney South 1232, Australia

New South Wales Environment Protection Authority, 2012b. Air Emissions Inventory for the Greater Metropolitan Region in New South Wales, Technical Report No. 7: 2008 Calendar Year On-Road Mobile Emissions, Environment Protection Authority, 59–61 Goulburn Street, Sydney South 1232, Australia

NRM 2015. *Mining lease surface areas – Queensland*. State of Queensland (Department of Natural Resources and Mines). Published 13 October 2015. Available at:at http://qldspatial.information.qld.gov.au/catalogue/

NRM, 2015, *Exploration and production permits - Queensland*. Available at http://qldspatial.information.qld.gov.au/catalogue/custom/detail.page?fid=%7BB0D192C5-4076-43E8-9A2C-94A0FA928AF9%7D

Queensland Government, 2013, Animal Care and Protection Amendment Regulation (No. 2) 2013, Explanatory Notes for SL 2013 No. 103. Available at https://www.legislation.qld.gov.au/LEGISLTN/SLS/RIS_EN/2013/13SL103E.pdf.

State of Queensland, Department of Natural Resources and Mines, 2010. Physical road network - Queensland.

Sustainable Table, 2015, Free Range Egg and Chicken Guide. Available at http://www.sustainabletable.org.au/Hungryforinfo/Free-range-egg-and-chicken-guide/tabid/113/Default.aspx.

CONTACT US

t 1300 363 400
+61 3 9545 2176
e enquiries@csiro.au
w www.csiro.au

FOR FURTHER INFORMATION

David Etheridge
t +61 3 9239 4590
e david.etheridge@csiro.au